

Copyright
by
Paul Frank Thompson, Jr.
2004

The Dissertation Committee for Paul Frank Thompson, Jr. certifies that this is the approved version of the following dissertation:

Interpreting the Earth's Time Varying Geopotential as Observed from Space and Comparisons to Global Models of Hydrologic Transport

Committee:

Byron D. Tapley, Supervisor

Srinivas V. Bettadpurr

Wallace T. Fowler

Cesar Ocampo

Clark R. Wilson

**Interpreting the Earth's Time Varying Geopotential as Observed from
Space and Comparisons to Global Models of Hydrologic Transport**

by

Paul Frank Thompson, Jr., B.S., M.S.

Dissertation

Presented to the Faculty of the Graduate School of

The University of Texas at Austin

in Partial Fulfillment

of the Requirements

for the Degree of

Doctor of Philosophy

The University of Texas at Austin

December 2004

Dedication

To the two most important women in my life—my mother, Ann, and my wife, Laura.

Acknowledgements

First, I wish to thank the members of my dissertation committee for their review of my dissertation as well as discussions regarding my research and academic education. I also wish to thank Byron Tapley and Srinivas Bettadpur for allowing me to do productive and interesting research as well as for their patience with me during the less productive time periods.

A number of individuals assisted with the analysis necessary to conduct the research contained in this dissertation, and I would like to thank them for their help:

- Don Chambers – provided the ocean circulation statistics based on GRACE gravity models.
- Jian-Li Chen – provided the Stokes coefficients for the annual variability found from the TOPEX/Poseidon data and the NCEP/NCAR CDAS-1 data analysis.
- Richard Eanes – conducted the analysis of the SLR data, providing a time series of spherical harmonic coefficients.
- Brian Gunter – provided the software development and algorithm testing of the parallel solver used in GRACE simulations and data processing, the Advanced Equation Solver for Parallel Systems (AESoP).

- Tatyana Pekker – provided analysis of the atmospheric pressure contribution to the geoid and converted the GLDAS output into geopotential coefficients
- John Wahr and Steve Jayne – provided spherical harmonic coefficients derived from the POP model and the CPC hydrology model

This research was supported in part by a NASA Graduate Student Researchers Program (GSRP) fellowship at the Goddard Space Flight Center and by NASA Grant NAG5-97213.

Interpreting the Earth's Time Varying Geopotential as Observed from Space and Comparisons to Global Models of Hydrologic Transport

Publication No. _____

Paul Frank Thompson, Jr., Ph.D.

The University of Texas at Austin, 2004

Supervisor: Byron D. Tapley

Measurements of temporal changes in Earth's gravitational field were measured using six years of satellite laser ranging (SLR) to Lageos-1 and Lageos-2 and the results were compared to geophysical models of mass variability for the atmosphere, ocean, and continental hydrology. Annual estimates of spherical harmonic gravity coefficients (degree and order four expansion) derived from the SLR observations when compared to combinations of the mass models had degree correlations that generally exceeded the 90% confidence limit and agreed to about the 1 mm level in terms of geoid height anomaly.

The Gravity Recovery and Climate Experiment (GRACE) is measuring Earth's gravitational field approximately every month at spatial scales of a few hundred kilometers. In order to achieve smaller temporal and spatial scales, it is necessary to account for the effects of short period, non-tidal, mass variability which was not previously included in other gravity determinations. Orbital simulations of GRACE showed that the highest degrees were impacted the most by unmodeled variability in the

atmosphere, oceans, and continental hydrology (a factor of ~20 increase in degree error in the case of the atmosphere). The use of approximate models gave the greatest reduction in aliasing error for the mid-degrees and higher; however, the lowest degrees (~2-5) were dominated by the sensitivity of the GRACE processing system to systematic error. GRACE data processing that used a combined atmosphere-ocean de-aliasing (AOD) model showed improvement in the gravity estimates consistent with the simulations: the shorter spatial wavelengths (higher degrees) were improved while the longest spatial wavelengths (particularly important for time-variable gravity studies) were relatively unaffected.

Monthly gravity solutions from GRACE resolved features on the order of 2-3 mm geoid height anomaly when smoothed to 400-km spatial scales. Comparisons with the Global Land Data Assimilation System (GLDAS) terrestrial water storage model indicated a high degree of correlation up to spatial wavelengths of 600 km or larger; a significant improvement over the spatial and temporal scales obtained with SLR observations. However, temporal variability in the degree 2 coefficients, particularly the zonal, seemed to be better resolved by SLR observations than by GRACE observations.

Table of Contents

List of Tables	xi
List of Figures	xii
Chapter 1: Introduction	1
1.1 Measuring Gravity from Space	1
1.2 Measurements of Time-Variable Gravity	3
1.3 GRACE	5
1.4 Study Outline and Objectives	6
Chapter 2: Annual Geopotential Variability from SLR and Global Hydrology Models	9
2.1 Introduction	9
2.2 Representing Variations in Geopotential	11
2.3 Annual Variability	13
2.4 SLR Data Analysis	14
2.5 Geophysical Models	31
2.5.1 Atmosphere	32
2.5.2 Ocean	33
2.5.3 Continental Hydrology	35
2.6 Comparison of Results	37
2.7 Discussion	43
Chapter 3: Aliasing Impact of Short Period, Non-Tidal, Temporal Mass Variability in Simulated GRACE Gravity Recovery	46
3.1 Introduction	46
3.2 Geophysical Models	48
3.2.1 Atmosphere	48
3.2.2 Ocean	49
3.2.3 Continental Hydrology	50
3.4 Simulation Procedure	52
3.5 Aliasing Error Definition	55

3.6	Results.....	59
3.7	Discussion.....	66
Chapter 4:	Atmosphere-Ocean De-Aliasing Model and GRACE	68
4.1	Introduction.....	68
4.2	Comparisons with TEG4.....	70
4.3	Time-Variable Gravity Perturbation	74
4.4	Ocean Circulation Statistics.....	82
4.5	Orbit Statistics.....	82
4.6	Discussion.....	84
Chapter 5:	GRACE Time-Variable Gravity and Continental Hydrology.....	86
5.1	Introduction.....	86
5.2	Methods.....	88
5.3	Continental Hydrology and GRACE Time-Variable Gravity	89
5.4	Annual Signal.....	93
5.5	Sub-Annual, Basin-Scale Variability.....	95
5.6	Spatial Resolution.....	113
5.7	Discussion.....	116
Chapter 6:	Conclusions and Recommendations	118
6.1	Conclusions.....	118
6.2	Future Work and Recommendations	121
Appendix A:	AOD Model Description and Implementation.....	125
A.1	Atmospheric Data	125
A.2	Ocean Model.....	126
A.3	Model Combination	128
A.4	Implementation	128
A.5	Background Geopotential Models	131
A.6	Simulation Validation.....	133
References.....		139
Vita		146

List of Tables

Table 2.1.	Annual cosine and sine amplitude in the geopotential determined from SLR to Lageos-1 and Lageos-2.....	30
Table 2.2.	Amplitude and phase of the annual variation of the normalized spherical harmonic coefficients estimated in the geopotential as determined by SLR observations to Lageos-1 and Lageos-2. See equations 2.8 and 2.9 for the definition of amplitude and phase.	31
Table 2.3.	Lageos-1 and Lageos-2 SLR observations of time-variable gravity compared to geoid variations predicted by various combinations of geophysical models. Complete from degree 2-4 and based on a 1° lat/lon grid.....	39
Table 2.4.	Degree correlations of the model combinations and SLR data for the cosine and sine components of the annual cycle.	42
Table 4.1.	Global statistics from ocean circulation velocities based on the GRACE gravity field solutions as compared to velocities from Levitus to 4000-m depth.....	82
Table 4.2.	Impact of the AOD model on orbit fits calculated from the GRACE gravity solutions. Values are RMS in cm.	83

List of Figures

Figure 2.1. Representative 12-day groundtrack for Lageos-1 (top) and Lageos-2 (bottom).....	15
Figure 2.2. $C_{2,0}$: SLR time series (solid line) with annual fit (dashed line).	18
Figure 2.3. $C_{2,1}$: SLR time series (solid line) with annual fit (dashed line).	19
Figure 2.4. $C_{2,2}$: SLR time series (solid line) with annual fit (dashed line).	19
Figure 2.5. $C_{3,0}$: SLR time series (solid line) with annual fit (dashed line).	20
Figure 2.6. $C_{3,1}$: SLR time series (solid line) with annual fit (dashed line).	20
Figure 2.7. $C_{3,2}$: SLR time series (solid line) with annual fit (dashed line).	21
Figure 2.8. $C_{3,3}$: SLR time series (solid line) with annual fit (dashed line).	21
Figure 2.9. $C_{4,0}$: SLR time series (solid line) with annual fit (dashed line).	22
Figure 2.10. $C_{4,1}$: SLR time series (solid line) with annual fit (dashed line).	22
Figure 2.11. $C_{4,2}$: SLR time series (solid line) with annual fit (dashed line).	23
Figure 2.12. $C_{4,3}$: SLR time series (solid line) with annual fit (dashed line).	23
Figure 2.13. $C_{4,4}$: SLR time series (solid line) with annual fit (dashed line).	24
Figure 2.14. $S_{2,1}$: SLR time series (solid line) with annual fit (dashed line).....	24
Figure 2.15. $S_{2,2}$: SLR time series (solid line) with annual fit (dashed line).....	25
Figure 2.16. $S_{3,1}$: SLR time series (solid line) with annual fit (dashed line).....	25
Figure 2.17. $S_{3,2}$: SLR time series (solid line) with annual fit (dashed line).....	26
Figure 2.18. $S_{3,3}$: SLR time series (solid line) with annual fit (dashed line).....	26
Figure 2.19. $S_{4,1}$: SLR time series (solid line) with annual fit (dashed line).....	27
Figure 2.20. $S_{4,2}$: SLR time series (solid line) with annual fit (dashed line).....	27
Figure 2.21. $S_{4,3}$: SLR time series (solid line) with annual fit (dashed line).....	28
Figure 2.22. $S_{4,4}$: SLR time series (solid line) with annual fit (dashed line).....	28

Figure 2.23. Maps of the cosine and sine components of the annual variation in the geoid due to atmosphere mass redistribution (complete from degree 2-4).	33
Figure 2.24. Maps of the cosine and sine components of the annual variation in the geoid due to ocean mass redistribution (complete from degree 2-4).	35
Figure 2.25. Maps of the cosine and sine components of the annual variation in the geoid due to continental water mass redistribution (complete from degree 2-4).	37
Figure 2.26. Maps of the cosine and sine components of the annual variation in the geoid as determined from the Lageos-1 and Lageos-2 SLR observations and from the sum of the combined geophysical models for Case 4.	40
Figure 3.1. RMS about the monthly mean of the time variable geopotential models used to generate simulated observations: ECMWF atmosphere (top), POP baroclinic ocean (middle), and NCEP continental hydrology (bottom).	51
Figure 3.2. Outline of the procedure for the GRACE orbital simulations.	53
Figure 3.3. Ground track coverage for the simulations. Every 10-second integration point is shown for the 30-day time span of the simulation.	54
Figure 3.4. Average difference between the ‘truth’ and ‘nominal’ time variable models. Degree difference is shown for the atmosphere and ocean models. Degree amplitude is shown for the continental hydrology model as no de-aliasing was attempted with that model type.	59

Figure 3.5. Atmosphere model simulation results. Degree error as defined in equation (3.5). Results are for error due to the ECMWF atmosphere (truth model) along with residual aliasing error after using the NCEP atmosphere (nominal model) as an approximate model of the ECMWF atmosphere.61

Figure 3.6. Atmosphere model simulation results. Error due to ECMWF atmosphere (top) and error after de-aliasing with NCEP atmosphere (bottom). Geoid anomaly, Gaussian smoothed with a 500-km radius.62

Figure 3.7. Ocean model simulation results. Degree error as defined in equation (3.5). Results are for error due to the baroclinic ocean (truth model) along with residual aliasing error after using the barotropic ocean (nominal model) as an approximate model of the baroclinic ocean. 63

Figure 3.8. Ocean model simulation results. Error due to baroclinic ocean (top) and error after de-aliasing with the barotropic ocean (bottom). Geoid anomaly, Gaussian smoothed with a 500-km radius.64

Figure 3.9. Continental hydrology model simulation results. Degree error as defined in equation (3.5). Results are for error due to the NCEP continental hydrology (truth model); no de-aliasing was attempted.65

Figure 3.10. Continental hydrology model simulation results. Error due to NCEP continental hydrology. Geoid anomaly, Gaussian smoothed with a 500-km radius.....66

- Figure 4.1. Degree error for the solutions processed with and without the AOD model for August 2002 as compared to TEG4 as well as the difference between the two. The differences relative to TEG4 are difficult to see at full scale (top), but are evident for the highest degrees (bottom). The average value of AOD was added to the with-AOD solutions before the comparisons were made, isolating the perturbation due to the short-period variability.....71
- Figure 4.2. Degree error for the solutions processed with and without the AOD model for November 2002 as compared to TEG4 as well as the difference between the two. The differences relative to TEG4 are difficult to see at full scale (top), but are evident for the highest degrees (bottom). The average value of AOD was added to the with-AOD solutions before the comparisons were made, isolating the perturbation due to the short-period variability.....72
- Figure 4.3. Degree error for the solutions processed with and without the AOD model for April 2003 as compared to TEG4 as well as the difference between the two. The differences relative to TEG4 are difficult to see at full scale (top), but are evident for the highest degrees (bottom). The average value of AOD was added to the with-AOD solutions before the comparisons were made, isolating the perturbation due to the short-period variability.....73

Figure 4.4. Comparisons of time variable gravity signals from August 2002 to November 2002 based on the with-AOD or the without-AOD gravity solutions. The average of the AOD model has been added to the with-AOD solutions in order to isolate the perturbations due to the short-period effects of the AOD model.....75

Figure 4.5. Comparisons of time variable gravity signals from November 2002 to April 2003 based on the with-AOD or the without-AOD gravity solutions. The average of the AOD model has been added to the with-AOD solutions in order to isolate the perturbations due to the short-period effects of the AOD model.....76

Figure 4.6. Comparisons of time variable gravity signals from August 2002 to April 2003 based on the with-AOD or the without-AOD gravity solutions. The average of the AOD model has been added to the with-AOD solutions in order to isolate the perturbations due to the short-period effects of the AOD model.....77

Figure 4.7. Time variable gravity estimates for the time period between the August and November 2002 solutions for both the without-AOD solutions (top) and with-AOD solutions (middle). Gaussian smoothed with a 600-km radius and the degree 2 coefficients removed. Peak amplitude of the difference between the two time-variable estimates was $-4.8/+3.2$ mm geoid height (bottom).....79

Figure 4.8.	Time variable gravity estimates for the time period between the November 2002 and April 2003 solutions for both the without-AOD solutions (top) and with-AOD solutions (middle). Gaussian smoothed with a 600-km radius and the degree 2 coefficients removed. Peak amplitude of the difference between the two time-variable estimates was -2.5/+2.3 mm geoid height (bottom).....	80
Figure 4.9.	Time variable gravity estimates for the time period between the August 2002 and April 2003 solutions for both the without-AOD solutions (top) and with-AOD solutions (middle). Gaussian smoothed with a 600-km radius and the degree 2 coefficients removed. Peak amplitude of the difference between the two time-variable estimates was -3.9/+3.9 mm geoid height (bottom).....	81
Figure 5.1.	Annual variability of the geoid from GRACE and GLDAS hydrology. Geoid height anomaly using a 400-km smoothing radius and with the degree 2 coefficients omitted.	94
Figure 5.2.	Time-variable gravity over South America in April/May 2002 for GRACE (top left) and GLDAS (top right), relative to the average of 14 monthly solutions. The degree 2 coefficients were omitted and a 400-km smoothing radius was used. Degree correlations between GRACE and GLDAS were computed for the global set of geopotential coefficients (bottom).....	97
Figure 5.3.	Same as Figure 5.2 for August 2002.....	98
Figure 5.4.	Same as Figure 5.2 for October 2002.	99
Figure 5.5.	Same as Figure 5.2 for November 2002.	100
Figure 5.6.	Same as Figure 5.2 for February 2003.....	101

Figure 5.7.	Same as Figure 5.2 for March 2003.....	102
Figure 5.8.	Same as Figure 5.2 for April 2003.....	103
Figure 5.9.	Same as Figure 5.2 for May 2003.....	104
Figure 5.10.	Same as Figure 5.2 for July 2003.....	105
Figure 5.11.	Same as Figure 5.2 for August 2003.....	106
Figure 5.12.	Same as Figure 5.2 for September 2003.....	107
Figure 5.13.	Same as Figure 5.2 for October 2003.	108
Figure 5.14.	Same as Figure 5.2 for November 2003.	109
Figure 5.15.	Same as Figure 5.2 for December 2003.....	110
Figure 5.16.	Comparisons of signals and errors. Observed geoid height differences relative to a mean geoid (top) and a representation of the expected errors at the same levels of smoothing (bottom) for the April 2002 (left) and April 2003 (right) solutions. A 600-km smoothing radius was used for 2003 and 1000-km for 2002 (degree 2 coefficients not included)..	115
Figure 6.1	Error estimates for GRACE based on simulated and empirical results. Simulation results represent a type of lower bound in the level of error achievable and the empirical results represent an upper bound on the level of error that has been achieved to date. The “measurement noise” and “aliasing” error are based on the aliasing simulations of chapter 3, while the calibrated errors are based on the real-data processing that produced the GRACE solutions used in chapter 5.....	123
Figure A.1.	Representative time series for $C_{2,2}$ (top) and $S_{2,2}$ (bottom) for the original AOD (solid line) and the AOT series created by removing the S2 semi-diurnal tide variability (dashed line).....	130

Figure A.2. Time-variable models of $C_{2,0}$ geopotential coefficient as used in GRACE processing for an August 2002 solution. Individual models are shown for a selected 3-day interval (top), while the total is shown for the entire solution time-span (bottom). Gaps in the time series are due to data omitted during processing.....	132
Figure A.3. Comparison of AOD model and NCEP atmospheric pressure in terms of degree amplitude for the month of August 2002. Also shown is representative error due to an optimistic assumption of measurement noise-only (see chapter 3)	134
Figure A.4. Average for the month August 2002 relative to the year 2001 mean shown for AOD model (top), NCEP atmosphere (middle), and the difference between the two (bottom). Note that the map scales reflects that the model differences are on the order of one-fifth the model signals.	135
Figure A.5. RMS about the mean for the month August 2002 for AOD model (top) and NCEP atmosphere (bottom).....	136
Figure A.6. History of geoid height for AOD taken along ground track during the August 2002 solution.	137
Figure A.7. Degree error using AOD data for August 2002 as the truth model and de-aliasing with NCEP atmosphere as the nominal model. Simulations conducted as in chapter 3. Representative error predicted for an unmodeled ocean and measurement noise-only are also shown.....	138

Chapter 1: Introduction

1.1 MEASURING GRAVITY FROM SPACE

The shape and character of Earth's gravitational field is directly linked to the density distribution within Earth's systems. Through the measurement of the geopotential, it is possible to learn about the shape of Earth and to place constraints on the density model of Earth's interior. Furthermore, temporal changes in the geopotential can be linked to mass redistribution within the various sub-systems of Earth. There are two basic methods currently used to measure gravity: terrestrial gravimetry and space-based techniques. Terrestrial methods are highly accurate at small spatial scales; however, it is difficult to get global coverage, particularly in a short time span. As the orbital motion of a satellite is largely determined by gravitational forces, it is possible to measure Earth's global geopotential field arising from perturbations of the orbits of spacecraft. Furthermore, it is possible to repeat these measurements over time in order to track the temporal changes in the geopotential.

Satellite geodesy began with the launch of the Sputnik spacecraft in 1957 and techniques of precise tracking of artificial satellites have continued to be the primary means of determining Earth's large-scale regional gravity features [e.g., *Nerem et al.*, 1995]. In particular, satellite laser ranging (SLR) systems developed in the mid-1960s and operating through the present have improved the precision of the range measurements to less than a centimeter [e.g., *Degnan*, 1993]. For example, Lageos-1, launched in 1976 to an altitude of about 6000 km, and Lageos-2, launched in 1992 at roughly the same altitude but at a different inclination, are two of the most useful

spacecraft for providing ranging measurements of adequate accuracy and precision for observing the Earth's global gravity field.

Shorter-wavelength terms decay rapidly with distance above the Earth's surface; therefore, accurate detection of these terms in the geopotential would require a low-altitude satellite. Unfortunately, low altitude satellites are subject to considerably larger non-gravitational forces, primarily from the atmosphere, and these can greatly degrade the gravity inversion at all wavelengths. Furthermore, the increased atmospheric drag requires extensive station keeping and reduces the lifetime of the mission. High-altitude satellites like Lageos, however, can provide useful gravity information only at relatively long wavelengths (approximately a degree and order 6 field at most [e.g., *Nerem et al.*, 2000]). While gravity models such as JGM-3, which is derived from observations using a number of satellites along with surface information, includes spherical harmonic coefficients out to only degree and order 70 [*Tapley et al.*, 1996]. A higher altitude is a reasonable compromise between an altitude low enough to provide good spatial resolution and yet it allows for an orbit high enough to minimize atmospheric drag effects. However, to make further advances in gravity modeling from space, technologies are needed to help alleviate the effects of non-gravitational forces while allowing for observations at smaller spatial scales [e.g., *Wolff*, 1969].

Satellite-to-satellite tracking is another successful method for determining the Earth's gravity field using spacecraft and it has a long history. It was first successfully demonstrated in 1968 while mapping the nearside gravity field of the Moon (in this case, treating Earth as a satellite of the Moon) [*Muller and Sjogren*, 1968], and was first employed for the determination of Earth's gravity field from using the Apollo spacecraft tracked by the Applied Technology Satellite [*Vonbun et al.*, 1980]. The development of this method has advanced considerably, resulting in high-accuracy Global Positioning

System (GPS) receivers now frequently used onboard orbiting satellites and allowing for nearly continuous tracking of any satellite. For example, the utility of GPS tracking is demonstrated through precise orbit determination and improvements in gravity field determination due to GPS tracking of TOPEX/POSEIDON [e.g., *Yunck et al.*, 1994; *Schutz et al.*, 1994; *Tapley et al.*, 1994].

1.2 MEASUREMENTS OF TIME-VARIABLE GRAVITY

Variations in Earth's mass distribution result in a corresponding change in the global geopotential, which has been observed using space geodetic techniques. Temporal variations in the Earth's gravitational field can be observed due to a variety of phenomenon that include luni-solar tides, atmospheric redistribution, ocean circulation, glacial isostatic readjustment, changes in snow cover, plate tectonics, and other geophysical phenomenon [*NRC*, 1997]. Some temporal variations in gravity such as those caused by ocean and solid Earth tides are well known because they are driven by precise frequencies and can be indirectly observed through other measurements (e.g., altimetry). Other gravitational variations due to the Earth's different sub-systems are more difficult to observe directly (e.g., deep aquifers) and may be best observed indirectly through their influence on orbiting spacecraft.

As with the Earth's static gravity field, only the longest spatial scales of the Earth's temporal gravity field have been observed with orbiting spacecraft. For example, the variations in the degree 1 coefficients of the gravity field (directly related to the location of the center of mass relative to the center of figure) have been determined using SLR data [e.g., *Watkins and Eanes*, 1993; *Eanes*, 1995]. SLR observations of the geocenter variations have been compared to geophysical models of atmosphere, ocean, and continental hydrology, helping to explain much of the variability in the geoid at the annual time scale [e.g., *Chen et al.*, 1999]. In particular, there has been an increasing

appreciation for the importance of continental hydrological process in explaining geocenter variations, for example, seasonal transport of water between the Northern and Southern Hemispheres due to soil moisture and snow cover variations has been observed through GPS tracking [*Bleweitt et al.*, 2001].

One of the temporal gravity variations with the longest history of observing from space would arguably be the second degree zonal coefficient, J_2 , first estimated using SLR tracking of Lageos-1 [*Yoder et al.*, 1983]. The variations are also associated with specific geophysical models; in particular, the change in J_2 corresponds to a change in the overall shape of Earth, which arises from glacial isostatic adjustment as the asthenosphere moves from the equator back to the poles in response to the removal of a previous ice load. The annual cycle of J_2 has also been studied extensively, with many studies concluding that much of the observed variation is caused by the mass redistribution in the atmosphere, though with substantial year-to-year variations [e.g., *Chao and Au*, 1991; *Gegout and Cazenave*, 1993; *Nerem et al.*, 1993; *Chao and Eanes*, 1995].

Shorter and shorter wavelengths of temporal variations in Earth's geopotential have been observed, though it has been found difficult to attribute all the annual cycle at these spatial scales as being due to atmospheric variability alone. For example, variations in J_3 determined from Lageos SLR data are not well predicted by the models of atmospheric mass redistribution alone [*Nerem et al.*, 1993; *Gegout and Cazenave*, 1993]. *Chao and Eanes* [1995] found that while the atmospheric variability helped to explain the magnitude of the variability for low, even-degree zonals, the phase was incorrect. However, they found that the agreement measurably improved with the inclusion of a continental hydrology model. Furthermore, there has been shown to be significant agreement, on annual time scales, between the degree 2 terms of the geopotential and

geophysical models of the combined effects of the atmosphere, ocean, and continental hydrology [Cazenave *et al.*, 1999; Nerem *et al.*, 2000].

A large class of seasonal, climate-related mass variability exists in Earth's fluid sub-systems where an increased knowledge of these systems would be of great interest to the oceanographic, hydrological, glaciological, and climate change communities [NRC, 1997]. The global measurement of the associated mass distribution and mass flux, through its effects on Earth's gravity, was the major motivation behind the development of GRACE [Tapley, *et al.*, 2004b]. Ultimately, accurate and ongoing measurements of gravity variations will aid in developing a new understanding of ocean heat storage [Jayne *et al.*, 2003], deep ocean currents [Wahr *et al.*, 2002], eustatic sea level rise, polar ice mass accumulation [Velicogna and Wahr, 2002; Wu *et al.*, 2002], ground water storage [Rodell and Famiglietti, 1999], and surface water [Alsdorf and Lettenmaier, 2003].

1.3 GRACE

The Gravity Recovery and Climate Experiment (GRACE) launched March 2002 is a dedicated satellite mission under the joint sponsorship of the National Aeronautics and Space Administration (NASA) and the Deutsches Zentrum für Luft und Raumfahrt (DLR). One key objective of GRACE is to map the global gravity field with a spatial resolution of ~400 km every 30 days for five years [Tapley and Reigber, 2001; Kim and Tapley, 2002]. Preliminary results have shown dramatic improvement in gravity field solutions relative to previous spacecraft geodesy mission [Tapley *et al.*, 2004a]. GRACE uses a microwave tracking system to obtain a biased measurement of the range between two identical satellites, each carrying GPS receivers and on board accelerometers [Dunn *et al.*, 2003]. The GRACE satellites are in a nearly circular, polar orbit, had a starting altitude of approximately 500 km, and will have nominal separation of approximately

200 km. The nominal mission is expected to allow the spacecraft to descend over its lifetime to a final altitude of approximately 300 km before reentry into Earth's atmosphere. The range-rate measurements derived from the observations are used to infer the gravitational field, and the on-board GPS receivers are used to determine the position of each spacecraft in a geocentric reference frame. Errors in the nonconservative force models (atmospheric drag, solar radiation pressure, etc.) for the low satellite are the primary limitations of the GRACE system for gravity field determination; on-board accelerometers are used to detect the non-gravitational effects so that they can be modeled correctly.

Because the satellites are in such a low orbit, the gravity field should be determined orders of magnitude more accurately and with more precision than other spacecraft-only methods. The variations in the monthly gravity solutions with this level of precision can be used to study a large variety of problems in a number of disciplines: changes in water and snow storage on continents, seafloor pressure variations, redistribution of ice and snow on the polar ice caps, and post-glacial rebound (PGR). In particular, global gravity models will be improved in areas where data was previously denied for political reasons (e.g., parts of Asia) or in areas logistically difficult to access from the ground (e.g., the poles). A good summary of applications for time-variable gravity applications is given by *NRC [1997]* and *Wahr et al. [1998]* summarize some of the expected GRACE time-variable gravity results as compared to geophysical models.

1.4 STUDY OUTLINE AND OBJECTIVES

The first objective of this study is to use pre-GRACE methods to document some of the temporal and spatial scales possible for time-variable gravity results as observed from spacecraft. The annual variations in the geopotential field as observed using SLR observations to Lageos-1 and Lageos-2 are discussed in chapter 2, and these observations

are compared to the variability predicted by models of the atmosphere, oceans, and continental hydrology. Approximately six years of data were analyzed in order to produce a time series of Stokes coefficients that was complete for degrees 2-4. Prior to the launch of GRACE, this analysis was representative of the spatial scales of the annual variability of the gravity field that was possible to detect using spacecraft-only observations. A comparison of these pre-GRACE results to time-variable gravity observed by GRACE helps to put the improvements by GRACE in context with previous methods. It also illustrates that SLR observations will continue to be useful in constraining the longest wavelengths of the time-variable gravity field as well as provide continuity for the time series prior to GRACE launch.

The second objective is to study one of the challenges associated with any gravity mission—reducing the impact of short-period variability on gravity estimates. While other sources of variability, such as ocean tides, have a long history of being used to improve gravity recovery from space, the new accuracy requirements for GRACE gravity recovery require a level of precision in the models of known variability beyond that used in previous spacecraft geodesy missions. The non-tidal, short period variations due to the atmosphere, ocean, and continental hydrology will significantly impact the gravity estimates if completely ignored [*Thompson et al.*, 2000]. Chapter 3 summarizes the results of a systematic, orbital simulation study of the impact on the GRACE gravity estimates due to non-tidal, short-period mass variability. Geophysical models of hydrologic mass variability in the atmosphere, oceans, and continents were used to study the aliasing effects due to completely unmodeled mass variability as well as the improvement possible using approximate models of this variability.

Chapter 4 discusses the implementation of the atmosphere-ocean de-aliasing (AOD) model adopted for GRACE processing and the impact of this model when used

with real data. This model is provided to reduce the error introduced into GRACE gravity recovery by the non-tidal, short-period variations of the atmosphere and ocean. It consists of a six-hour time series of geopotential coefficients from the combination of an atmosphere model and an ocean model driven by the atmospheric model winds. Gravity solutions done with the AOD model used during processing were compared to gravity solutions produced without the model. A variety of tests were used to demonstrate the improvement obtained by using this model, and the results were compared to the simulation results.

Finally, the results from the time series of monthly gravity estimates of GRACE were studied and compared to continental hydrology (that is, the largest source of mass variability variations expected to be observed in the monthly GRACE gravity solutions). These results were used to show the improvement in time-variable gravity detection as detected by GRACE. The latest sequence of monthly gravity solutions obtained from GRACE is discussed in chapter 5. The annual cycle along with the monthly estimates relative to the mean are presented and discussed. These observations are compared to estimates of geoid variations computed from a continental hydrology model.

Chapter 6 is a summary of the key results of this dissertation, along with conclusions and recommendations for future work.

Chapter 2: Annual Geopotential Variability from SLR and Global Hydrology Models

A six-year span of satellite laser ranging (SLR) to the Lageos-1 and Lageos-2 spacecraft was analyzed to determine the annual variation of a set of spherical harmonic coefficients of the Earth's gravity field complete in degree 2-4. These observations were compared to the annual variability predicted by a suite of geophysical models describing changes in the distribution of mass in the atmosphere, ocean, and continental hydrology. The SLR observations were able to distinguish between two different hydrologic models as well as the ocean models to a lesser degree, but were unable to distinguish between the models selected for the atmosphere. The set of spherical harmonic, geopotential coefficients derived from the satellite observations and the preferred combination of the geophysical models agreed to about 1 mm RMS in geoid height, and had degree correlations that generally exceeded the 90% confidence limit. This level of agreement implied that SLR can continue to contribute to the time-variable gravity studies for the longest wavelengths even with the improved level of accuracy of GRACE gravity solutions, particularly for the degree 2 coefficients.

2.1 INTRODUCTION

Relative to the timescales over which spacecraft observations are available, the Earth can be treated as a closed system in which mass and angular momentum are conserved. Mass redistributes itself in the Earth system on a variety of temporal and spatial scales, reflecting complex interrelated processes in the oceans, atmosphere, groundwater, glacial/polar ice, among others. These mass variations are observable through the perturbations in the orbits of near-earth spacecraft, with SLR being one

method of measuring those perturbations. In the past 30 years, the precision of SLR has progressed from meters to millimeters; this has led to a steady improvement in geophysical models of mass variability.

The gravity field of the Earth varies due to many different phenomena, however, at seasonal periods the principal contributions are expected to be due to redistribution of water mass in the atmosphere [e.g., *Chao and Au*, 1991], the oceans [e.g., *Wahr et al.*, 1998], and on the continents [e.g., *Chao and O'Connor*, 1988; *Rodell and Famiglietti*, 1999]. Due to the limitations of Lageos SLR analysis, a degree and order four expansion (corresponding to a wavelength of roughly 10,000 km) is the best that can be recovered for annual time scales. SLR data and geophysical models have shown good agreement for seasonal variations of the low degree zonal gravitational coefficients, [*Chao and Eanes*, 1995; *Cheng and Tapley*, 1999; *Gegout and Cazenave*, 1993; *Nerem et al.*, 1993], the position of the Earth's geocenter (the location of the crust-fixed reference frame relative to the center-of-mass) [*Chen et al.*, 1999], and the degree 2, order 1 coefficients [*Cazenave et al.*, 1999].

Herein, analysis of SLR data from Lageos-1 and Lageos-2 is compared to the combined effects of a variety of contemporary, global geophysical models. Three basic types of models were considered: atmospheric, oceanic, and land hydrology. Different model permutations were formed and some success was achieved in being able to rank each combination when compared with SLR observations. In particular, it was found that the one of the two continental hydrology models examined was better at explaining the annually varying geoid that was computed from the combined Lageos-1 and Lageos-2 SLR data analysis, most noticeably for the sine component of the annual variability. The results of this study will help put into context both the improvements and limitations of

the recent time-variable gravity results due to GRACE [e.g., see *Tapley et al.*, 2004b; *Chambers, et al.*, 2004; *Wahr, et al.*, 2004].

2.2 REPRESENTING VARIATIONS IN GEOPOTENTIAL

The geopotential is commonly described by a set of gravitational spherical harmonic coefficients, C_{lm} and S_{lm} , where l and m are the degree and order, respectively [e.g., *Kaula*, 1966]. With the appropriately defined basis functions, these coefficients can be used to describe the effect that an arbitrary mass distribution has on the geopotential. A scalar geopotential field, U , as a function of position, (r, ϕ, λ) can be given by

$$U(r, \phi, \lambda) = \frac{GM}{r} \sum_{l=0}^{\infty} \sum_{m=0}^l \left(\frac{a}{r}\right)^l \bar{P}_{lm}(\sin \phi) [C_{lm} \cos m\lambda + S_{lm} \sin m\lambda] \quad (2.1)$$

where r is the radial distance from Earth's center, ϕ is the latitude, λ is the longitude, G is the gravitational constant, M is the mass of the Earth, a is the average radius of the Earth, and \bar{P}_{lm} are the normalized associated Legendre polynomials. The distribution of mass within the Earth enters equation (2.1) indirectly through the spherical harmonic coefficients which are integral multipoles of the density. Throughout this study, the normalization for the \bar{P}_{lm} is consistent with *Kaula* [1966], specifically

$$\int_0^{2\pi} \int_{-\pi/2}^{\pi/2} \left[\bar{P}_{lm}(\sin \phi) \begin{Bmatrix} \cos \\ \sin \end{Bmatrix} m\lambda \right]^2 \cos \phi \, d\phi \, d\lambda = 4\pi. \quad (2.2)$$

The normalized associated Legendre polynomials are related to the unnormalized associated Legendre polynomials, P_{lm} , by

$$\bar{P}_{lm} = \left[(2 - \delta_{0m})(2l + 1) \frac{(l - m)!}{(l + m)!} \right]^{1/2} P_{lm} \quad (2.3)$$

where δ is the Kronker delta function, and the associated Legendre polynomials can be defined by

$$P_{lm}(\mu) = \frac{(1 - \mu^2)^{m/2}}{2^l l!} \frac{d^{l+m}}{d\mu^{l+m}} (\mu^2 - 1)^l \quad (2.4)$$

One special group of coefficients that has a long history of use is the zonals, J_l , where $m=0$ and

$$J_l = -\sqrt{2l + 1} C_{l0}. \quad (2.5)$$

Detailed treatment of gravitational potential and how it relates to orbit perturbations [e.g., *Kaula*, 1966] and surface mass anomalies [e.g., *Chao*, 1994; *Wahr, et al.*, 1998] can be found in the literature.

Temporal variations of the geopotential can be taken into account by allowing for time-dependent $C_{lm}(t)$ and $S_{lm}(t)$, where t is time. Furthermore, a finite change in the coefficients for a specific time interval, $t_2 - t_1$, can be represented as $\Delta C_{lm} = C_{lm}(t_2) - C_{lm}(t_1)$ and $\Delta S_{lm} = S_{lm}(t_2) - S_{lm}(t_1)$. Variations and perturbations in geopotential are commonly represented in terms of a geoid anomaly as it allows for the same information (potential) to be described in equivalent but more intuitive units (height). The shape of the geoid anomaly, ΔN , relative to a reference surface can also be described by the set of spherical harmonic coefficients, ΔC_{lm} and ΔS_{lm} , for the variation in potential, ΔU , and the two

quantities are simply related by $\Delta N = \Delta U/g$, where g is the acceleration due to gravity at the Earth's surface ($g = GM/a$), a scalar.

$$\Delta N(\varphi, \lambda) = a \sum_{l=0}^{\infty} \sum_{m=0}^l \bar{P}_{lm}(\sin \varphi) [\Delta C_{lm} \cos m\lambda + \Delta S_{lm} \sin m\lambda] \quad (2.6)$$

Maps of the geoid anomaly as a function of latitude and longitude are a means of illustrating a set of geopotential, spherical harmonic coefficients, but in units of height instead of potential. Examples of this type of map are used extensively in this study to illustrate variability or errors in the geopotential as measured by spacecraft observations or as predicted by geophysical models of mass variability. The degree 0 and degree 1 terms are specifically excluded from this study and are not represented in any of the maps that follow.

2.3 ANNUAL VARIABILITY

Annual variations of a time series of geopotential coefficients, $C_{lm}(t)$ and $S_{lm}(t)$ can be described as

$$\left\{ \begin{array}{l} C_{lm} \\ \text{or} \\ S_{lm} \end{array} \right\} = A_{lm} \cos(\omega t) + B_{lm} \sin(\omega t) + E_{lm} \quad (2.7)$$

where ω is the annual frequency ($1/365.25 \text{ days}^{-1}$), t is time after January 1st at 0-hr UTC, A_{lm} and B_{lm} are the cosine and sine amplitude respectively, and E_{lm} is the mean. This representation is equivalent to describing the annual variation in terms of amplitude and phase, though care must be taken to explicitly define the phase. In the results that follow the amplitude, α_{lm} , and phase, φ_{lm} , were defined such that

$$\left\{ \begin{array}{l} C_{lm} \\ \text{or} \\ S_{lm} \end{array} \right\} = \alpha_{lm} \cos(\omega t - \varphi_{lm}) + E_{lm} \quad (2.8)$$

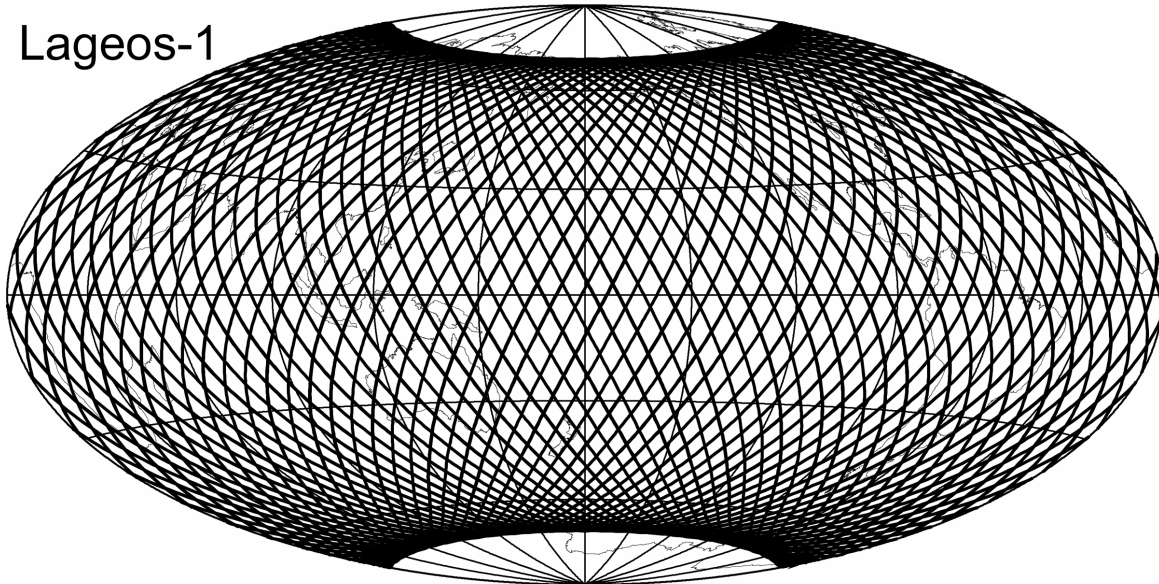
where

$$\begin{aligned} \alpha_{lm} &= \sqrt{A_{lm}^2 + B_{lm}^2} \\ \varphi_{lm} &= \tan^{-1} \left(\frac{B_{lm}}{A_{lm}} \right) \end{aligned} \quad (2.9)$$

2.4 SLR DATA ANALYSIS

Lageos-1, launched in 1976, is regarded as one of the most precisely tracked targets using SLR. It has an altitude of ~ 5900 km, well above the Earth's atmosphere, and thus non-gravitational forces are quite small. However, estimating gravity variations using a single satellite imposes significant limitations on spatial and temporal resolution. With the launch of Lageos-2 in 1992, two targets at roughly the same altitude but different inclinations (109.84° for Lageos-1, 52.63° for Lageos-2) became available for geophysical studies. This orbit geometry is at a high enough altitude to minimize the effects of drag, but low enough to allow for a good spatial resolution. Examples of the different orbital geometries of the two spacecraft are illustrated in terms of representative ground track coverage in Figure 2.1.

Lageos-1



Lageos-2

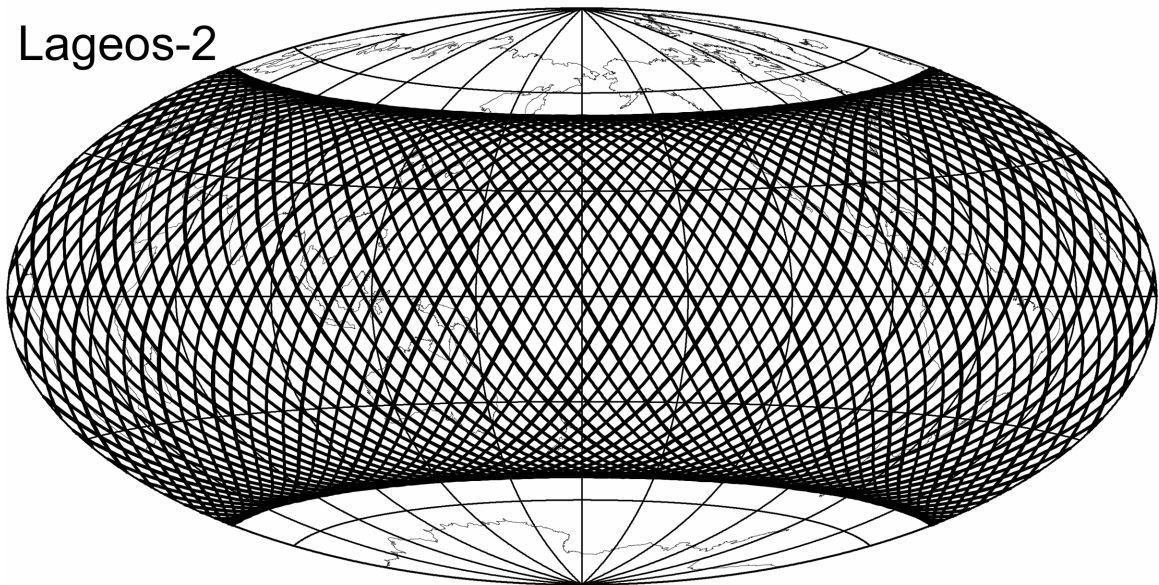


Figure 2.1. Representative 12-day groundtrack for Lageos-1 (top) and Lageos-2 (bottom)

Summarized here is the method used to produce the time-series of geopotential coefficients based on the SLR data; a more detailed description of the procedure for analyzing the SLR observation residuals from a long-arc analysis of the Lageos-1 and Lageos-2 is discussed in *Eanes* [1995] and *Eanes and Bettadpur* [1995]. Six years of SLR observations (November 1992 - November 1998) were processed to obtain a time series of coefficients complete through degree 2-4. Two distinctly different methods were used to compute the even zonals, $C_{2,0}$ and $C_{4,0}$, and to compute the remaining coefficients. The temporal variations in the even zonals were computed from a linear combination of the observed residual node rates of Lageos-1, $\delta\dot{\Omega}_1$, and Lageos-2, $\delta\dot{\Omega}_2$, as:

$$\begin{aligned} J_2 &= -0.00621\delta\dot{\Omega}_1 \sin I_1 - 0.02038\delta\dot{\Omega}_2 \sin I_2 \\ J_4 &= 0.08576\delta\dot{\Omega}_1 \sin I_1 + 0.05501\delta\dot{\Omega}_2 \sin I_2 \end{aligned} \quad (2.10)$$

where the coefficients are orbit element-dependent constants that can be determined from Kaula's theory [*Kaula*, 1966], J_2 and J_4 are related to $C_{2,0}$ and $C_{4,0}$ by equation (2.5), and I_1 and I_2 are the orbit inclinations of Lageos-1 and Lageos-2 respectively. Thus, the even zonal coefficients are determined solely from the long period perturbations to the orbit.

The variations in the other coefficients (i.e., other than $C_{2,0}$ and $C_{4,0}$) are determined directly from the SLR observations while adjusting 12-day estimates of the spherical harmonic coefficients, range biases for each tracking station, and the geocenter vector, along with daily estimates of the satellite state and polar motion. The partial derivatives of the range, ρ , with respect to the coefficients are computed from Kaula's theory:

$$\frac{\partial \rho}{\partial C_{lm}} = \frac{\partial \rho}{\partial a_\alpha} \frac{\partial a_\alpha}{\partial C_{lm}} \quad (2.11)$$

$$\frac{\partial a_\alpha}{\partial C_{lm}} = \sum_{pq} \left(\frac{\partial a_\alpha}{\partial C_{lm}} \right)_{pq}$$

where a_α are the orbital elements, C_{lm} represents all of C_{lm} and S_{lm} , and the summation is performed over all p and q that are significant, but not including secular and long period terms. Therefore, $C_{3,0}$ was determined solely from short-period perturbations (minimizing the influence of the ‘‘Lageos Anomaly’’ [Metris *et al.*, 1997]), and the even degree non-zonal coefficients were primarily determined from the m -daily perturbations in the inclination, ascending node, and along-track. The residual RMS for the six years of SLR observations was about 8 mm.

The background models employed were similar to the 1996 IERS Conventions [McCarthy, 1996]; for example, a secular change to J_2 and variations due to the 18.6 year tide [Eanes, 1995]. The most important deficiency was the omission of the effect of anelasticity on rotational deformation, which would introduce small signals into the $C_{2,1}$ and $S_{2,1}$ estimates at the annual and Chandler Wobble periods; however, these signals are much smaller than those arising from mass redistribution. The time-variable signal observed by the SLR data, therefore, represents the variability that has been omitted in the background models during processing. Specifically, this signal will be dominated by the unmodeled mass re-distribution due to the atmosphere, oceans, and water on the continents. This can be contrasted with the time-variable gravity observations made by GRACE (chapter 5) which were processed with a model of the non-tidal variability in the atmosphere and oceans. The time-variable signal as observed by GRACE should be due predominately to continental hydrology along with some residual, unmodeled signal due

to the atmosphere and oceans. This does not make a comparison between the two methods (GRACE vs. SLR) impossible; however, care must be taken to properly account for time-variable signals that were removed in once case but not the other (as a consequence of the gravity estimation process).

The outcome of the SLR data analysis was a 6-yr time series of Stokes coefficients complete through degrees 2-4. The $C_{2,0}$ and $C_{4,0}$ coefficients were computed at 3-day intervals while the other coefficients were computed at 12-day intervals. The time series for each coefficient was then fit to the model in equation (2.7) in a least-squares sense, thereby providing an estimate of the annual variability as represented by the values found for the A_{lm} and B_{lm} . The time series of geopotential coefficients found from the SLR observations and the corresponding annual fit are shown in Figures 2.2-2.22.

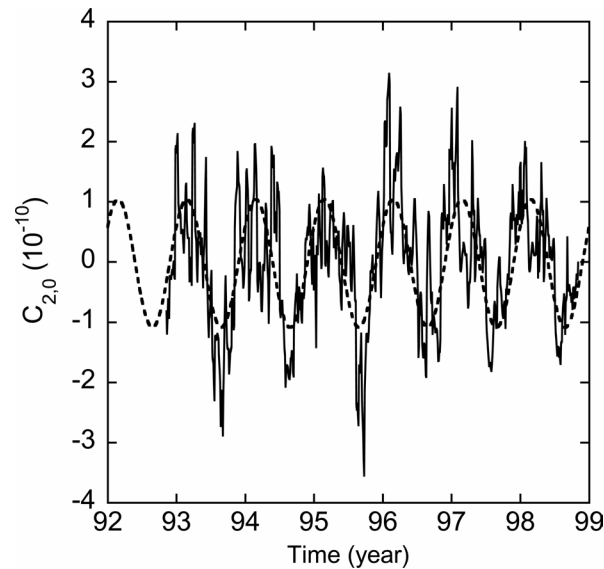


Figure 2.2. $C_{2,0}$: SLR time series (solid line) with annual fit (dashed line).

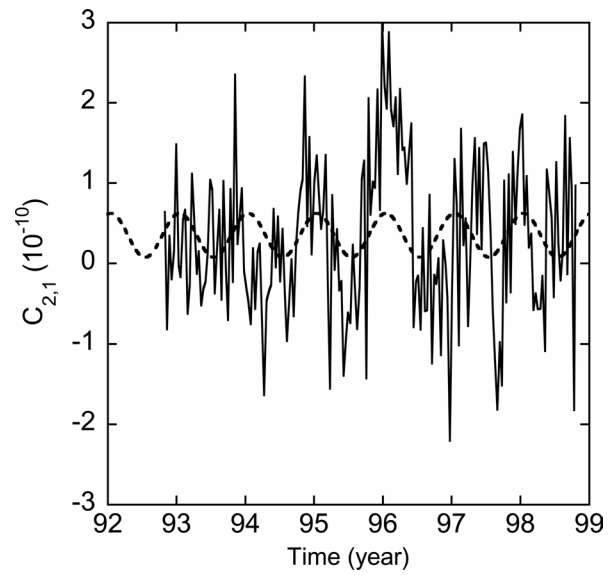


Figure 2.3. $C_{2,1}$: SLR time series (solid line) with annual fit (dashed line).

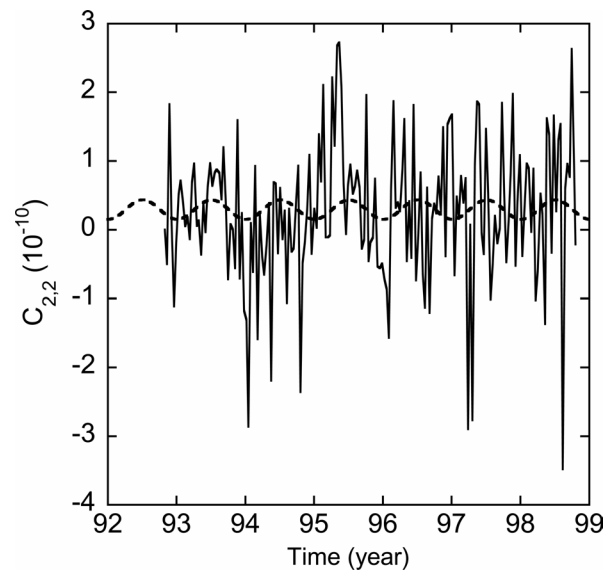


Figure 2.4. $C_{2,2}$: SLR time series (solid line) with annual fit (dashed line).

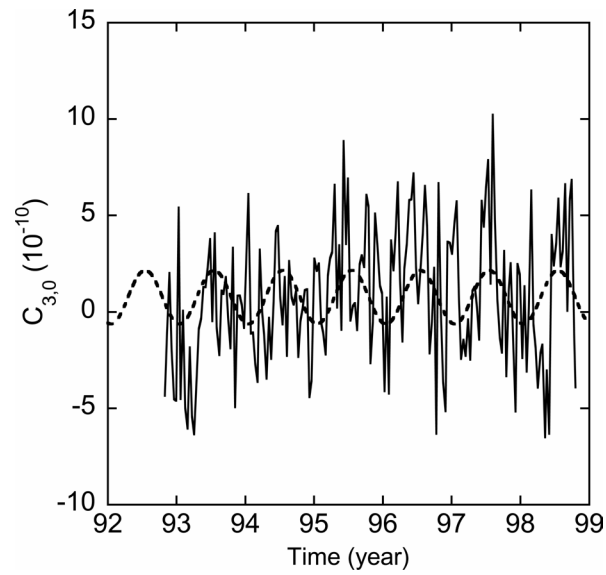


Figure 2.5. $C_{3,0}$: SLR time series (solid line) with annual fit (dashed line).

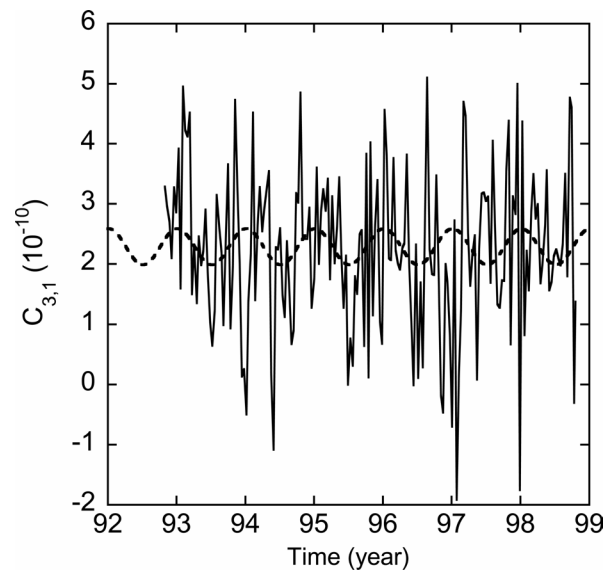


Figure 2.6. $C_{3,1}$: SLR time series (solid line) with annual fit (dashed line).

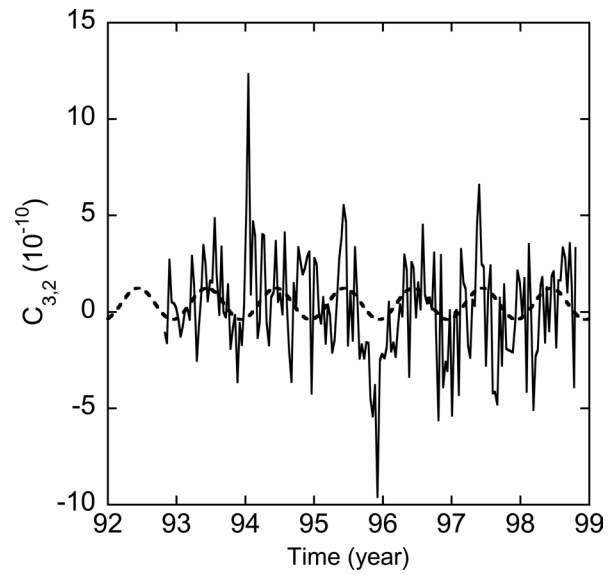


Figure 2.7. $C_{3,2}$: SLR time series (solid line) with annual fit (dashed line).

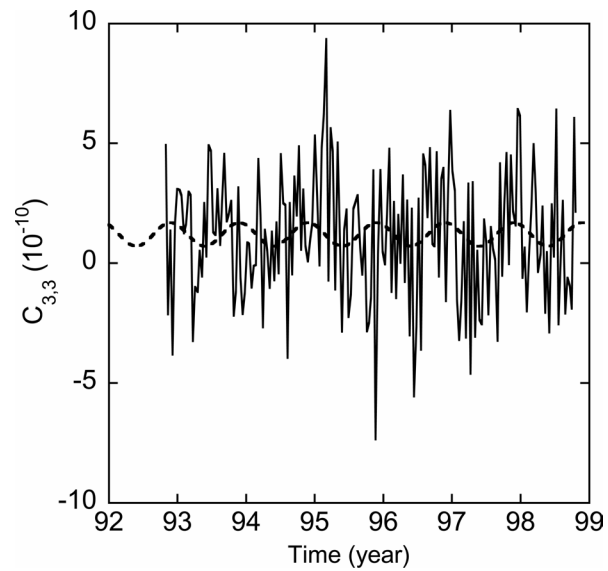


Figure 2.8. $C_{3,3}$: SLR time series (solid line) with annual fit (dashed line).

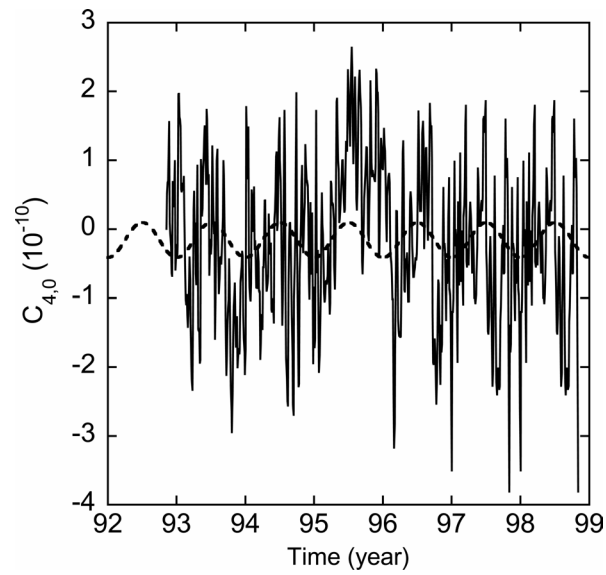


Figure 2.9. $C_{4,0}$: SLR time series (solid line) with annual fit (dashed line).

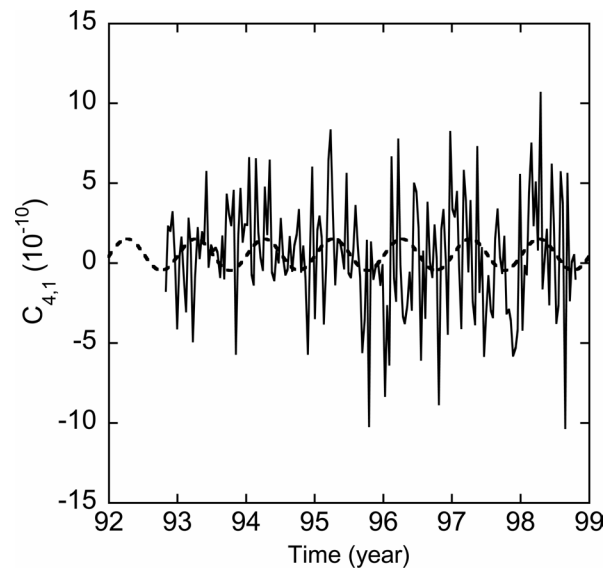


Figure 2.10. $C_{4,1}$: SLR time series (solid line) with annual fit (dashed line).

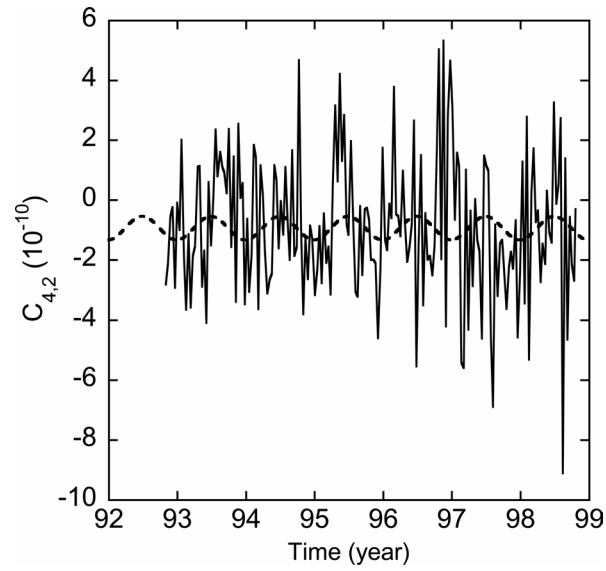


Figure 2.11. $C_{4,2}$: SLR time series (solid line) with annual fit (dashed line).

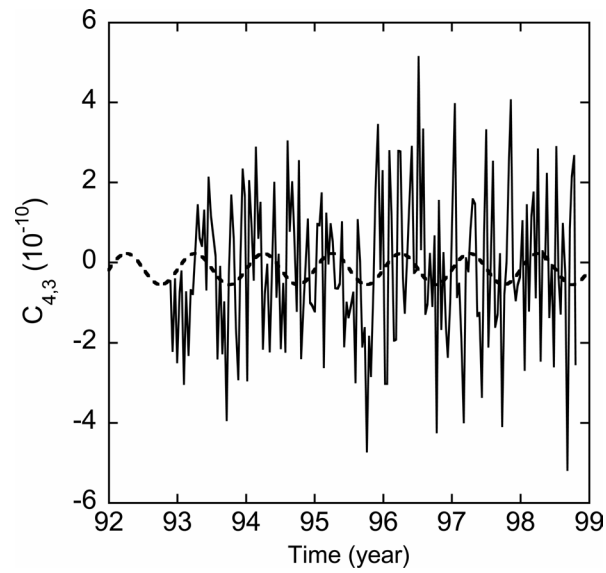


Figure 2.12. $C_{4,3}$: SLR time series (solid line) with annual fit (dashed line).

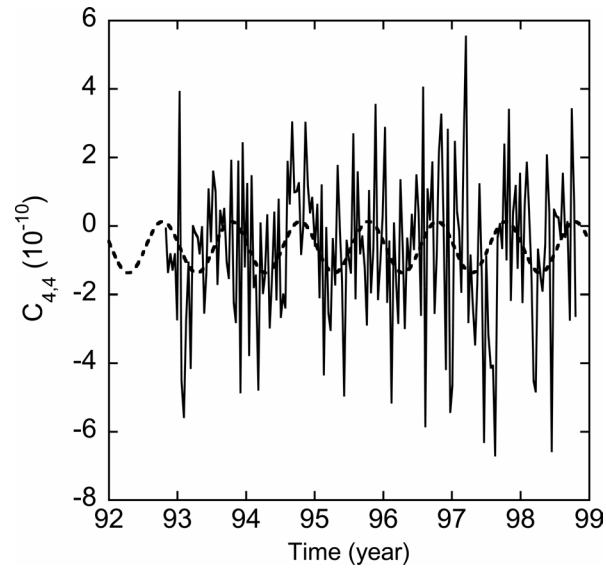


Figure 2.13. $C_{4,4}$: SLR time series (solid line) with annual fit (dashed line).

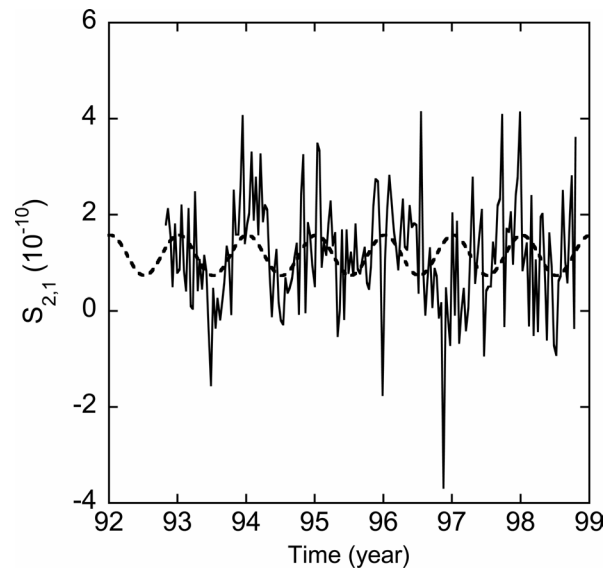


Figure 2.14. $S_{2,1}$: SLR time series (solid line) with annual fit (dashed line).

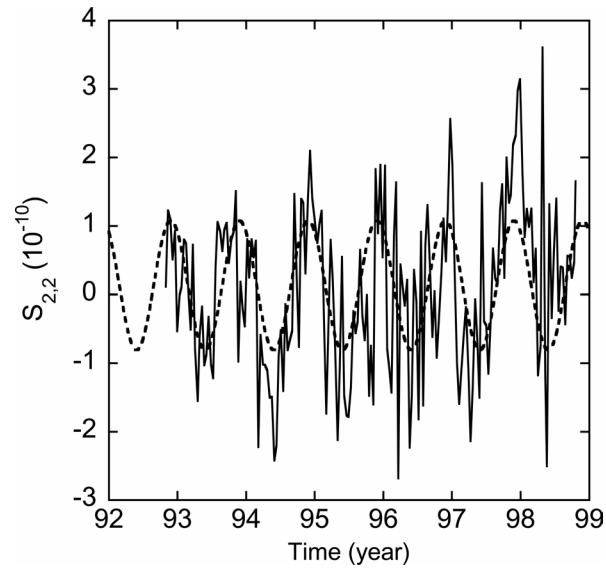


Figure 2.15. $S_{2,2}$: SLR time series (solid line) with annual fit (dashed line).

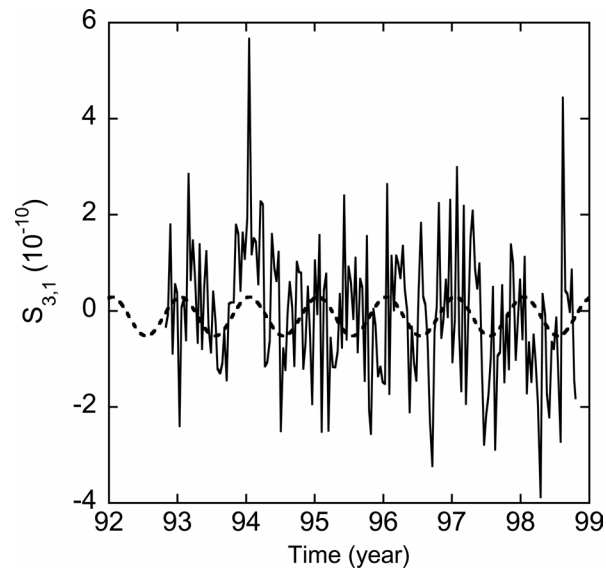


Figure 2.16. $S_{3,1}$: SLR time series (solid line) with annual fit (dashed line).

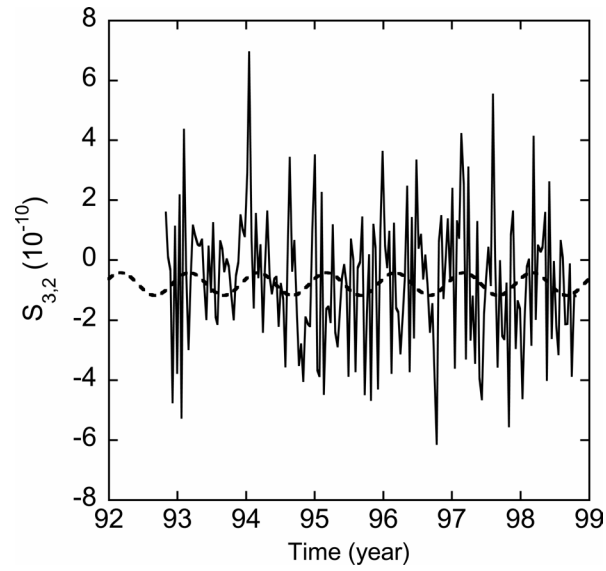


Figure 2.17. $S_{3,2}$: SLR time series (solid line) with annual fit (dashed line).

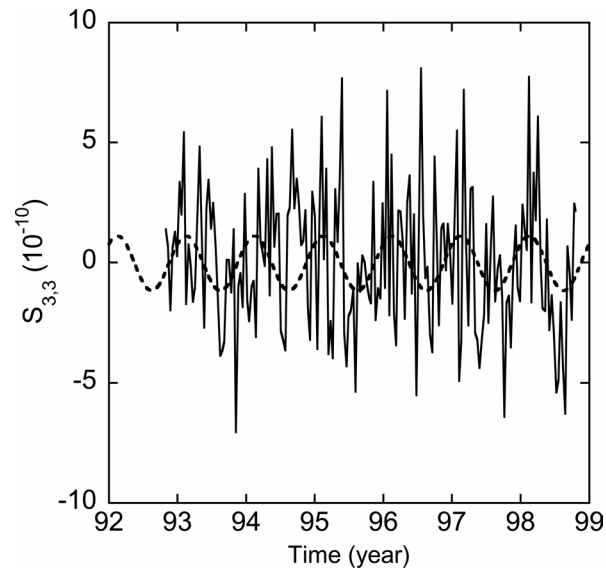


Figure 2.18. $S_{3,3}$: SLR time series (solid line) with annual fit (dashed line).

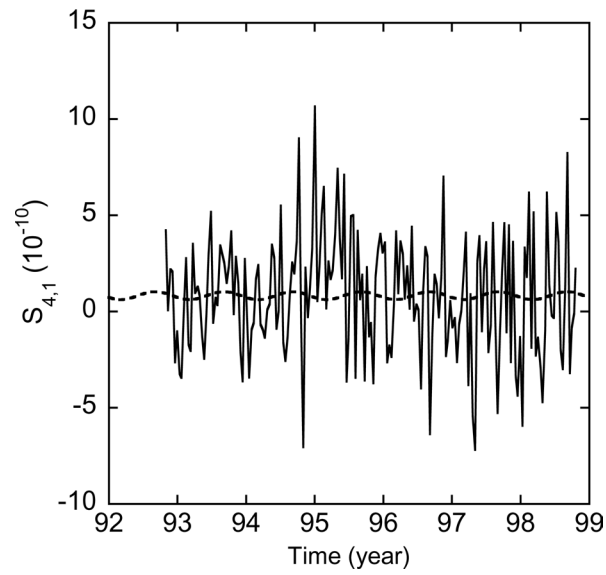


Figure 2.19. $S_{4,1}$: SLR time series (solid line) with annual fit (dashed line).

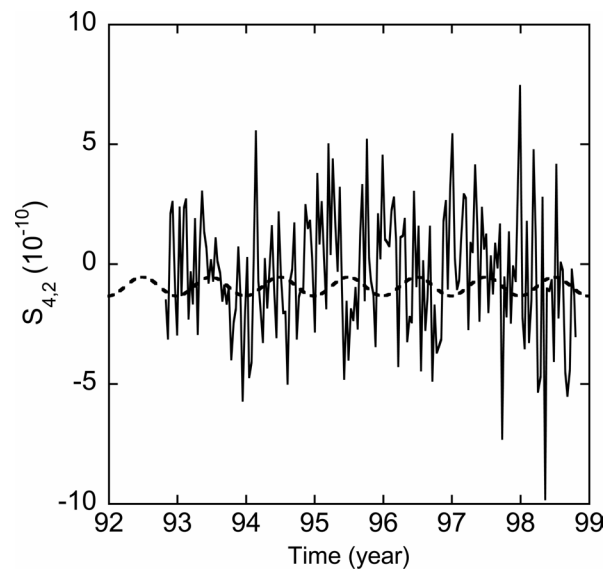


Figure 2.20. $S_{4,2}$: SLR time series (solid line) with annual fit (dashed line).

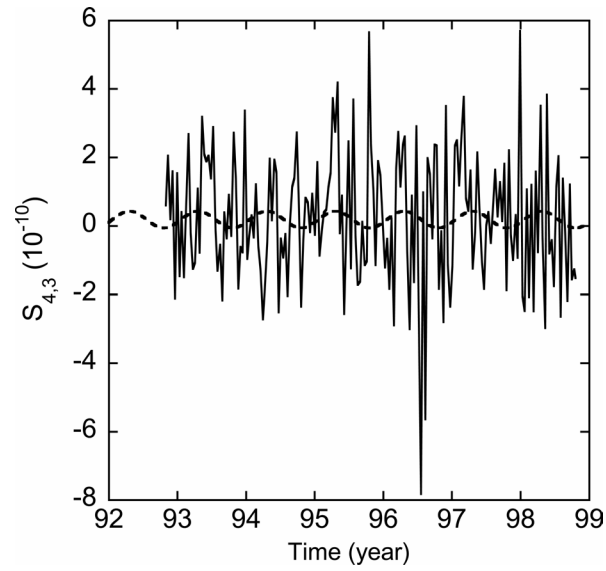


Figure 2.21. $S_{4,3}$: SLR time series (solid line) with annual fit (dashed line).

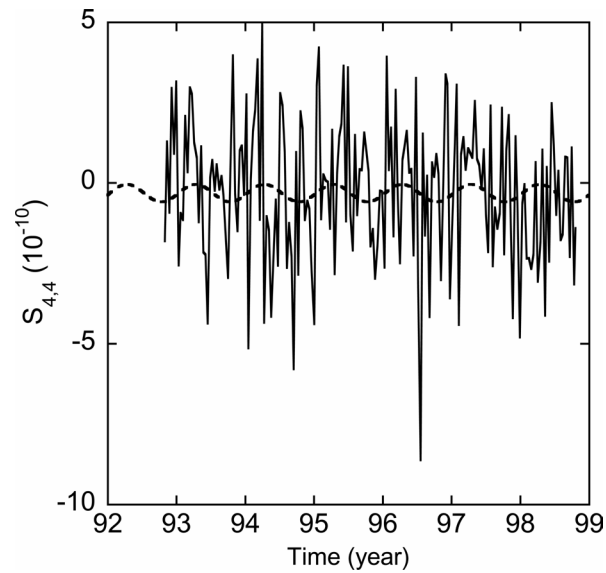


Figure 2.22. $S_{4,4}$: SLR time series (solid line) with annual fit (dashed line).

The SLR tracking data used in this study was not adequate for estimating and completely separating all the coefficients for a degree and order 4 gravity field, a limitation inherent in using long-period orbit perturbations from a small number of satellites. Some of the estimated spherical harmonic coefficients were highly correlated, and in some cases their specific values had little meaning (Table 2.1). However, maps of the annual cosine and sine variations of the gravity field can be meaningful because large areas of Earth's surface exist where the annual variations were adequately resolved. The values of the individual A_{lm} and B_{lm} (cosine and sine terms, respectively) were also converted into terms of amplitude and phase defined by equations (2.8) and (2.9) and shown in Table 2.2; this is primarily to allow for comparisons with other studies [e.g., *Cheng and Tapley, 1999; Cazenave et al., 1999*]. The amplitude and phase values should be interpreted with caution due to the previously mentioned issues with correlation, large errors in some specific coefficients, and the ambiguity that arises from different definitions for amplitude and phase as used by various authors.

l	m	$C_{lm} (10^{-10})$		$S_{lm} (10^{-10})$	
		Cosine	Sine	Cosine	Sine
2	0	0.61	0.87		
2	1	0.26	0.08	0.42	0.06
2	2	-0.14	-0.01	0.78	-0.53
3	0	-1.32	-0.40		
3	1	0.30	0.03	0.38	0.12
3	2	-0.76	0.27	0.17	0.34
3	3	0.40	-0.29	0.79	0.82
4	0	-0.26	-0.01		
4	1	-0.11	0.98	-0.09	-0.18
4	2	-0.39	0.03	0.44	0.71
4	3	-0.02	0.39	-0.08	0.23
4	4	0.17	-0.73	-0.05	0.27

Table 2.1. Annual cosine and sine amplitude in the geopotential determined from SLR to Lageos-1 and Lageos-2.

l	m	Amplitude $C_{lm} (10^{-10})$	Phase $C_{lm} (\text{deg})$	Amplitude $S_{lm} (10^{-10})$	Phase $S_{lm} (\text{deg})$
2	0	1.06	54.8		
2	1	0.27	16.5	0.42	7.6
2	2	0.14	184.1	0.94	326.0
3	0	1.38	196.9		
3	1	0.30	5.6	0.40	17.6
3	2	0.81	160.1	0.38	63.0
3	3	0.49	324.4	1.14	46.0
4	0	0.26	181.5		
4	1	0.99	96.4	0.21	244.2
4	2	0.39	176.3	0.84	58.1
4	3	0.39	92.8	0.24	109.3
4	4	0.75	283.3	0.27	101.4

Table 2.2. Amplitude and phase of the annual variation of the normalized spherical harmonic coefficients estimated in the geopotential as determined by SLR observations to Lageos-1 and Lageos-2. See equations 2.8 and 2.9 for the definition of amplitude and phase.

2.5 GEOPHYSICAL MODELS

A variety of different types of geophysical models were considered for comparisons with the SRL observations. The objective of this study was to test a representative sub-set of models but not every possible model type. Spacecraft will be affected by the total mass variability exhibited on Earth. However, as previously discussed, the SLR observations to Lageos-1 and Lageos-2 were processed along with various background models in order to remove some of that variability (e.g., ocean tides). Three basic types of models were considered: atmospheric, oceanic, and continental

hydrology; spherical harmonic coefficients of the geopotential were computed from gridded mass variations derived from each model. The three model types considered here should represent most of the variability that was omitted from the processing of the SLR observations. Various permutations of the geophysical models were used to construct reasonable approximations of the geopotential variations as observed by Lageos-1 and Lageos-2.

2.5.1 Atmosphere

The change in the total atmospheric mass integrated vertically above a point is proportional to the change in atmospheric pressure, since the atmosphere is close to being hydrostatic. Thus atmospheric pressure can be used to compute the temporal variations of the gravity field caused by the atmosphere. Atmospheric pressure grids from the European Center for Medium-range Weather Forecasts (ECMWF) [ECMWF, 1995] and the National Center for Environmental Prediction (NCEP) Reanalysis Project [Kalnay *et al.*, 1996] were used to compute the annual cycle of the geopotential. These two models assimilate a variety of meteorological measurements in order to adjust the dynamical equations describing the evolution of the atmosphere in time. Both models contained pressure data at 6-hr intervals. The NCEP model was processed using data from 1975-1996 (21 years), while the ECMWF model was available for the time span of 1990-1996 (6 years). Furthermore, prior to computing the global geopotential field in these calculations, the change in atmospheric mass was set to zero at every oceanic grid point. The reason for this step is that the ocean response to pressure variations is expected to be very nearly an inverted barometer (IB) response at periods in excess of a few days [Ponte *et al.*, 1991]; the response of the underlying ocean surfaces is such that there is no net change in pressure at the sea floor.

The geoid anomaly calculated for the annual terms (A_{lm} and B_{lm} terms in equation (2.7)) of both atmospheric models is illustrated in Figure 2.23. Note that most of the power in the annual signal is contained in the cosine component (winter-summer), and very little in the sine component (spring-fall). The major mode observed in the sine component was attributed to $C_{2,0}$.

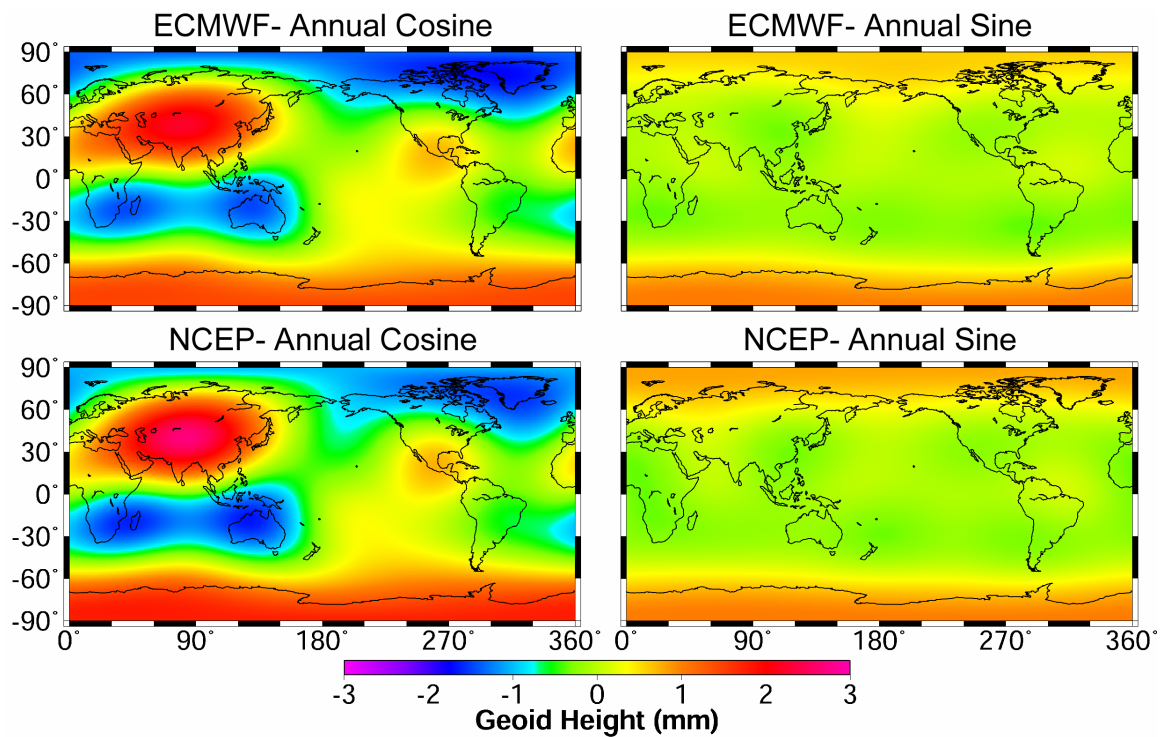


Figure 2.23. Maps of the cosine and sine components of the annual variation in the geoid due to atmosphere mass redistribution (complete from degree 2-4).

2.5.2 Ocean

The seasonal gravitational variations caused by ocean mass redistribution were studied using two distinctly different approaches: a numerical model approach and one derived from spacecraft observations. The numerical model used was a variant of the

Parallel Ocean Program developed at Los Alamos National Laboratory [*Dukowicz and Smith, 1994*] and as modified by *Wahr et al. [1998]* (hereafter referred to as POP in this study). The model was output for the time period of 1991-1995 (five years) at a 3-day time step. It included a free surface, with realistic bathymetry, and was driven by 6-hourly surface winds provided by the ECMWF. Forcing from atmospheric pressure variations was not included. The ocean model was integrated on a global grid with 192 (longitude) x 128 (latitude) x 32 (depth) points. Additionally, the mode model used the Boussinesq approximation, which conserves volume and not mass. The change in ocean mass at each point on the grid was found by integrating through the water column. This global surface mass distribution was converted into a time series of equivalent geopotential.

In the second model (referred to as TOPEX in this study), oceanic mass load variations were estimated from sea level anomalies using the TOPEX/Poseidon Geophysical Data Record, which covers regions between $\pm 66^\circ$ latitude. The conversion to geopotential coefficients is described in detail by *Chen et al. [1999]*. Over four years of data were used (cycles 10-168) with the 1997/1998 El Niño time periods explicitly removed. All media, instrument, and geophysical corrections were applied, including ionosphere delay, wet and dry troposphere delay, electromagnetic bias, tides, and the IB response. However, several changes were made to update models and correct errors. The steric component involves no mass changes, so it is estimated and subtracted using the WOA94+OISST steric model. The non-steric sea level anomalies were converted into oceanic mass load change and used to compute corresponding contributions to the geopotential field.

These two ocean data sources, POP and TOPEX, are dramatically different in their approaches and result in significant inter-model differences in the annual geoid

variations (Figure 2.24). The magnitude of the geoid variation due to the oceans is four to five times smaller in magnitude than that due to the atmospheric and continental hydrology sources. Due to this reduced signal relative to the other model types (i.e., atmosphere and continental hydrology), it was difficult to determine which model best represented the variability as observed by the SLR observations.

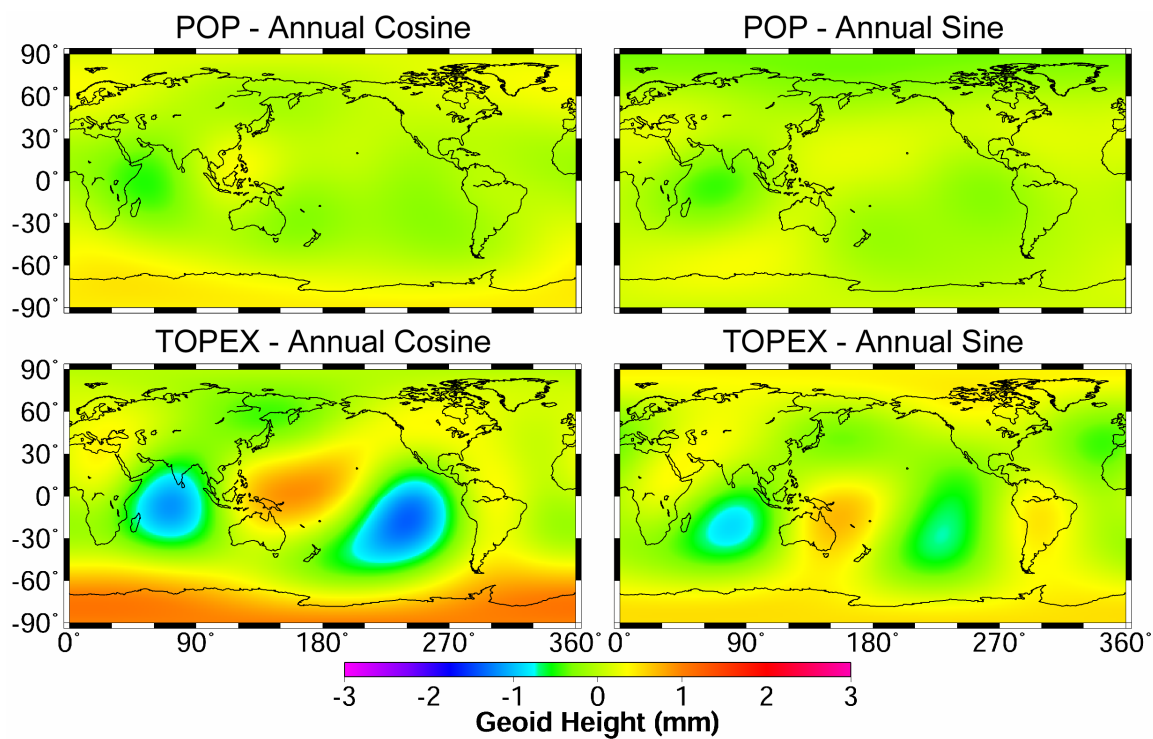


Figure 2.24. Maps of the cosine and sine components of the annual variation in the geoid due to ocean mass redistribution (complete from degree 2-4).

2.5.3 Continental Hydrology

Two different models were considered for the contribution of continental water mass variation—one computed from Climate Prediction Center (CPC) data and another from the NCEP 40-year reanalysis model, referred to as the NCEP-NCAP Data

Assimilation System (CDAS-1) and herein called the CDAS-1 model. *Wahr et al.* [1998] describe the details of estimating the annual cycle in the geopotential due to CPC model. Using the method described by *Huang, et al.* [1996], the CPC data was used to generate a globally gridded monthly time series of surface mass due to effects of (soil moisture) + (snow mass). The annual variability in the geopotential was calculated using the time period of 1989-1993 (5 years). The analysis of the CDAS-1 model is described by *Chen et al.* [1998; 1999]. It consists of monthly gridded soil moisture and snow depth fields. The soil moisture data included two layers; the first layer covers the top 10cm of the soil, and the second layer covers from 10 cm to 200 cm depth. The annual cycle was determined from data during the time period of 1958-1997 (40 years).

No attempt was made to estimate surface mass variability on the Antarctica continent in either model. In fact, variations on the sea ice attached to the continental shelf are excluded in this study as no geophysical model adequately models this system. Furthermore, there is no data available for water in the deeper layers (~1-2 meters or deeper) for any location on the globe. In addition, the CDAS-1 model does not assimilate precipitation and surface fluxes important for predicting soil moisture and snow depth. While these may be significant omissions that impact the overall accuracy, the magnitude of the geoid anomaly produced by what is contained in these models is still significant and on the same order of mass variations due to the atmosphere. The most notable difference in the annual cycle predicted by these models was the difference in phase as highlighted by the very different character observed in the two maps of the cosine component of the annual variability (Figure 2.25). The magnitude of the annual variability due to the two hydrology models is comparable, but the timing of peak magnitudes differs significantly.

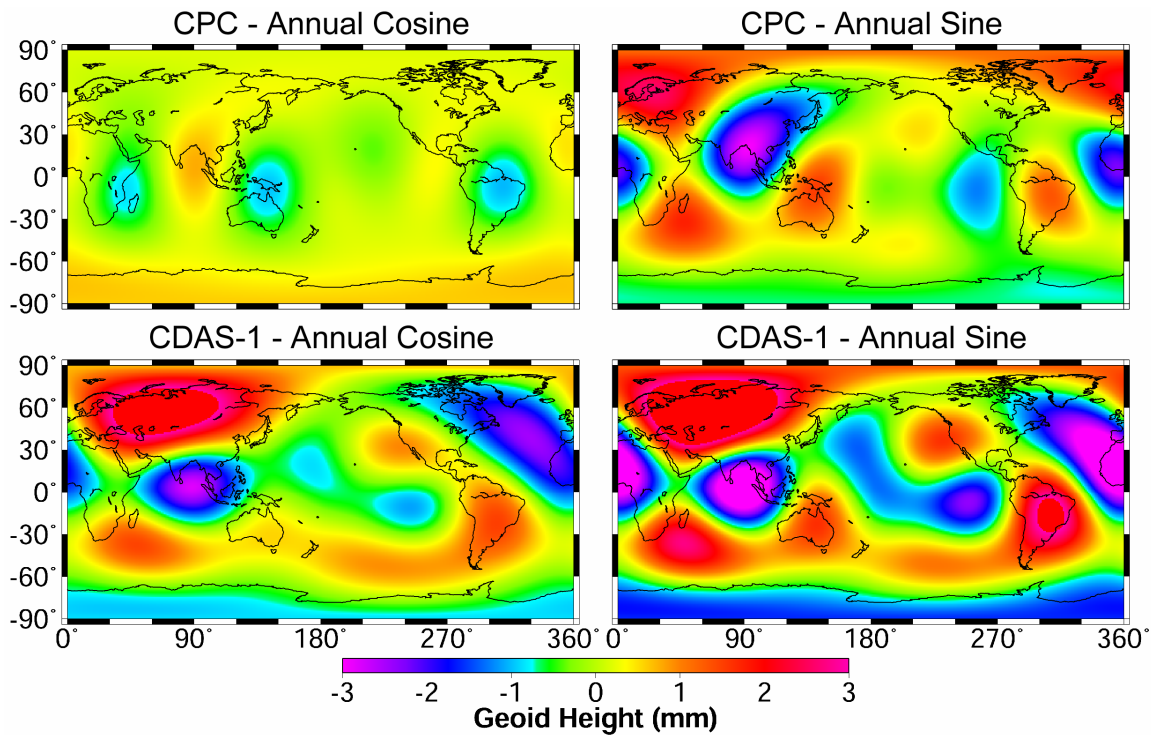


Figure 2.25. Maps of the cosine and sine components of the annual variation in the geoid due to continental water mass redistribution (complete from degree 2-4).

2.6 COMPARISON OF RESULTS

The SLR measurements of the time-varying gravity field observe the combined effects of all sources of mass variation in Earth’s systems. Thus, results from the geophysical models that are the major contributors to the seasonal variation of the gravity field were combined in a variety of permutations of three model types (atmosphere, ocean, and continental hydrology). These models represent variability that was not explicitly removed as a consequence of data processing, in other words, “science by omission”. It is difficult to say that any particular combination model exactly matches the SLR results on a coefficient by coefficient basis. However, the geoid height anomaly

calculated from the complete set of coefficients and degree correlations can produce comparisons that indicate a clear correlation between the SLR observations and the geophysical models (Table 2.3). Based on correlation between maps of geoid on a 1° lat/lon grid, the “best” model combination appeared to be Case 4 or Case 8, which differed only in the atmospheric model used. For reasons discussed later, Case 4 is the preferred model combination and the comparison with the Lageos SLR analysis is shown in Figure 2.26.

Case	Atmo. Model	Ocean Model	Hydro. Model	Cosine		Sine	
				Correl.	rms (mm)	Correl.	rms (mm)
1	NCEP	POP	CDAS-1	0.62	1.42	0.49	1.60
2	NCEP	POP	CPC	0.81	0.92	0.63	1.06
3	NCEP	TOPEX	CDAS-1	0.67	1.37	0.50	1.69
4	NCEP	TOPEX	CPC	0.83	0.89	0.63	1.09
5	ECMWF	POP	CDAS-1	0.62	1.36	0.49	1.54
6	ECMWF	POP	CPC	0.82	0.91	0.63	1.05
7	ECMWF	TOPEX	CDAS-1	0.67	1.31	0.50	1.63
8	ECMWF	TOPEX	CPC	0.83	0.87	0.64	1.07
9	NCEP	None	None	0.85	0.90	0.50	1.19
10	NCEP	None	CPC	0.81	0.92	0.59	1.12
11	NCEP	None	CDAS-1	0.59	1.45	0.46	1.66
12	ECMWF	None	None	0.84	0.94	0.45	1.22
13	ECMWF	None	CPC	0.81	0.92	0.59	1.10
14	ECMWF	None	CDAS-1	0.58	1.42	0.46	1.60

Table 2.3. Lageos-1 and Lageos-2 SLR observations of time-variable gravity compared to geoid variations predicted by various combinations of geophysical models. Complete from degree 2-4 and based on a 1° lat/lon grid.

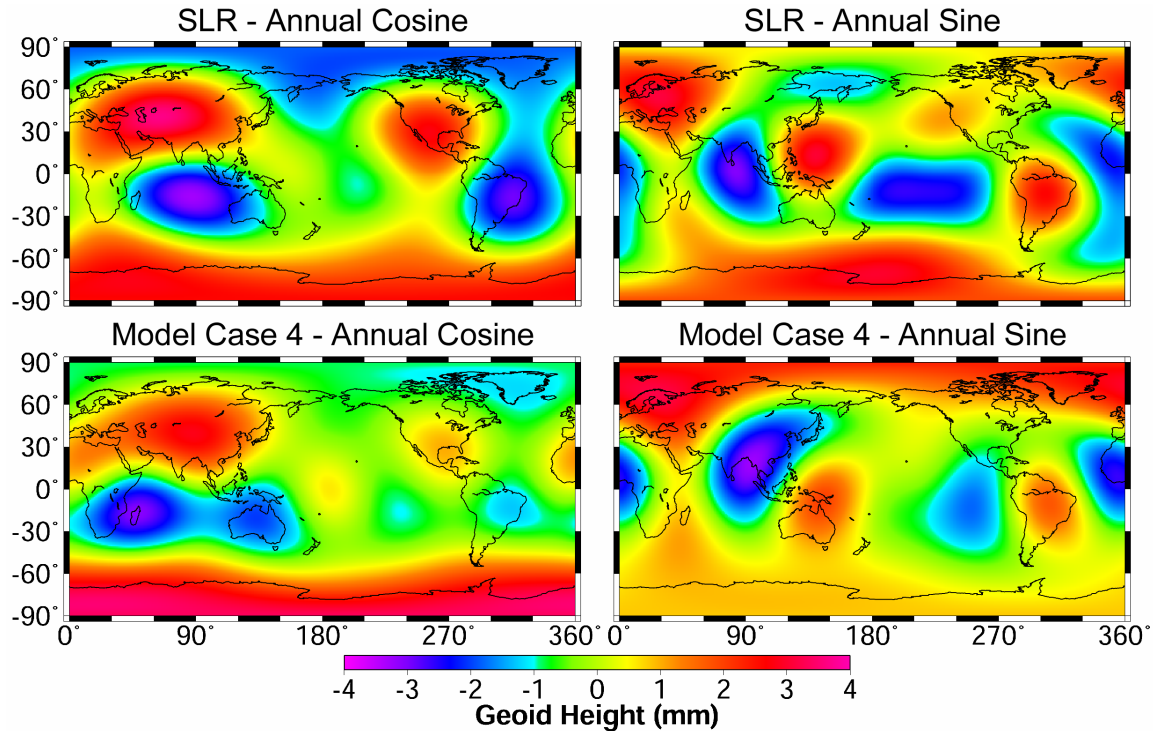


Figure 2.26. Maps of the cosine and sine components of the annual variation in the geoid as determined from the Lageos-1 and Lageos-2 SLR observations and from the sum of the combined geophysical models for Case 4.

Correlations between maps can be an imprecise method of quantifying the correlation between two sets of spherical harmonic coefficients, and meaningful confidence limits are best made by segregating the correlation by degrees [Eckhardt, 1984]. The scale of a spatial feature in the geoid is related to the spherical harmonic degree (half-wavelength $\approx 20,000/l$); therefore, a measure of the power at given wavelengths can be described by the degree variance

$$\sigma_l^2 = \sum_{m=0}^l (C_{lm}^2 + S_{lm}^2), l \geq 1 \quad (2.12)$$

while a comparison between two sets of global harmonics, set A and set B, can be made with the degree correlation,

$$r_l = \frac{1}{\sigma_l^{(A)} \sigma_l^{(B)}} \sum_{m=0}^l (C_{lm}^{(A)} C_{lm}^{(B)} + S_{lm}^{(A)} S_{lm}^{(B)}), l \geq 1 \quad (2.13)$$

Of course, these statistics can also be computed based not only on the full amplitude coefficients, but also coefficients differences, that is, ΔC_{lm} and ΔS_{lm} . Correlations were computed for the components of the annual geoid variability computed from the SLR data and for each geophysical model combination that was considered (Table 2.4). Using this metric, every geophysical model improved the comparison for some wavelengths while degrading the comparison for other wavelengths.

Case	Atmo. Model	Ocean Model	Hydro. Model	Cosine			Sine		
				$l=2$	3	4	$l=2$	3	4
1	NCEP	POP	CDAS	0.78	0.60	0.63	0.86	0.32	0.69
2	NCEP	POP	CPC	0.83	0.75	0.48	0.68	0.48	0.81
3	NCEP	TOPEX	CDAS	0.68	0.66	0.65	0.88	0.36	0.70
4	NCEP	TOPEX	CPC	0.69	0.82	0.58	0.80	0.53	0.79
5	ECMWF	POP	CDAS	0.77	0.60	0.59	0.87	0.35	0.69
6	ECMWF	POP	CPC	0.83	0.73	0.41	0.61	0.53	0.80
7	ECMWF	TOPEX	CDAS	0.66	0.66	0.62	0.89	0.38	0.69
8	ECMWF	TOPEX	CPC	0.67	0.81	0.54	0.75	0.58	0.78
9	NCEP	None	None	0.80	0.79	0.69	0.86	0.37	0.07
10	NCEP	None	CPC	0.86	0.74	0.46	0.69	0.41	0.80
11	NCEP	None	CDAS	0.80	0.56	0.62	0.81	0.28	0.70
12	ECMWF	None	None	0.75	0.79	0.63	0.83	0.49	-0.11
13	ECMWF	None	CPC	0.86	0.73	0.39	0.62	0.46	0.79
14	ECMWF	None	CDAS	0.79	0.56	0.59	0.82	0.31	0.70

Table 2.4. Degree correlations between the model combinations and SLR data results for both the cosine and sine components of the annual cycle.

Again, there was no clear indication of the “best” model combination for all degrees (spatial wavelengths) based on degree correlations. In a relative sense, specific models did produce consistently better correlations with the SLR data when compared to the correlations found from a different model of the same type. The NCEP atmosphere performed better than the ECMWF atmosphere, the TOPEX ocean model performed

better than the POP model, and the CPC continental hydrology performed better than the CDAS-1 model. Significant improvement in the degree correlations for the sine component was found when the CPC continental hydrology was combined with an atmosphere model (relative to the degree correlation for the atmosphere-only models in Case 9 and Case 12). However, there was one notable exception to the improvement, and that was a degradation observed in the degree 2 correlations for many of the model combinations. This was not an unexpected result as the TOPEX ocean model and both of the continental hydrology models are not strictly global. By explicitly omitting the polar latitudes, these models can underestimate the contribution of mass variability to the spherical harmonic coefficients that are more affected by large-scale changes at the poles, e.g., $C_{2,0}$.

2.7 DISCUSSION

Good agreement was found between the annual gravity cycle derived from the SLR data and from that predicted by various combinations of models of the atmosphere, ocean, and continental hydrology. Studies have shown previously that SLR measurements from Lageos-1 and the predictions of global atmospheric circulation models for the evolution of the low order, zonal harmonics agree quite well [*Chao and Au, 1991; Nerem, et al., 1993*]. However, it was clear from this study that in order to explain sine term of the annual geoid variations observed by the Lageos SLR, a source of mass variability other than atmospheric was required. Much of the power in the sine term was explained by the continental hydrology models, even given the significant known deficiencies in those models.

Based on geoid map comparisons, the NCEP and ECMWF pressure fields compared equally well to the SLR results. Even though the NCEP model showed slightly better performance in terms of degree correlation and was selected for the “preferred”

model combination, the difference was not statistically significant. For the ocean models, the altimetry-based model (TOPEX) performed slightly, but consistently, better than the numerical model output (POP). The most significant difference was observed in the comparison between the continental hydrology models, with the CPC model clearly out-performing the CDAS-1 model. This may be due to the particular nature of the deficiencies of the CDAS-1 model; it has been found that on a regional basis the maximum and minimum magnitudes did not occur at the appropriate times (i.e., the phase was wrong), and the frequency of the variations was not consistent with known forcings [Rodell and Famiglietti, 1999]. While an extensive regional validation was not done with the CPC model, a comparison with an independent soil moisture data set for Illinois found good agreement between the data and CPC model predictions [Huang *et al.*, 1996].

A considerable omission in all the models considered was the lack of a reasonable model of the mass variability in the Antarctic. There are few observations within the continent, and there are additional complications with the observations along the continental boundary. This omitted variation is not negligible since the Antarctic ice sheet mass change may represent a 2 mm/yr sea level change when considering realistic rheological parameters [James and Ivins, 1997]. Furthermore, unlike the northern ice cap, the seasonal sea ice around Antarctica cannot simply be included in the oceanic term. This ice shelf is not completely detached from the continental land mass, and it is under a varying amount of stress as the sea level changes. A non-linear coupling exists between the Antarctic ice shelf and sea level changes, making it necessary to devise a coupled model for this interaction between the ocean and continental hydrology. Since these omissions are characteristic of many continental hydrology models, one of the best methods to observe these unmodeled mass variations may be satellite-observed gravity variations (e.g., GRACE). It may be possible to significantly constrain these types of

hydrology models given the temporal (approximately monthly) and spatial (a few hundred kilometers) scales of the geopotential that will be observed by GRACE.

Chapter 3: Aliasing Impact of Short Period, Non-Tidal, Temporal Mass Variability in Simulated GRACE Gravity Recovery

Using orbital simulations of the Gravity Recovery and Climate Experiment (GRACE) spacecraft, the effects on gravity recovery due to short period, non-tidal temporal mass variability in the atmosphere, ocean, and continental hydrology were examined. The magnitude of the aliasing error was strongly correlated with the power of the high-frequency variability of the models. Degree error relative to measurement error increased by a factor of ~ 20 due to atmospheric aliasing (corresponding to geoid anomalies of approximately 1 mm at 500 km wavelengths), by a factor of ~ 10 due to the ocean model, and by a factor of ~ 3 due to the continental hydrology model. De-aliasing done with approximate models of the mass variability gave the greatest reduction in aliasing error for the mid-degrees and higher. For the atmosphere, the remaining, residual aliasing error was $\sim 1/5$ that of the aliasing error due to a completely unmodeled atmosphere. A barotropic ocean model reduced the aliasing error due to a baroclinic model to nearly the level of measurement noise. Aliasing error due to the continental hydrology model studied was found to be relatively small in comparison to the atmospheric and oceanic model results. The error at the lowest degrees ($\sim 2-5$) was dominated by the sensitivity of the GRACE processing system to systematic error and did not correlate with the level of error introduced by any of the time-variable mass models.

3.1 INTRODUCTION

GRACE is designed to recover the Earth's gravity field at approximately monthly intervals with a spatial resolution of a few hundred kilometers. The nominal product is a piecewise constant series of gravity solutions tied to monthly epochs. As a consequence

of unmodeled variability in the geopotential taking place during the solution time span, the GRACE mission samples the variability in such a way that the gravity fields it recovers will differ from the average geopotential during that time span. This short period variability can alias into the longer period gravity estimates at a variety of spatial scales, affecting the accuracy of the gravity results. The GRACE data processing strategy, therefore, includes using detailed knowledge of the time-varying potential as a function of time in order to reduce measurement residuals. Preliminary estimates of the GRACE error budget did not specifically address temporal aliasing due to mass redistribution [e.g., *Kim* 2000; *Kim and Tapley*, 2002], though some level of aliasing was accounted for in the estimating the error budget for GRACE science return [*Wunsch and Zlotnicki*, 1999]. Furthermore, the time-variable gravity predictions made in preparation for GRACE data are based on the assumption of non-aliased error estimates, though they did recognize that the error estimates were limited by this assumption [e.g., *Wahr et al.*, 1998; *Rodell and Famiglietti*, 1999; *Nerem et al.*, 2003].

Orbital simulations by *Thompson et al.* [2000] show that the impact of short-period variability in hydrologic systems produces aliasing error comparable to the level of error produced by measurement noise alone, though partial modeling of the variability reduced this error significantly. While relatively slow variations were captured by the simulated estimation process, the gravity estimates were corrupted by aliasing of short-period mass variability into other spatial and temporal scales. Herein is discussed the aliasing error that resulted from mass variability models of the atmosphere, ocean, and continental hydrology used in the presence of measurement noise comparable to what had been assumed in previous studies. This aliasing error was characterized relative to the error floor due to measurement noise-only, the benefits of using alternative models of the short period mass variability were quantified (also known as de-aliasing), and processing

guidelines for GRACE were established (e.g., approximate models will improve the gravity solutions).

3.2 GEOPHYSICAL MODELS

A collection of geophysical models was selected that are representative of variability in three different hydrologic systems of the Earth. It was not the purpose of this study to test every available model; rather it is to highlight the impact of different spectra of mass variability on the GRACE gravity solutions along with the benefits of using approximate models to reduce this error. The convention for representing and fully normalizing the geopotential coefficients in the discussion that follows is the same as in chapter 2. Detailed examples of geoid height calculations and representations can also be found elsewhere in the literature [e.g., *Kaula*, 1966; *NRC*, 1997; *Wahr et al.*, 1998].

3.2.1 Atmosphere

Atmospheric pressure grids available at 6-hr intervals were used from the European Center for Medium-range Weather Forecasts (ECMWF) [*ECMWF*, 1995] and the National Center for Environmental Prediction (NCEP) Reanalysis Project [*Kalnay et al.*, 1996] for the month of January, 1990. These models assimilated a variety of meteorological measurements in order to adjust the dynamical equations that describe the evolution of the atmosphere in time. The change in the total atmospheric mass integrated vertically above a point is proportional to the change in atmospheric pressure, since the atmosphere is close to being hydrostatic [*Chao and Au*, 1991]. Prior to computing the global geopotential field due to the atmosphere, the change in atmospheric mass was set to zero at every oceanic grid point. The reason for this step is that the ocean response to pressure variations is expected to be closely approximate an inverted barometer (IB) response at periods in excess of a few days [*Ponte et al.*, 1991]. In the simulation

procedure described later, the ECMWF atmosphere was used as the ‘true’ model and NCEP as the ‘nominal’ model. The yearly mean for 1990 was removed from both models. Notable differences exist between these models at relatively short time scales [e.g., *Velicogna et al.*, 2001] and in regions where there is a sparsity of meteorological data, for example, Antarctica.

3.2.2 Ocean

A variant of the Parallel Ocean Program (POP) developed at Los Alamos National Laboratory [*Dukowicz and Smith*, 1994] was used to compute two different time series of ocean mass variability. The origin of this model begins with a standard Bryan-Cox-Semtner global ocean model [*Bryan*, 1969; *Semtner*, 1986]. The initial stream function formulation of this model was changed by *Dukowicz and Smith* [1994] to one based on a surface formulation of the barotropic mode. The final form of the POP model used in this study is discussed by *Wahr et al.* [1998].

The POP model was integrated on a global grid, had a free surface, and supported realistic bathymetry. The model was driven by six-hourly surface winds provided by NCEP; forcing from atmospheric pressure variations was not included. The model conserved volume but not mass (Boussinesq approximation). The nature of the differences between the two ocean model types is not the same as for the atmospheric models, though the simulation procedure to estimate the effects due to temporal aliasing was identical. The model chosen to represent the ‘true’ model was generated by using the fully baroclinic capability of the POP (i.e., vertical density variations were allowed). Barotropic conditions were applied in the POP run (i.e., constant density) to generate the model used to de-alias the baroclinic ocean variability, the ‘nominal’ model in the simulation procedure described later. The reason for testing the effects of this difference in model formulation is that even though a baroclinic model is better at tracking long-

term variability, but a barotropic model is computationally cheaper while still accurate for short-period variability. The disadvantage of the barotropic model is that the response of such a model on time scales longer than approximately 100 days or so is significantly different from that of the real ocean [Tierney *et al.*, 2000]. However, the long-term effects of this type of model can be removed from the GRACE data after the estimate for the gravity solution has been completed.

3.2.3 Continental Hydrology

For the contribution of continental water mass variations, a series of geopotential coefficients was computed from a global grid of soil moisture and snow mass data generated by NCEP [Kalnay *et al.*, 1996]. Chen *et al.* [1999] describe the details of the computations to generate geopotential coefficients from this data set. The yearly mean was removed and the month of January 1990 was selected for the simulations. It is important to note that this model does not include water storage variations below a depth of two meters; furthermore, variability over the Antarctic continent and Greenland was specifically excluded. Clearly, this model omits important aspects of the true variability, but these deficiencies are representative of many of the contemporary global continental hydrology models.

The differences between the models' spectra of variability at sub-monthly periods (Figure 3.1) will result in different sampling by GRACE and different aliasing error characteristics. The atmospheric variability has considerable power at the diurnal and semi-diurnal periods, as well as significant power at other periods. Variability in the ocean models was significantly less in terms of spatial extent and magnitude. While the magnitude of the variability in the NCEP continental hydrology model seemed to be comparable regionally to that of the ocean or atmosphere models, the monthly variability was nearly secular and contained little power at sub-monthly periods.

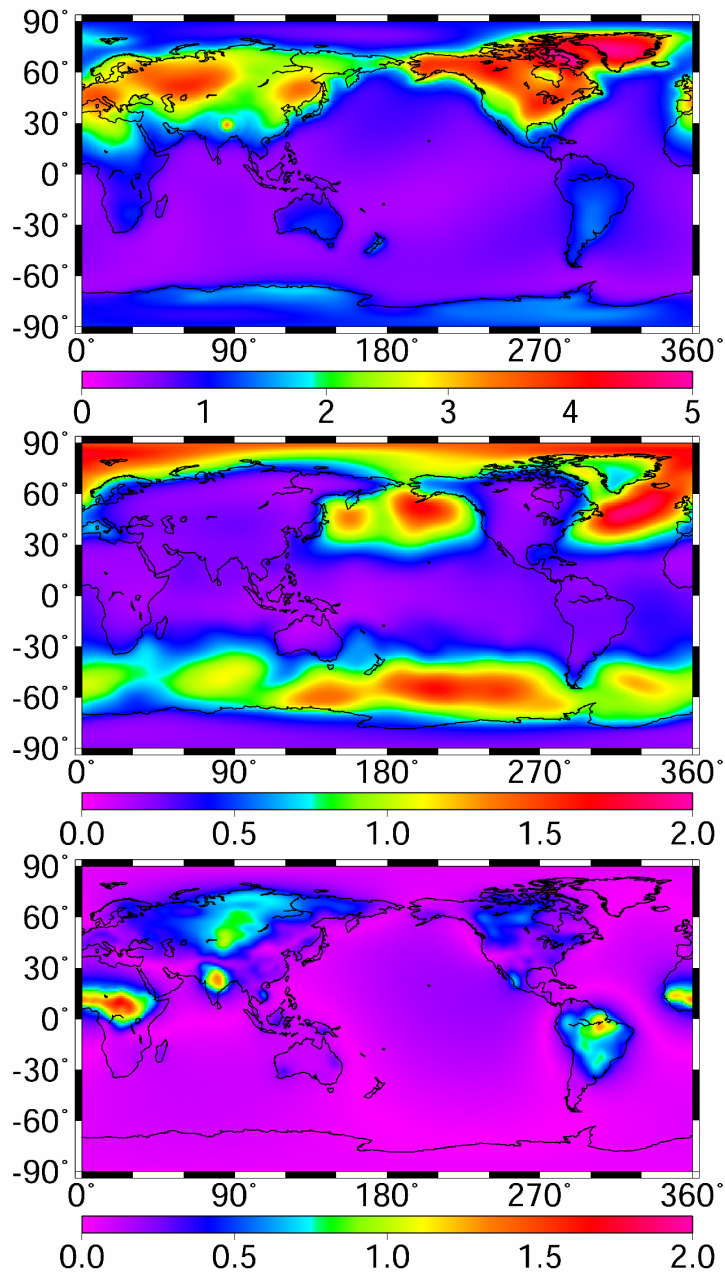


Figure 3.1. RMS about the monthly mean of the time variable geopotential models used to generate simulated observations: ECMWF atmosphere (top), POP baroclinic ocean (middle), and NCEP continental hydrology (bottom).

3.4 SIMULATION PROCEDURE

Summarized here is the method used to generate simulated GRACE observations and to estimate the resulting geopotential field in the presence of these simulated observations. The simulation procedure for studying time variable gravity and other related effects is comparable to previous simulation studies for GRACE [e.g., *Kim*, 2000; *Kim and Tapley*, 2002; *Roesset*, 2003]. Extensive details of the simulation method and software employed can be found in *Kim* [2000]. In brief, the Multi-Satellite Orbit Determination Program (MSODP), which was developed at The University of Texas, Center for Space Research (UT-CSR) to process and simulate Global Positioning System (GPS) observations [*Rim*, 1992] and modified to include GRACE observation types, was used to create noisy measurements of both double-differenced GPS range observations and range-rate derived from K-band ranging (KBR) for 30 consecutive one-day arcs. The background models used in this procedure represent the ‘truth model’ in the simulation universe; in particular, the time variable geopotential models used to represent the short-period temporal mass variations were specified. The simulated observations along with an alternative ‘nominal model’ for geopotential variations were used to obtain an estimate of the ‘true’ gravity. The best estimate of the gravity field was found by minimizing the measurement residuals in the least-squares sense; calculated through the use of the Advanced Equation Solver for Parallel Systems (AESoP) program developed to support the computational requirements of GRACE data processing [*Gunter*, 2004]. An outline of the GRACE simulation procedure used for this study is illustrated in Figure 3.2; additional discussion regarding the different types of gravity models denoted in the flowchart is contained in section 3.5.

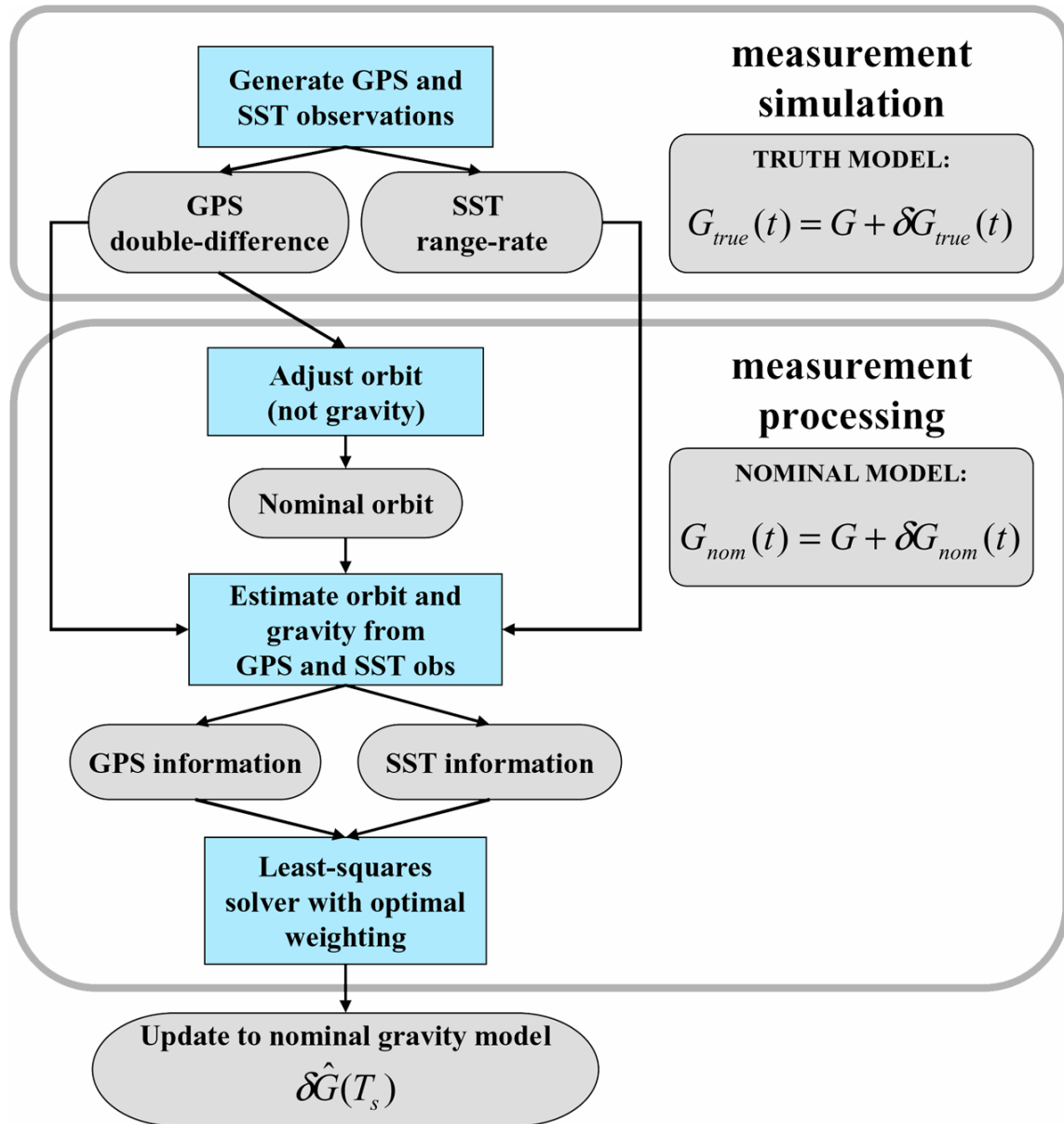


Figure 3.2. Outline of the procedure for the GRACE orbital simulations.

The initial conditions were the same for each simulation and were selected to be representative of an evenly spaced 30-day ground track (Figure 3.3). The inclination was 89° , the nominal separation angle between the two GRACE satellites was 2° , and the

altitude was 462 km. This orbital geometry results in a separation distance between the spacecraft of roughly 239 km and an orbit period of approximately 93 min. A 10-second interval was used for the integration time-step and for outputting the simulated KBR and GPS observations. Geopotential field models and estimates were limited to spherical harmonic degrees from 2-60.

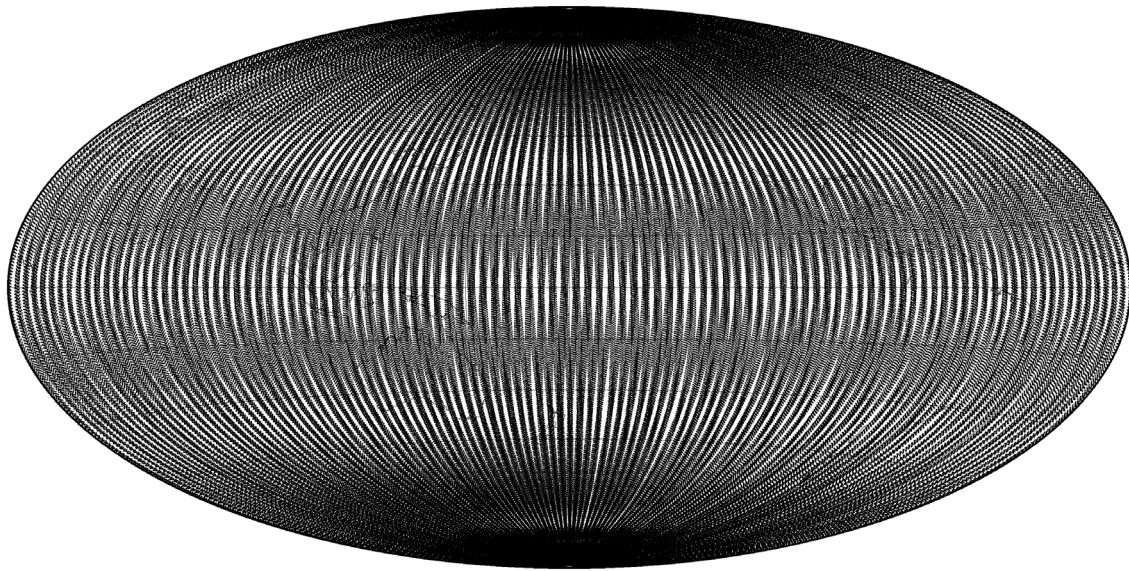


Figure 3.3. Groundtrack coverage for the simulations. Every 10-second integration point is shown for the 30-day time span of the simulation.

Residual or unmodeled measurement error was treated in part through the use of empirical parameters, i.e., not model parameters. These included 1-cycle-per-revolution (1-cpr) and tangential acceleration parameters used to adjust the orbit trajectories. Low-low satellite empirical parameters were also used to adjust the low-low satellite-to-satellite tracking (SST) measurements between the two GRACE spacecraft. One of the primary results of *Thompson et al.* [2000] was regarding the impact of the number of empirical parameters on the gravity estimates: too few parameters and the estimate error increases as signal power is placed into the gravity estimates, too many parameters and

the desired gravity signal is partially placed into the other empirical parameters. The parameters in this study were selected to reduce some of the systematic error that was present, but were limited in number in order to prevent further corruption of the gravity parameters.

The degree 0 and degree 1 terms deserve some discussion, as they are excluded from the GRACE results in this study (chapters 3-5). While the degree 0 term can be non-zero for a specific sub-system of the Earth's variability, it is assumed to be constant for the entire Earth. This term is proportional to the total mass of the Earth, which does not change on the timescales of interest for spacecraft observations. The degree 1 terms are proportional to the geocenter, that is, the location of the center of mass of the Earth system relative to the geographic center. Though the individual mass sub-systems can have a non-zero change in the degree 1 components, the GRACE spacecraft processing model assumes a coordinate system with an origin coincident with the geocenter (i.e., degree 1 terms vanish).

3.5 ALIASING ERROR DEFINITION

The definition of aliasing error used follows that given in *Thompson et al.* [2000]; it is repeated herein but with additional discussion. The purpose of these simulations was to gain a quantitative understanding of the effect of aliasing error on the GRACE mission and how it will manifest itself in the gravity field estimate. It is impossible to know the true impact of aliasing error, or any unmodeled error source, as it would require perfect knowledge of the error source. The combination of a static geopotential and a time-variable geopotential used in generating the simulated observations represented the total 'true' geopotential, while the estimated geopotential and the 'nominal' time-variable geopotential used to compute the estimate represented a best-fit estimate to the simulated observations. The differences between these two characterizations of the geopotential, on

average, provided a measure of the solution accuracy and gives a measure of the sensitivity of the simulation procedure to differences between the ‘truth’ versus ‘nominal’ time-variable mass models.

During a particular simulation, one model was designated as the truth model and was used to generate all the appropriate spacecraft observations and measurements that are representative of real GRACE observations. A second model was designated as the nominal model and was used to process the simulated measurements and to obtain a gravity estimate, in the least-squares sense. It is the error in the nominal model (i.e., differences from the truth model) as well as inherent limitations in the estimation process that produces a difference between the gravity field estimate and the ‘true’ geopotential.

In symbolic form, the geopotential coefficients for the truth model as a function of time, t , were specified as:

$$G_{true}(t) = G + \delta G_{true}(t) \quad (3.1)$$

where G is a static field (i.e., no time-variable component), and $\delta G_{true}(t)$ is the perturbation due to the ‘true’ time-variable potential. The computation of the estimate assumed a nominal field different from the truth model represented by

$$G_{nom}(t) = G + \delta G_{nom}(t). \quad (3.2)$$

where $\delta G_{nom}(t)$ is the nominal perturbing time variable model relative to the same static field.

An update to the nominal background gravity model was found such that the measurement residuals were minimized. This update is a set of constant corrections to

the spherical harmonic geopotential coefficients during the data span, T_s , and represents the gravity information contributed by GRACE:

$$\delta\hat{G}(T_s) = L\{Y_i - f(G_{nom}(t_i)), i = 1, \dots, m\} \quad (3.3)$$

where L represents the linearized least-squares problem over m time steps, Y_i are the observations, and $f(G_{nom}(t_i))$ are the computed measurements based on nominal models. The $Y-f$ differences are the pre-fit residuals that are also commonly represented in other references by $O-C$ or (observed-computed) [e.g., Tapley *et al.*, 2004c]. The update in equation (3.3) is a measure of the mismatch between the truth model and the nominal model. However, there are errors introduced due to aliasing, measurement noise, averaging, as well as due to the nature of the estimation procedure; therefore, the update can only be approximated such that

$$\delta\hat{G}(T_s) \approx \langle G_{true}(t) \rangle - \langle G_{nom}(t) \rangle \quad (3.4)$$

where $\langle \rangle$ denotes a time average. By introducing an error term, ε , to make this an equality and combining with equations (3.1) and (3.2), total error in the simulated solutions was defined as

$$\varepsilon \equiv \delta\hat{G}(T_s) - (\langle \delta G_{true}(t) \rangle - \langle \delta G_{nom}(t) \rangle). \quad (3.5)$$

In this study $\delta G_{true}(t)$ was non-zero for all of the simulations. The full aliasing impact due to a completely unmodeled system was realized by setting $\delta G_{nom}(t)=0$. The impact of partially modeling the true variability (i.e., de-aliasing) was found using a non-zero $\delta G_{nom}(t) \neq \delta G_{true}(t)$.

Accounting for the average difference between the truth and nominal background models (Figure 3.4) is critical because this difference can be erroneously described as aliasing error. This is not error in the gravity recovery, but un-modeled gravity signal that is correctly captured by the estimation process. The accuracy of background models on average will limit the ability to interpret the gravity field estimates as arising directly from mass changes due continental hydrology [*Wahr et al.*, 1998; *Velicogna et al.*, 2001]. Fortunately, the differences in background models for periods on the order of the solution time span or longer are something that can be corrected for after the gravity estimation process is complete. The same is not true for the effects of short-period temporal variability.

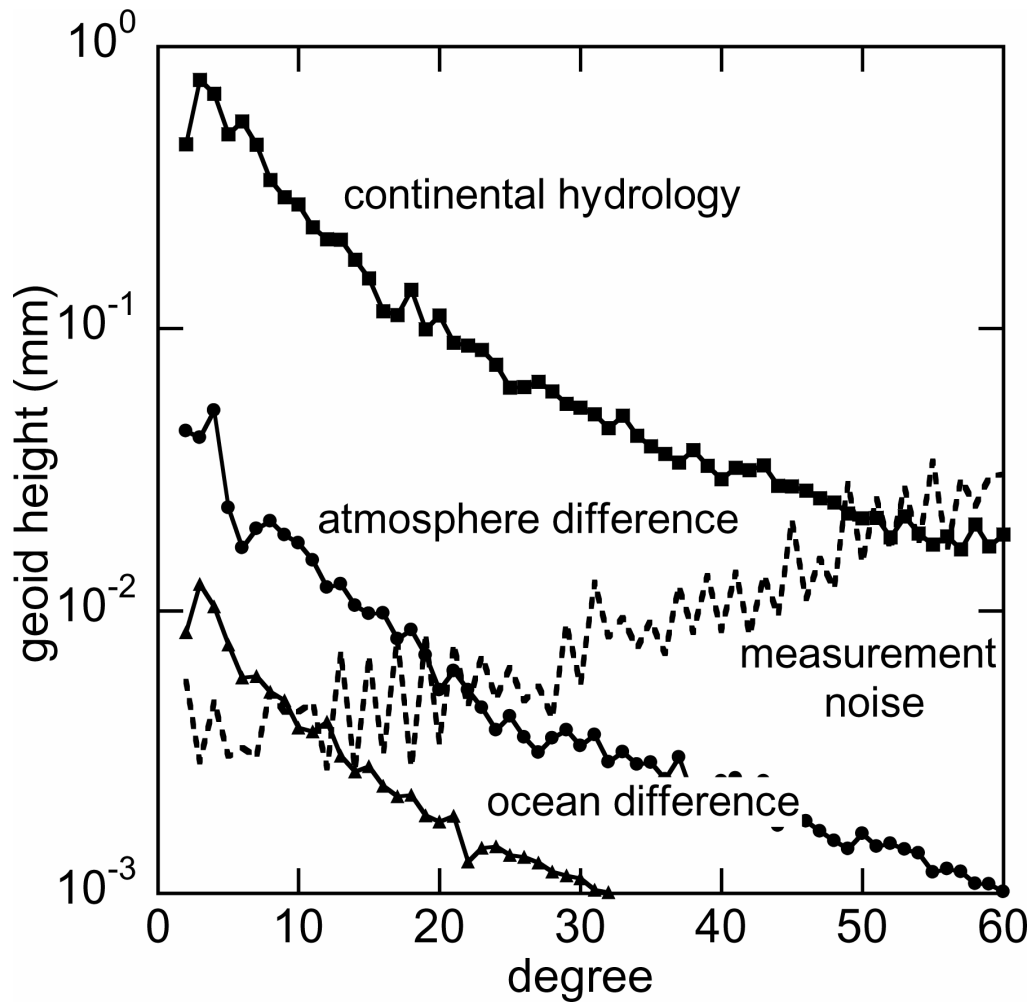


Figure 3.4. Average difference between the ‘truth’ and ‘nominal’ time variable models. Degree difference is shown for the atmosphere and ocean models. Degree amplitude is shown for the continental hydrology model as no de-aliasing was attempted with that model type.

3.6 RESULTS

First, a representative error floor was established in the absence of any time-variable geopotential model error. Depending upon the particular parameterization used, the error in this static gravity case can vary in the details, but the general characteristics of the error in gravity recovery remain [Thompson *et al.*, 2000]. The resulting error was

obtained when only measurement noise was considered as an error source. This error floor was a result that the aliasing simulations can approach but will never exceed; it is comparable to the GRACE error estimates by *Kim* [2000]. This simulation is denoted as “measurement noise” and is included as a reference in all the degree error plots shown in Figures 3.5, 3.7, and 3.9.

The orbital simulations conducted with the atmospheric models showed that the aliasing error due to completely ignoring the short-period variability of the ECMWF atmosphere increased the degree error by an order of magnitude (Figure 3.5), though it should be noted that this also assumes that other error sources were reduced to the level of the simulated measurement noise. Using the NCEP atmosphere as a nominal model in an attempt to de-alias the estimate was most successful at reducing error for the middle to high degrees (approximately $>$ degree 7). The lowest degrees (longest wavelengths) were affected the least; however, this was not a feature specific to these aliasing error simulations. There was no correlation between the unique characteristics of the input models (Figures 3.1 and 3.4) and the features observed at the errors at the lowest degrees for the gravity estimate. The low degree error was found to be dominated by the fact that the GRACE system solution methods for the lowest degrees are particularly sensitive to systematic errors. This feature (particularly for degree 2) is something that remains consistent throughout all of the simulations discussed in this study, is observed in other simulations studies [e.g., *Thompson et al.*, 2000; *Kim*, 2000], and is present in gravity estimates derived from processing of real GRACE data (John Ries, personal communication, 2003). It is important to note that degree error curves do not give an indication of the spatial structure of the error that may exist (Figure 3.6), and this error may not be geographically correlated with the variability in the input models (Figure 3.1). This was particularly noticeable for regions that did not contain any error in the time-

variable model. The aliasing error due to completely unmodeled atmosphere (i.e., ECMWF truth model, static nominal model) was present over ocean areas even though the construction of the atmosphere model specifically removed variability over the ocean areas.

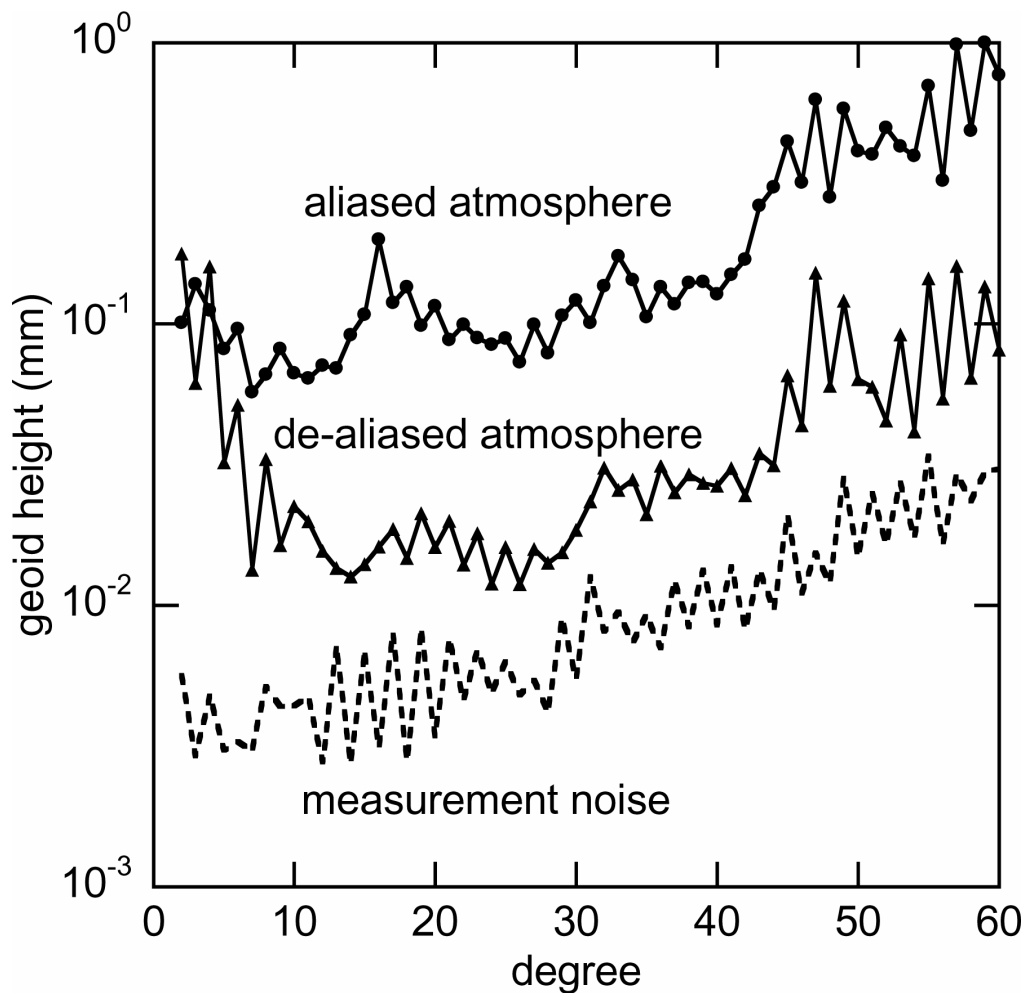


Figure 3.5. Atmosphere model simulation results. Degree error as defined in equation (3.5). Results are for error due to the ECMWF atmosphere (truth model) along with residual aliasing error after using the NCEP atmosphere (nominal model) as an approximate model of the ECMWF atmosphere.

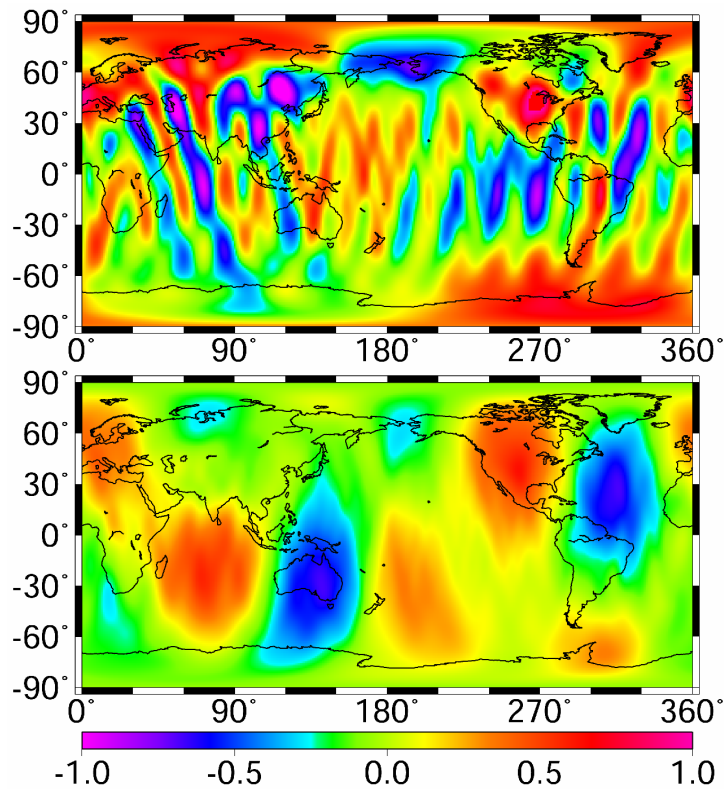


Figure 3.6. Atmosphere model simulation results. Error due to ECMWF atmosphere (top) and error after de-aliasing with NCEP atmosphere (bottom). Geoid anomaly, Gaussian smoothed with a 500-km radius.

Results of the ocean model aliasing and de-aliasing simulations (Figure 3.7 and 3.8) reflected the reduced magnitude and relatively weaker short period variability of the ocean models. The error had a qualitatively similar structure to that observed in the simulations done with the atmospheric models, although it was significantly reduced in overall magnitude. As noted previously in the other simulations, this set of results with the ocean models also indicated relatively more error at the lowest degrees. This set of simulations did not address the overall question of aliasing caused by differences between the POP ocean model and other competing ocean models. The key result was that a

barotropic ocean model can be used to de-alias the baroclinic model successfully, reducing the error nearly to the limit of the measurement noise above \sim degree 10.

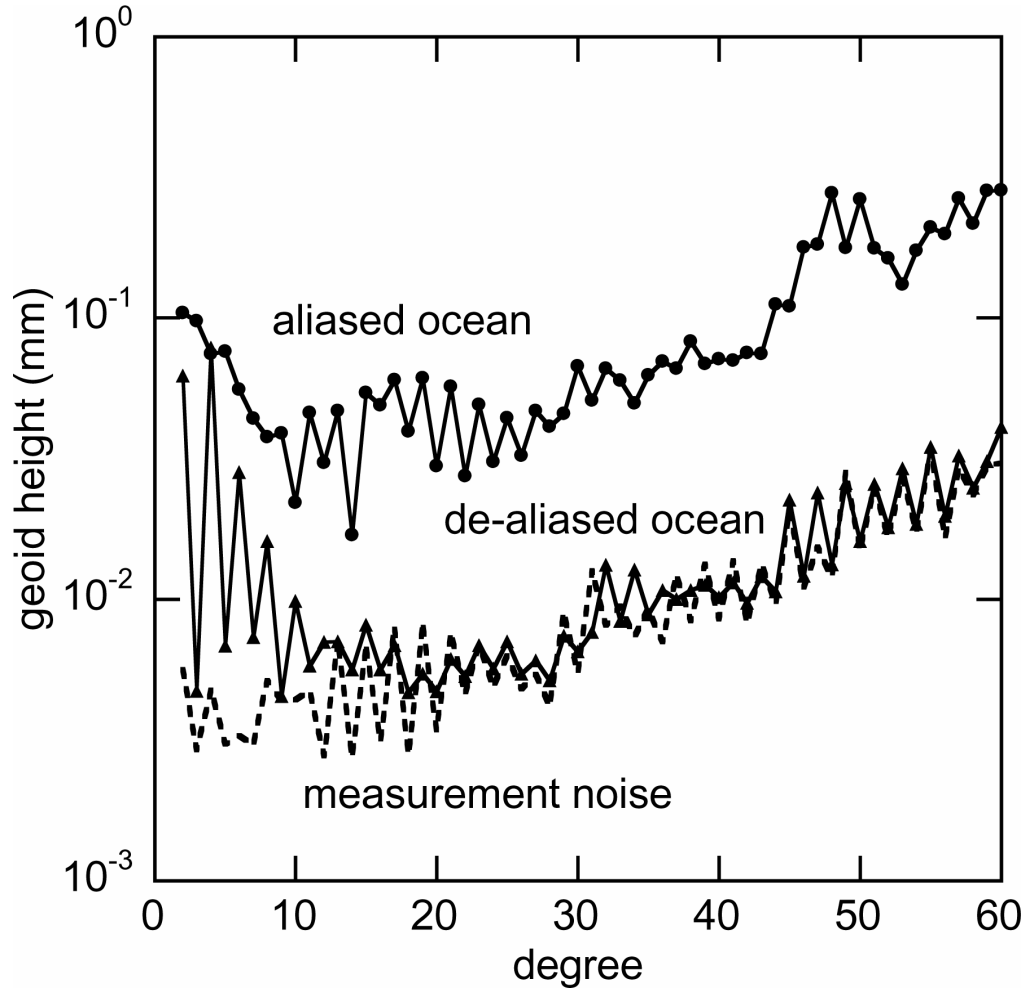


Figure 3.7. Ocean model simulation results. Degree error as defined in equation (3.5). Results are for error due to the baroclinic ocean (truth model) along with residual aliasing error after using the barotropic ocean (nominal model) as an approximate model of the baroclinic ocean.

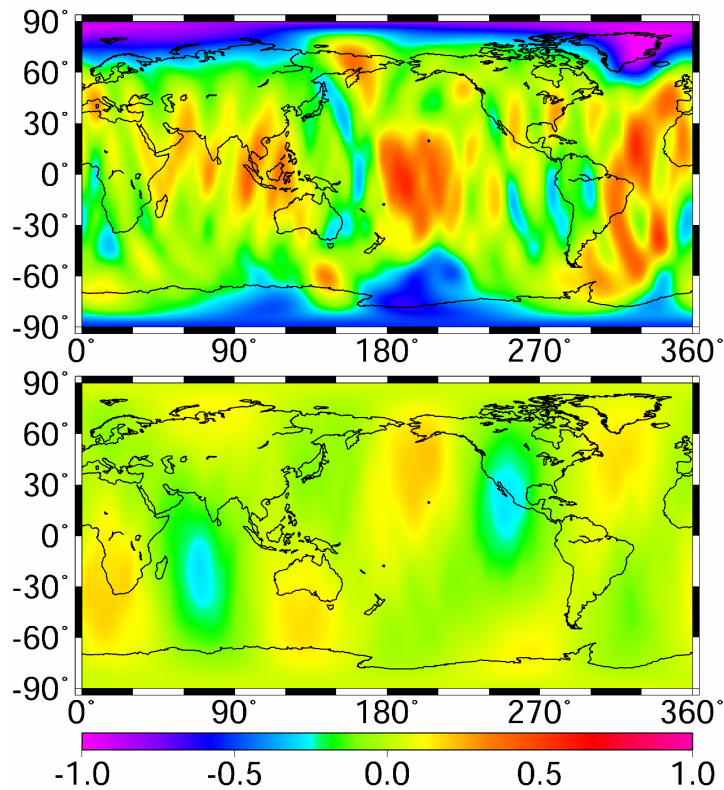


Figure 3.8. Ocean model simulation results. Error due to baroclinic ocean (top) and error after de-aliasing with the barotropic ocean (bottom). Geoid anomaly, Gaussian smoothed with a 500-km radius.

Though large at seasonal periods [e.g., *Wahr et al.*, 1998; *Nerem et al.*, 2000], the NCEP continental hydrology model contained little variability at sub-monthly periods that would allow for aliasing in the gravity estimates. The simulation results with a continental hydrology model (Figures 3.9 and 3.10) produced a significantly smaller amount of error relative to the atmosphere and ocean model simulations, even below the level of error found for the partially de-aliased atmosphere. Another conclusion is that the simulation with the continental hydrology model illustrated that the relatively large mean omitted in the ‘nominal model’ (see Figure 3.4) was largely recovered by the gravity estimation procedure.

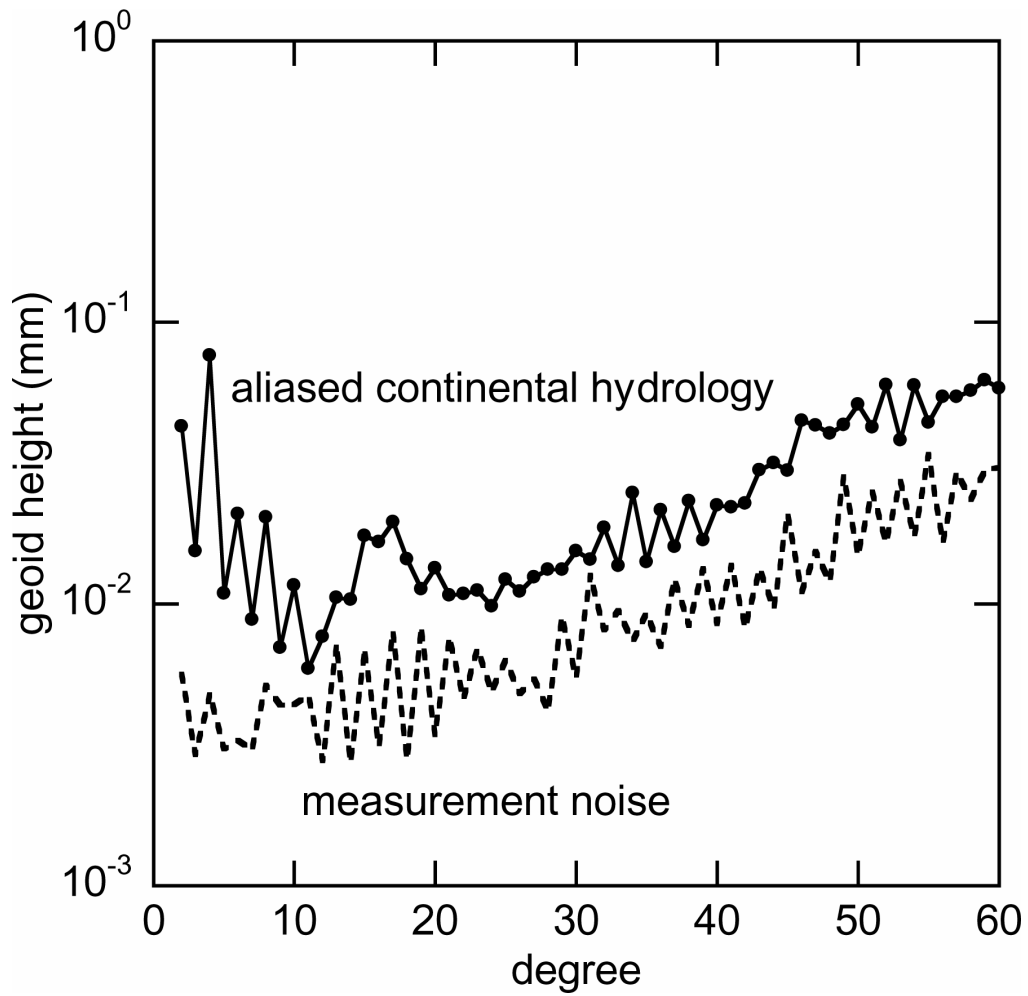


Figure 3.9. Continental hydrology model simulation results. Degree error as defined in equation (3.5). Results are for error due to the NCEP continental hydrology (truth model); no de-aliasing was attempted.

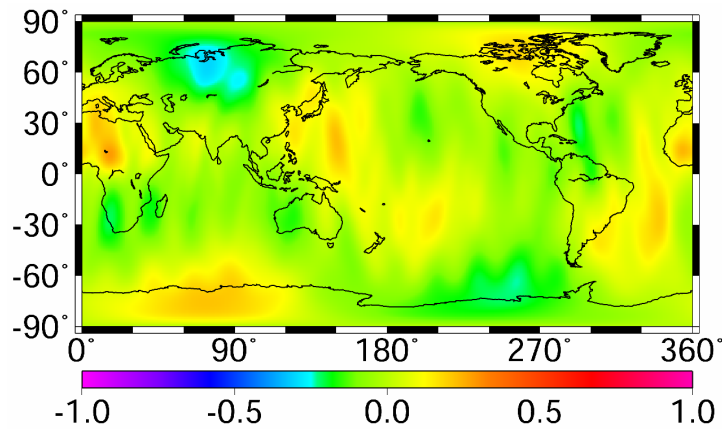


Figure 3.10. Continental hydrology model simulation results. Error due to NCEP continental hydrology. Geoid anomaly, Gaussian smoothed with a 500-km radius.

3.7 DISCUSSION

The benefits of de-aliasing were most evident at the middle to higher degrees, while the error at the lowest degrees ($\sim 2-5$) was dominated by other aspects of the GRACE processing methods. Qualitatively, the level of aliasing error was strongly correlated to the shorter-period power present in the models. It is important that the background time variable models used in GRACE processing contain a reasonably accurate representation of the short-period content in Earth's systems. Accurate estimates of the uncertainty in these models are needed in order to predict the level of aliasing error that may be present from using these models. For example, atmospheric fields from ECMWF and NCEP are partially correlated [Wahr *et al.*, 1998; Velicogna *et al.*, 2001], and the predicted reduction in error may be optimistic.

Competitive models sufficiently different from the POP model were not used to assess the inherent accuracy of ocean models in general. The de-aliasing simulations with the ocean models primarily tested the assumption that a barotropic model was

sufficient for describing high-frequency ocean behavior. The slowly varying baroclinic ocean response was captured by the estimate and did not result in significant aliasing. A barotropic model is currently used to model the shorter period, non-tidal ocean variability for the production of GRACE gravity estimates (discussed further in chapter 4) [*Ali and Zlotnicki, 2003*].

Aliasing error predictions based on an NCEP-class continental hydrology are limited by the lack of reasonable short-period variability. The aliasing error due to a model with such a temporal spectrum was below the level even of an optimistic estimate of the residual error present after partially de-aliasing the atmospheric effects. This result may have not been unexpected as an NCEP-class model may be of limited value in assessing variability at the monthly time scales, requiring models with higher spatial and temporal resolutions in order to compare with expected GRACE gravity recovery [e.g., *Rodell and Famiglietti, 1999*]. As significant improvements are made in both the accuracy and temporal resolution of continental hydrology models, these results and conclusions should be revisited.

Chapter 4: Atmosphere-Ocean De-Aliasing Model and GRACE

GRACE data processing uses a combined atmosphere-ocean model in order to reduce the effects of temporal aliasing that may be caused by non-tidal, short period mass variability of the atmosphere and ocean. The atmosphere+ocean de-aliasing (AOD) model is generated from six-hour global atmospheric data from ECMWF combined with a barotropic ocean model. Upon implementing this model in GRACE processing, the greatest impact was found to be a reduction of error at the highest degrees. Furthermore, there was either improvement or no measurable change in the orbit fits and oceanographic circulation statistics for the solutions processed using the AOD model. The impact at the lowest degrees of the gravity field, which is important for time-variable gravity studies, was not significantly affected by the use of the AOD model

4.1 INTRODUCTION

The nominal product produced by the GRACE processing system is a piecewise constant series of gravity solutions at approximately monthly intervals. The gravity estimates will be corrupted by aliasing of short period mass variability into other spatial and temporal scales (see chapter 3 and *Thompson et al.* [2000]). Selected models of temporal mass variability are used to reduce these effects: solid Earth and oceanic tides, selected secular variations, pole-tide effects, and a combination of atmospheric pressure variations and the response of a barotropic ocean model driven by European Centre for Medium-Range Weather Forecasts (ECMWF) atmospheric pressure and winds. While there is a history in orbit determination of using models to reduce the degradation in gravity recovery due to the time-variable geopotential (see, e.g., see chapter 2), the increased sensitivity of the GRACE measurements requires that an *a priori* model for the

non-tidal, short period variability due to the atmosphere and ocean be included during the gravity estimation procedure.

GRACE data processing has adopted an atmosphere-ocean de-aliasing (AOD) model provided by GeoForschungsZentrum Potsdam (GFZ) [Gruber and Peters, 2003] in order to reduce the effects of the non-tidal, short period variability of the atmosphere and ocean. The AOD product is based on 6-hr global data from the ECMWF combined with a barotropic ocean model driven by ECMWF atmospheric winds. Herein is discussed the implementation of the AOD model in GRACE processing and the perturbation in the gravity field estimates due to using the AOD model relative to gravity field estimates that did not use the AOD model. At a minimum, the impact of using an AOD model will need to show no degradation in orbit determination, measurement residuals, or covariance of the gravity fields. It was found those gravity solutions that used the AOD models performed consistently better or the same as those gravity solutions processed without the AOD model.

The outcome of using the AOD model with real GRACE data was consistent with the results of aliasing simulations in chapter 3, though there was an increased level of noise and systematic error beyond that assumed in the simulations. In particular, any impact on the lowest degrees was within the level of error expected for GRACE solutions while the higher degrees showed significant improvement (discussed in the following sections). Three, approximately monthly, time spans of data were selected to test the effects of the AOD model—August 2002, November 2002, and April 2003. Two gravity solutions were computed for each of the time spans; they differed only by whether or not the AOD model was used as a nominal background model during the processing of the observations (“with-AOD” vs. “without-AOD”). All other methods and data were held fixed for the two solution types. An important caveat is that these gravity solutions were

based on a preliminary release of the data and the resulting error estimates are not necessarily representative of the current or future level of accuracy possible from GRACE data processing.

4.2 COMPARISONS WITH TEG4

Using the AOD model resulted in a measurable, incremental improvement in the gravity solutions. While it was not possible to attribute any change in the lowest degrees to an improvement, there was significant improvement at the highest degrees when compared to the TEG4 gravity model [Tapley *et al.*, 2000] (Figures 4.1-4.3). The TEG4 model is considered more to be a more accurate gravity model at the highest degrees when compared to satellite-only gravity solutions; it uses surface-based observations to better constrain the high-degree features that are not well resolved by spacecraft observations. Differences between the TEG4 model and GRACE models were most evident by an upturn in the degree differences starting at approximately degree 90. The error at those highest degrees was consistently less for the with-AOD solutions relative to the without-AOD solutions and was most evident at approximately degrees greater than 90. This decrease in the relative error indicated that the with-AOD solutions are more accurate at those higher degrees.

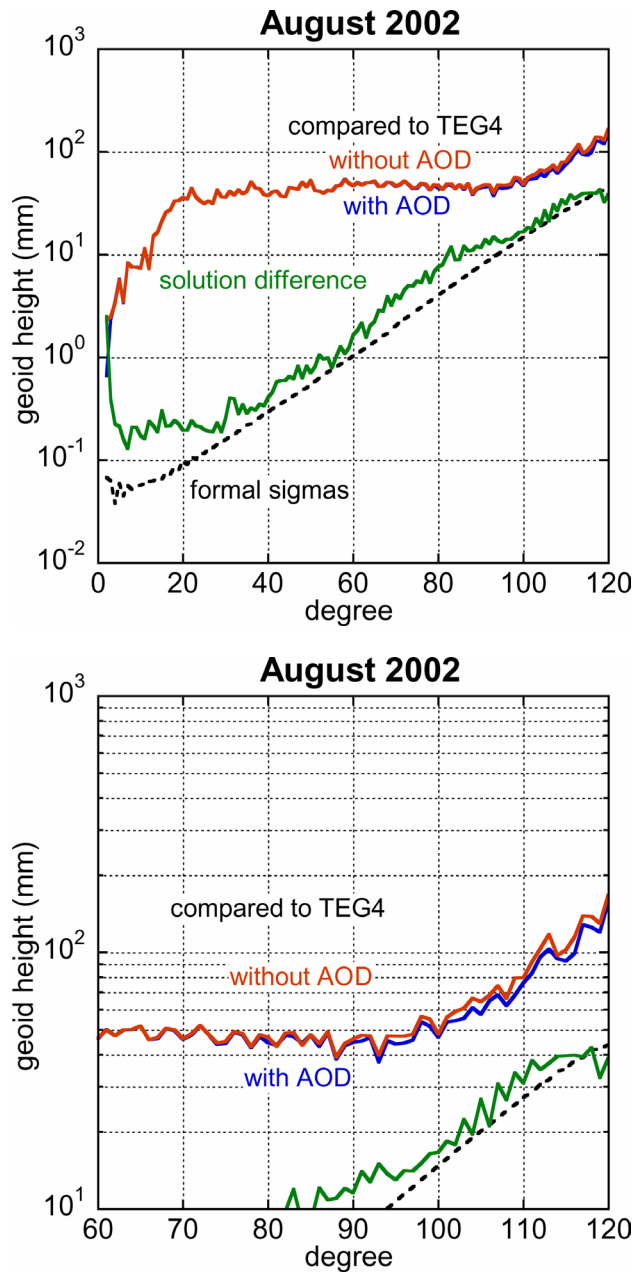


Figure 4.1. Degree error for the solutions processed with and without the AOD model for August 2002 as compared to TEG4 as well as the difference between the two. The differences relative to TEG4 are difficult to see at full scale (top), but are evident for the highest degrees (bottom). The average value of AOD was added to the with-AOD solutions before the comparisons were made, isolating the perturbation due to the short-period variability.

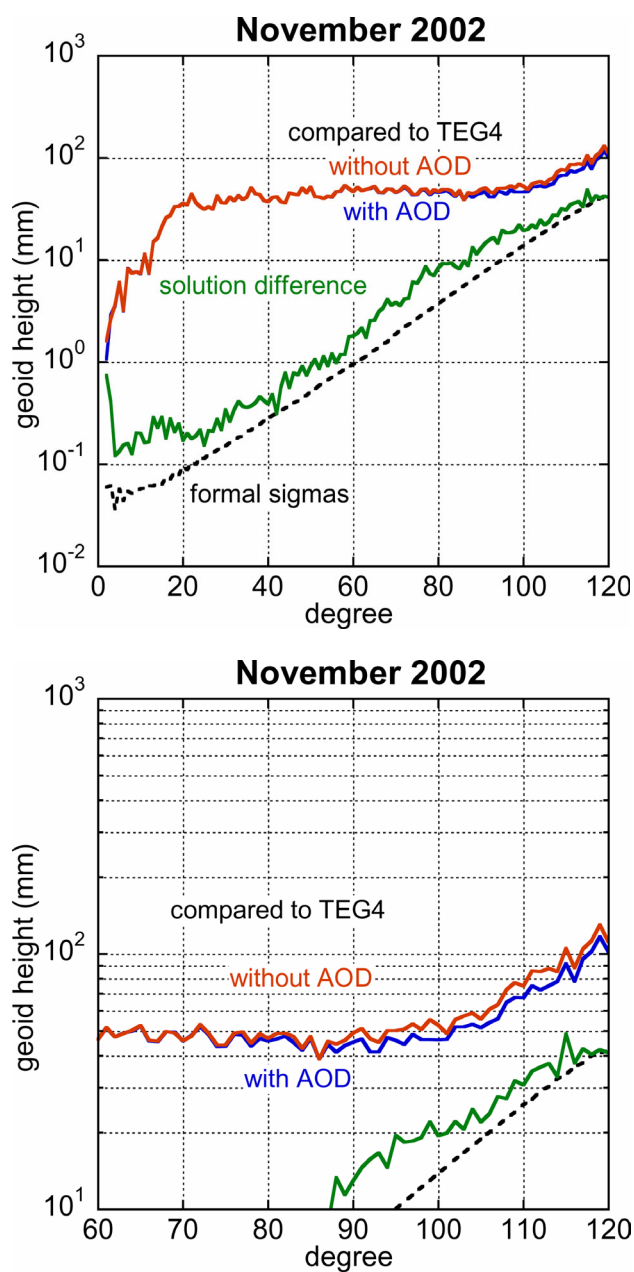


Figure 4.2. Degree error for the solutions processed with and without the AOD model for November 2002 as compared to TEG4 as well as the difference between the two. The differences relative to TEG4 are difficult to see at full scale (top), but are evident for the highest degrees (bottom). The average value of AOD was added to the with-AOD solutions before the comparisons were made, isolating the perturbation due to the short-period variability.

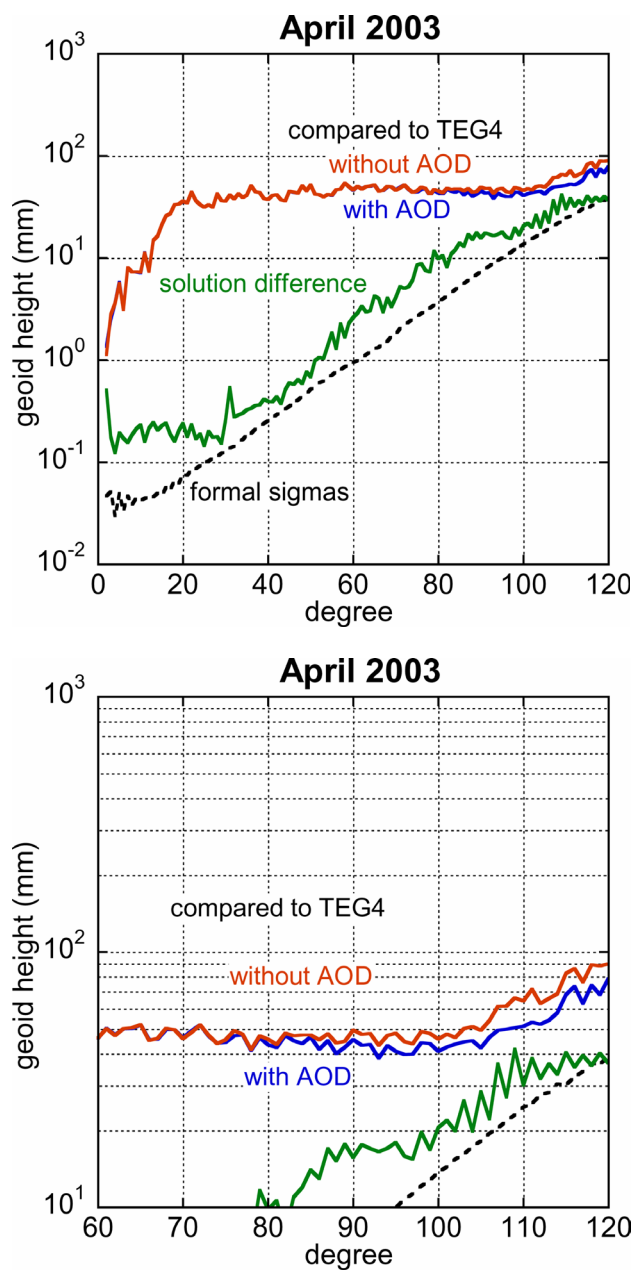


Figure 4.3. Degree error for the solutions processed with and without the AOD model for April 2003 as compared to TEG4 as well as the difference between the two. The differences relative to TEG4 are difficult to see at full scale (top), but are evident for the highest degrees (bottom). The average value of AOD was added to the with-AOD solutions before the comparisons were made, isolating the perturbation due to the short-period variability.

4.3 TIME-VARIABLE GRAVITY PERTURBATION

Of particular interest is the impact of the short-period variability on time-variable gravity interpretation based the monthly GRACE gravity solutions. Three permutations are possible with the solution set being considered: August 2002 to November 2002, November 2002 to April 2003, and August 2002 to April 2003. Prior to comparing with-AOD and without-AOD solutions, the average of the AOD model that was effectively removed as a consequence of the processing methods was added to the with-AOD gravity solutions. This procedure results in time-variable gravity observations that contained signal due to a combination of continental hydrology, the atmosphere, and the oceans.

Illustrated in Figures 4.4-4.6 are comparisons of time-variable gravity interpretations for the three permutations. In terms of degree amplitude, the perturbation due to the AOD sub-monthly variability caused a consistent reduction in the power contained in the time-variable gravity results at all but the lowest degrees. The significant power at the higher degrees, approximately greater than degree 20, cannot be attributed to real geophysical signal and must be interpreted as error. The reduction in this power at the higher degrees, therefore, indicated that the with-AOD solutions were consistently more accurate than the without-AOD solutions. It is difficult to assess if the perturbation below ~degree 10 can also be attributed to improvement as it was difficult to detect any significant perturbation at the lower degrees (i.e., longer wavelength spatial features). A key point is that, the lowest degrees that are most critical for time-variable gravity studies were influenced the least by the usage of the AOD model. This real-world data experience is consistent with the simulation results of chapter 3.

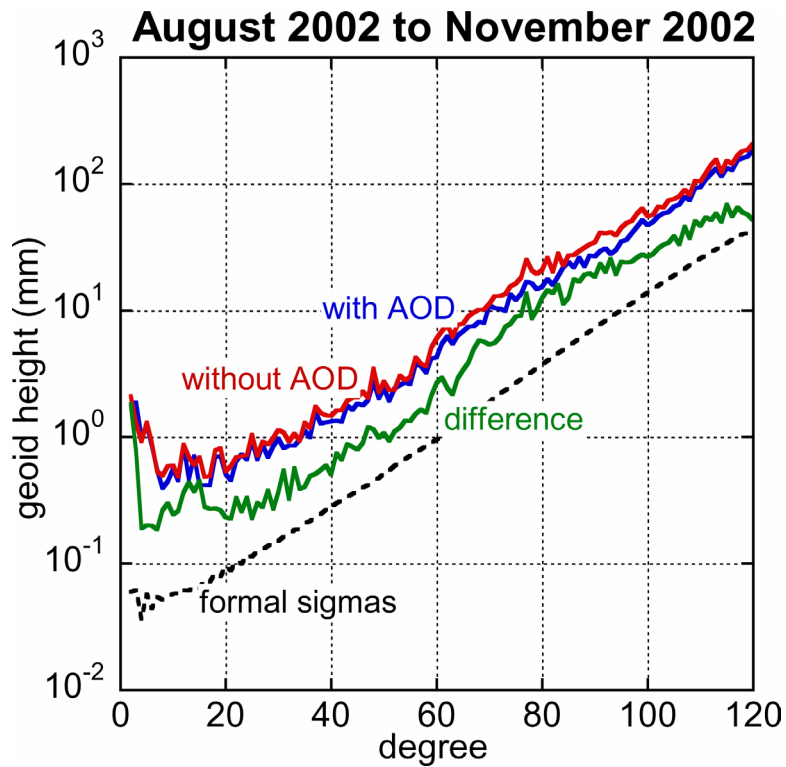


Figure 4.4. Comparisons of time variable gravity signals from August 2002 to November 2002 based on the with-AOD or the without-AOD gravity solutions. The average of the AOD model has been added to the with-AOD solutions in order to isolate the perturbations due to the short-period effects of the AOD model.

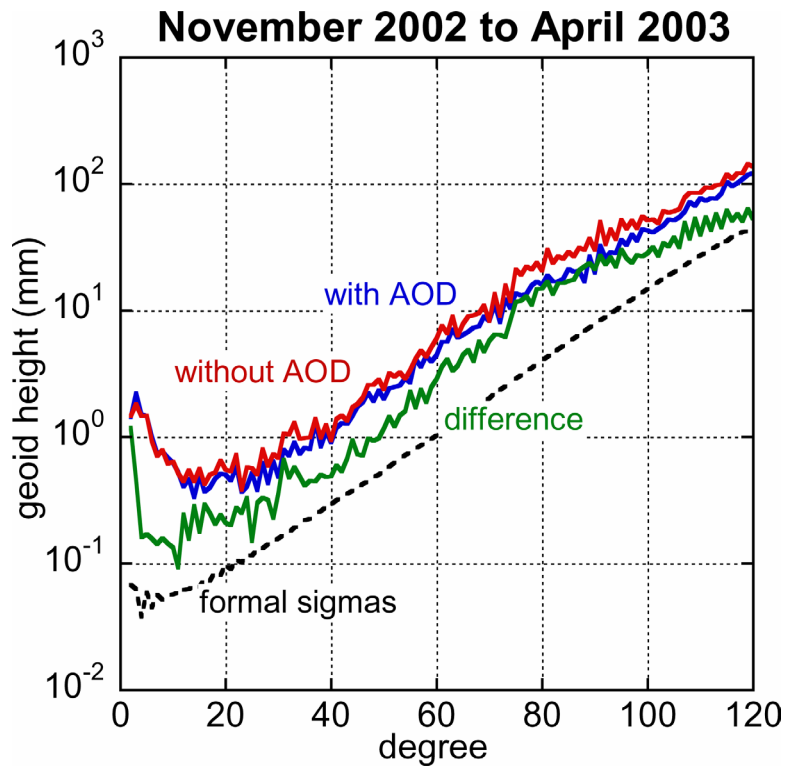


Figure 4.5. Comparisons of time variable gravity signals from November 2002 to April 2003 based on the with-AOD or the without-AOD gravity solutions. The average of the AOD model has been added to the with-AOD solutions in order to isolate the perturbations due to the short-period effects of the AOD model.

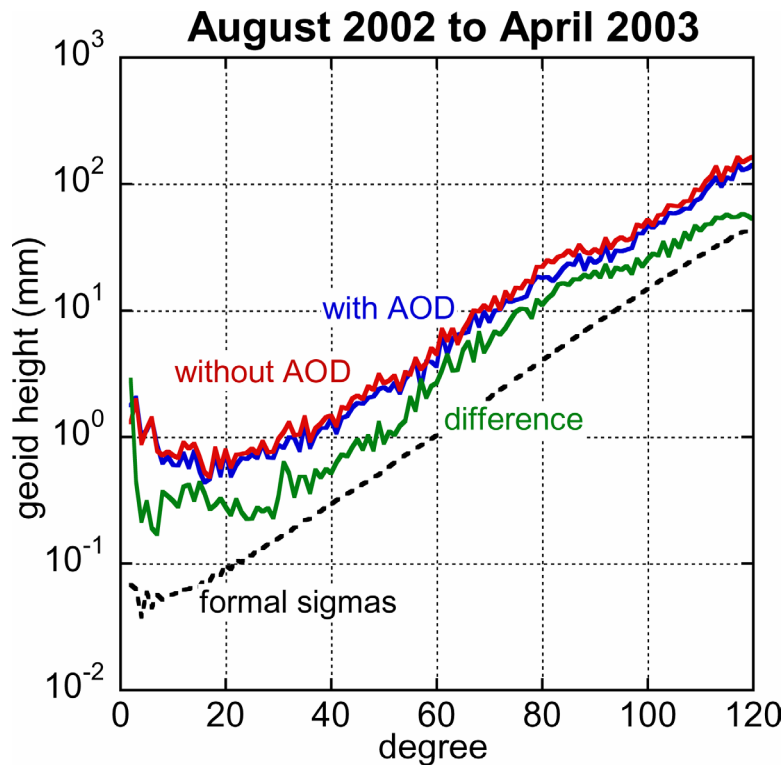


Figure 4.6. Comparisons of time variable gravity signals from August 2002 to April 2003 based on the with-AOD or the without-AOD gravity solutions. The average of the AOD model has been added to the with-AOD solutions in order to isolate the perturbations due to the short-period effects of the AOD model.

What do these results look like in a spatial sense? In order to isolate the long-wavelength features important for time variable gravity studies, the coefficient differences were Gaussian smoothed using a 600-km effective radius [see *Jekeli, 1981*] and the degree 2 coefficients were removed. The total amplitude of the time variable signal was found to be significantly larger (~5 times) than any perturbation that may have been introduced by the effects of the short-period variability in AOD model (Figures 4.7-4.9). Depending on the months selected, the peak magnitudes of geoid anomaly for the global maps of the time-variable signal were as large as 20 mm (e.g., August 2002 to

April 2003). However, the maximum difference between the time-variable solutions based on if they were the with-AOD or without-AOD solutions was only on the order of 4 mm at 600-km wavelengths (bottom panels, Figure 4.7-4.9). Also, there were no obvious spatial patterns that appear in the time-variable gravity maps that could be correlated with geophysical phenomenon in the atmosphere and ocean. For example, the error did not appear preferentially over the land or ocean, except in the sense that the global surface is mostly oceanic. Furthermore, these differences in time-variable gravity interpretations between the with-AOD and without-AOD solutions appeared to be within the level of error for any GRACE gravity solution conducted with the data and processing methods available for this study (John Ries, personal communication, 2004). Therefore, while there was consistent reduction in errors at the highest degrees for the with-AOD solutions, the time-variable gravity interpretation at the long spatial wavelengths was not limited by the impact of the short-period, mass variability in the atmosphere and oceans as represented in the AOD model.

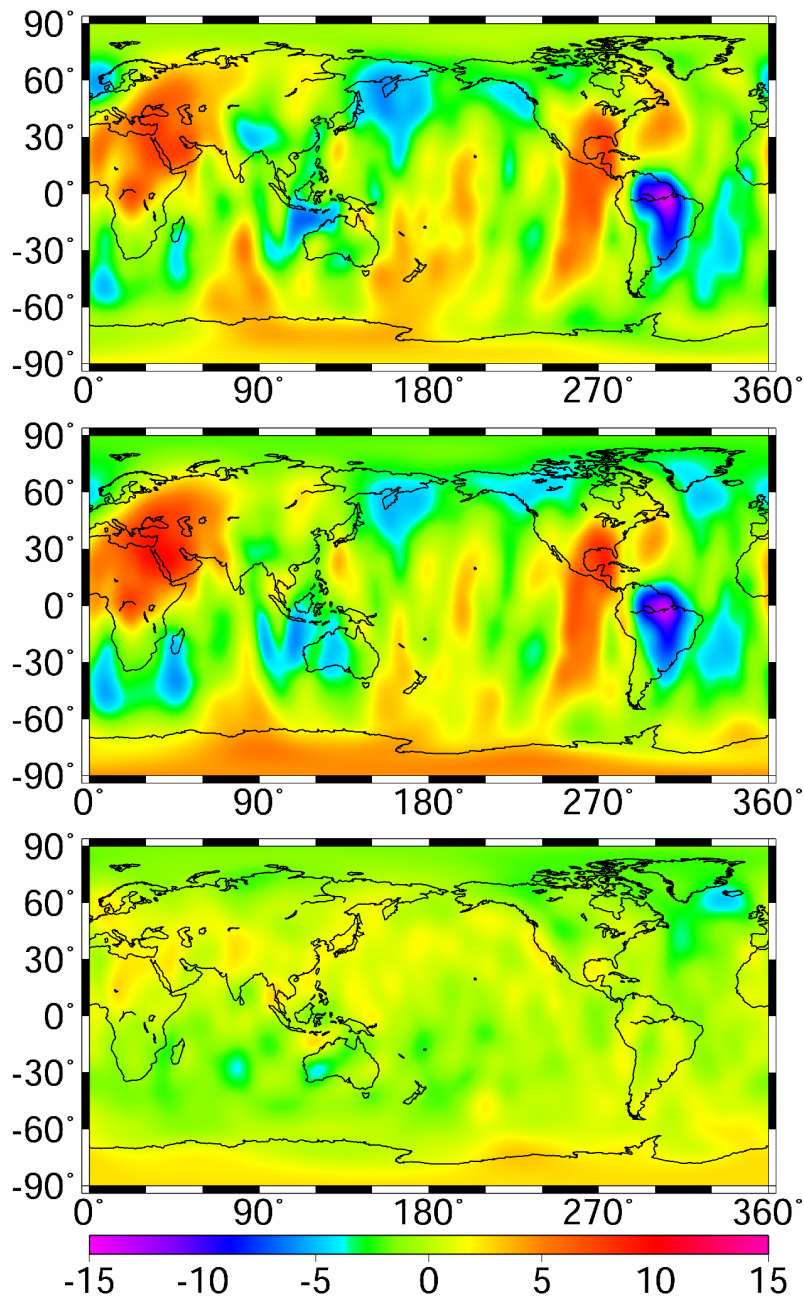


Figure 4.7. Time variable gravity estimates for the time period between the August and November 2002 solutions for both the without-AOD solutions (top) and with-AOD solutions (middle). Gaussian smoothed with a 600-km radius and the degree 2 coefficients removed. Peak amplitude of the difference between the two time-variable estimates was $-4.8/+3.2$ mm geoid height (bottom).

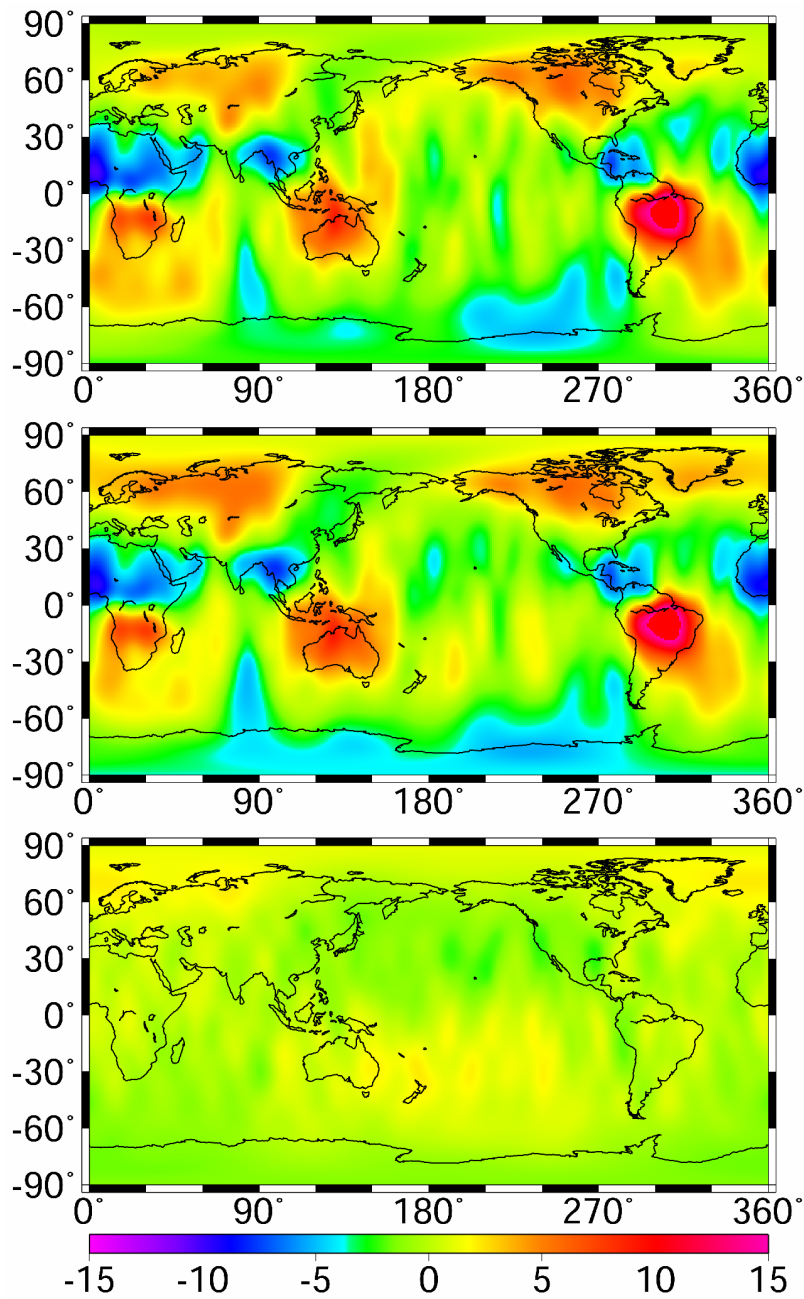


Figure 4.8. Time variable gravity estimates for the time period between the November 2002 and April 2003 solutions for both the without-AOD solutions (top) and with-AOD solutions (middle). Gaussian smoothed with a 600-km radius and the degree 2 coefficients removed. Peak amplitude of the difference between the two time-variable estimates was $-2.5/+2.3$ mm geoid height (bottom).

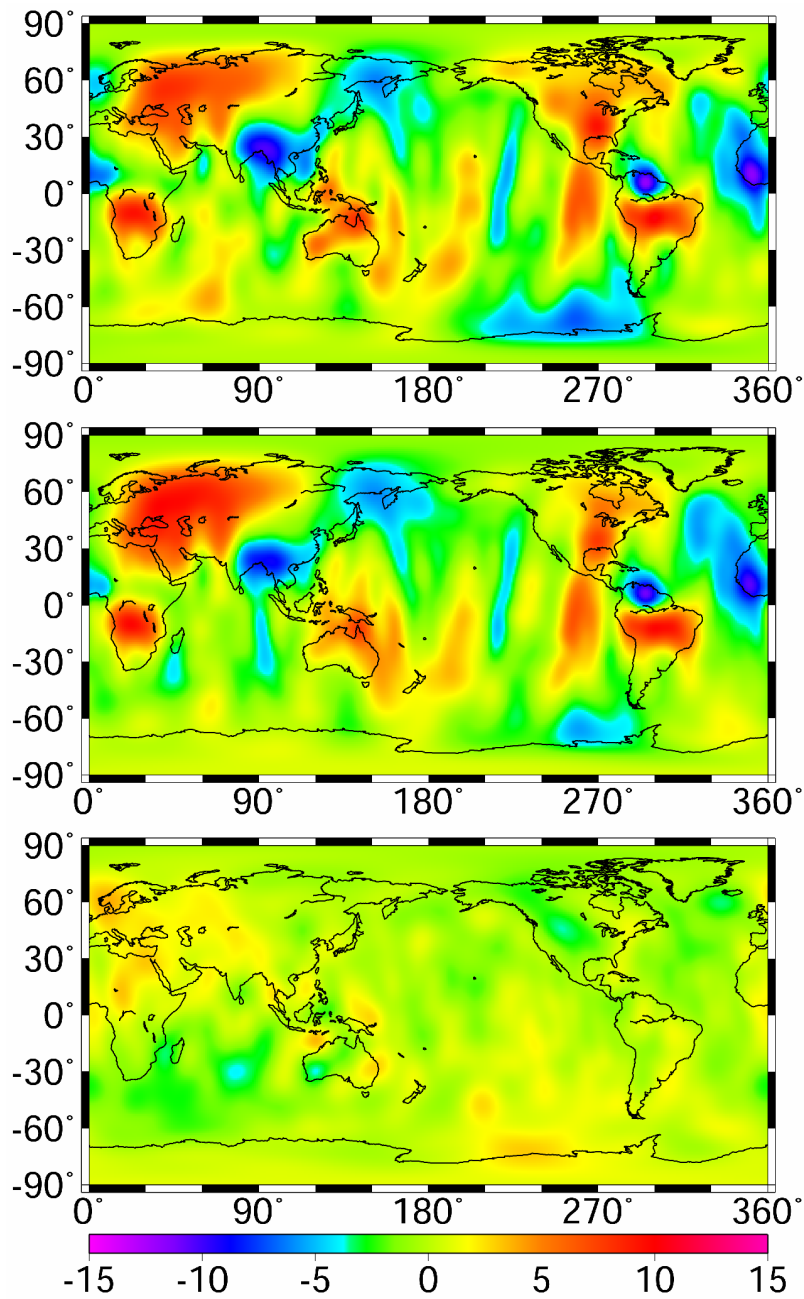


Figure 4.9. Time variable gravity estimates for the time period between the August 2002 and April 2003 solutions for both the without-AOD solutions (top) and with-AOD solutions (middle). Gaussian smoothed with a 600-km radius and the degree 2 coefficients removed. Peak amplitude of the difference between the two time-variable estimates was $-3.9/+3.9$ mm geoid height (bottom).

4.4 OCEAN CIRCULATION STATISTICS

Geostrophic currents based on the set of six gravity solutions were calculated and compared to those based on a mean hydrographic surface [Tapley *et al.*, 2003] (Table 4.1). The comparisons resulted in statistics indicating no change or improvement for with-AOD solutions relative to the without-AOD, where improvement was indicated by a reduction in the residual RMS and a higher correlation. The zonal RMS and correlations were unaffected, which was mainly an indicator of the limitations of the test and that correlations above 0.93 are difficult to achieve. The differences were significant, however, for the meridional component, which indicated an improvement in the higher degree sectorials or near sectorials for the with-AOD solutions.

	August 2002		November 2002		April 2003	
	with AOD	without AOD	with AOD	without AOD	with AOD	without AOD
Zonal						
RMS (cm/s)	2.59	2.61	2.59	2.58	2.57	2.59
correlation	0.93	0.93	0.93	0.93	0.93	0.93
Meridional						
RMS (cm/s)	3.13	3.27	3.15	3.38	3.22	3.47
correlation	0.49	0.46	0.49	0.44	0.46	0.41

Table 4.1. Global statistics from ocean circulation velocities based on the GRACE gravity field solutions as compared to velocities from Levitus to 4000-m depth.

4.5 ORBIT STATISTICS

Orbit fits for a variety of spacecraft were computed based on the six gravity solutions. The results show a slight, overall improvement for the with-AOD solutions

relative to the without-AOD solutions (Table 4.2). In those instances where a particular test seemed to be inconclusive, the results were found to be within the inherent uncertainty of the test. For example, the Lageos-1 and Lageos-2 fits are particularly sensitive to the low degree harmonics, especially the degree 2 zonal, $C_{2,0}$. The spread of values shown in Table 4.2 is indicative of the larger relative error for the $C_{2,0}$ coefficient in any GRACE solution (John Ries, personal communication, 2004) and it was not a consequence of the difference between the with-AOD and without-AOD solutions. The difference in the rms values was most significant for STELLA and WESTPAC due to their higher sensitivity to more of a range of spherical harmonic coefficients.

	August 2002		November 2002		April 2003	
	with AOD	without AOD	with AOD	without AOD	with AOD	without AOD
ICESAT	2.1	2.1	2.0	2.0	1.7	1.8
LAGEOS-1	0.94	1.22	1.00	1.09	1.10	1.05
LAGEOS-2	0.92	1.31	0.96	1.00	1.09	1.03
STARLETE	3.3	3.5	2.5	2.4	2.8	3.1
STELLA	3.9	4.9	3.3	4.0	3.0	3.5
WESTPAC	5.3	5.9	4.9	5.4	5.1	5.6

ICESAT - seven 30-hour arcs, Cd, w/ 1/revs
 LAGEOS-1 and -2 - ten 3-day arcs, daily Ct, 3-day 1/rev
 STARLETTE - 5-day arcs, daily Cd, w/ 1/revs
 STELLA - 5-day arcs, daily Cd, w 1/revs
 WESTPAC - 6-day arcs, daily Cd, w/ 1/revs

Table 4.2. Impact of the AOD model on orbit fits calculated from the GRACE gravity solutions. Values are RMS in cm.

4.6 DISCUSSION

Accuracy consistently improved for solutions that used the AOD model during processing (i.e., the with-AOD solutions) in order to reduce the effects of short-period mass variability. The highest degrees were better resolved when compared to a model that included surface gravity observations (i.e., TEG4). Ocean circulation statistics improved, particularly for the meridional component, which indicated improvement in the higher degree sectorials and near-sectorials. Orbit fits for other spacecraft from using the with-AOD gravity solutions indicated overall improvement, for those spacecraft orbits more sensitive to a range of spherical harmonic degrees, or no significant change in orbit fits.

Time-variable gravity interpretations at relatively long wavelengths (> 600 km) were not significantly impacted by the use or lack of the AOD model. The lowest degrees showed differences consistent with the level of error to be expected in any single gravity solution for the data and processing methods used at the time of this study. A reduction in time-variable amplitude at about degree 10 or greater indicated less error in the with-AOD solutions; the signal at those shortest spatial wavelengths is dominated by error rather than real geophysical signal.

It is important to note that as the accuracy of the GRACE solutions improves overall, the AOD model will have a more significant impact on accuracy (see, e.g., chapter 3) but not necessarily the most significant impact. More significant improvements in accuracy have been observed through the use of cleaner data (i.e., better editing of bad data points) or improved processing methods. Furthermore, errors arising from all the different sources of short-period mass variability will need to be considered from both modeled sources (e.g., ocean tides, solid body tides) and unmodeled sources

(e.g., continental hydrology) as their uncertainties may currently be or may later become larger than the errors in the AOD model components.

Chapter 5: GRACE Time-Variable Gravity and Continental Hydrology

Current gravity solutions from GRACE resolved features on monthly time scales with a geoid height accuracy of 2-3 mm for spatial scales greater than ~600 km, the amount of error depending on the specific temporal and spatial scale of interest. For annual time scales or regions with the largest variability, spatial scales on the order of 400 km were resolved. The annual cycle in the geoid variations peaked predominately in the spring and fall seasons, with amplitudes up to ~10 mm observed in some regions. On the South American continent basin-scale variability on monthly time scales was resolved, with a clear separation observed between the large Amazon watershed and the smaller watersheds to the north. Comparisons with the Global Land Data Assimilation System (GLDAS) terrestrial water storage estimates and GRACE observations indicated a high degree of correlation for both the annual signal and month-to-month variations up to spatial wavelengths of 600 km or larger. Usage of these GRACE products ultimately depended on the desired ratio of signal vs. error.

5.1 INTRODUCTION

Observations of the temporal variations in the Earth's gravity field on monthly time scales or longer will help constrain global models of mass variability and exchange within the land, ocean and atmospheric components of the Earth's sub-systems. This is particularly significant for sub-systems that have been otherwise extremely difficult to observe and monitor with other methods, e.g., deep ocean currents and deep aquifers. In the past, SLR has been used to determine the very long wavelength seasonal gravitational changes due to mass exchange between the atmosphere, ocean, and continental water sources (see, e.g., chapter 2) [*Nerem et al.*, 2000; *Cazenave et al.*, 1999; *Chao and Au*,

1991]. These have been limited in resolution due to the limitations in geographic distribution of the tracking data and the limited sensitivity of high altitude satellites. The GRACE mission was implemented to provide global measurements of these same phenomena, but with a much finer spatial resolution and to a greater accuracy than previously possible [Tapley *et al.*, 2004a].

The Gravity Recovery and Climate Experiment (GRACE) is a dedicated satellite mission whose objective is to map the global gravity field with unprecedented accuracy and with a spatial resolution of 400 km every 30 days for five years. The GRACE mission, launched on March 17, 2002, consists of two identical satellites in near circular orbits at ~500 km altitude, separated from each other by approximately 220 km along-track, and linked by a highly accurate inter-satellite, K-Band microwave ranging system. Each satellite carries GPS receivers and attitude sensors and high precision accelerometers to measure the surface forces. Through the dynamical evolution of the orbits, the inter-satellite distance change, which is extracted from phase measurements of the K-Band signal transmitted between the two satellites, contains implicitly the influence of the globally integrated mass distribution and its movements within the Earth system.

This study describes a methodology for extracting time-variable gravity information from the GRACE science products and discusses some of the initial results from the mission. The level of signal vs. error was found to vary for each particular application. Ultimately, the interpretation of the GRACE products depended on the procedure for defining the “average” geopotential during a time-span: the nature of the time-variable signal that has been removed as a consequence of data processing (e.g., solid body tides, ocean tides, AOD model), by gaps in the data (sometimes one day or longer in duration), temporal scales (e.g., annual vs. monthly), and spatial scales (e.g., global vs. annual).

5.2 METHODS

The temporal variations in the geopotential field were observed by the GRACE processing system as a sequence of piecewise constant, approximately monthly, estimates of the set of geopotential spherical harmonic coefficients. The monthly gravity estimates from GRACE were obtained as variations relative to a well-defined a priori gravity model. Due to the limitations of ground-track coverage, the sub-monthly variability of the geopotential is difficult to observe accurately. Because of this, it is advantageous to adopt models for well known time-variable geophysical processes that are better determined from techniques other than GRACE. The modeled geophysical variations included the solid Earth and oceanic tides, selected secular variations, pole-tide effects, and a combination of atmospheric pressure variations and the response of a barotropic ocean model driven by ECMWF atmospheric pressure and winds [Gruber and Peters, 2003].

As was previously mentioned in chapter 2, the interpretation of time-variable gravity as observed from orbiting spacecraft depended upon the assumptions made regarding mass variations that took place during the time interval being processed. By including *a priori* models of the nominal variability, some of the signal as observed by the spacecraft are effectively removed from the sequence of geopotential estimates, leaving any time-variable signal as arising from the omitted geophysical phenomenon. This “science by omission” for the SLR study in chapter 2 led to interpreting the time-variable gravity observations as having been due to the combined effects of the atmosphere, oceans, and continental hydrology. In the case of GRACE, non-tidal variations in the atmosphere and ocean were accounted for through the use of the atmosphere+ocean de-aliasing (AOD) model as discussed in chapter 4 and appendix A. Consequently, the GRACE gravity estimates contain information about mass variability

due to the signal introduced by geophysical phenomenon not already modeled and the residual signal (on average) from omissions in the *a priori* models (see the grace processing handbooks for details of the GRACE processing methods, <http://www.csr.utexas.edu/grace/publications/handbooks>). It is possible to compare the time-variable gravity results of SLR and GRACE as long as the differences in processing philosophy are properly accounted for.

5.3 CONTINENTAL HYDROLOGY AND GRACE TIME-VARIABLE GRAVITY

Continental hydrologic variations are the largest omitted phenomena from the suite of *a priori* gravity models used in GRACE data processing, and are thus the dominant un-modeled mass signal that should be evident in a sequence of monthly gravity estimates, though it is not the only source of variability. The gravity information as defined by the GRACE products for a specific time span of data, T_s , consists of a set of geopotential coefficients, $G(T_s)$, such that

$$G(T_s) = G_{static} + \delta\hat{G}(T_s) \quad (5.1)$$

where G_{static} is the static part of the *a priori* field used in processing and $\delta\hat{G}(T_s)$ is the update found relative to the nominal field that best reduced the measurement residuals. Consistent with what was previously defined in equation (3.3), this update is found as a set of constant corrections to the spherical harmonic geopotential coefficients during the data span, T_s , and represents the gravity information contributed by GRACE:

$$\delta\hat{G}(T_s) = L\{Y_i - f(G_{nom}(t_i)), i = 1, \dots, m\} \quad (5.2)$$

where L represents the linearized least-squares problem over m time steps, Y_i are the GRACE observations, $G_{nom}(t_i)$ is the *a priori* geopotential background model, and $f(G_{nom}(t_i))$ are the predicted measurements. Then following the form of equation (A.1) with slightly different notation, the nominal background model, $G_{nom}(t_i)$, at a specific data point at time t_i can be given by

$$G_{nom}(t_i) = G_{static} + \delta G_{aod}(t_i) + \delta G_{ot}(t_i) + \delta G_{st}(t_i) + \delta G_{pt}(t_i) + \delta G_{sec}(t_i) \quad (5.3)$$

where the individual contributions from time-variable geopotential models are the AOD model, δG_{aod} , ocean tides, δG_{ot} , solid Earth tides, δG_{st} , pole-tide, δG_{pt} , and secular variations, δG_{sec} . It is important to note that while the nominal background model, G_{nom} , contains a static part, G_{static} , they do not necessarily have the same mean over a solutions time-span. That is,

$$\langle G_{static} \rangle \neq \langle G_{nom} \rangle \quad (5.4)$$

for all possible T_s , where the brackets, $\langle \rangle$, denote a time average. Therefore, while the terms “mean-field” and “static-field” are often used interchangeably, they both customarily refer to only the static part of the background *a priori* model, G_{static} , and not necessarily the true average or “mean-field” for the entire *a priori* geopotential model.

Following the thread of the discussion for equations (3.4) and (3.5), the update, $\delta \hat{G}(T_s)$, represents the difference between the true geopotential, G_{true} , and the *a priori* nominal field, G_{nom} , in a least-squares sense; it will only approximately be equal to the average difference between the true and nominal fields,

$$\delta\hat{G}(T_s) \approx \langle G_{true}(t_i) \rangle - \langle G_{nom}(t_i) \rangle. \quad (5.5)$$

Updates to the nominal background geopotential consist of unmodeled variability (e.g., continental hydrology and baroclinic ocean), omissions and errors in the background models on average (e.g., ocean tides), and errors introduced by the estimation process (e.g., aliasing error or data noise). The primary component of the unmodeled variability is believed to be due to continental hydrology, therefore the update can be represented by

$$\delta\hat{G}(T_s) = \langle G_{hydro}(t_i) \rangle + \langle \varepsilon G_{nom}(t_i) \rangle + \varepsilon_{other}(T_s) \quad (5.6)$$

where $\langle G_{hydro}(t_i) \rangle$ is the time-averaged continental hydrology signal for all times processed during T_s , $\langle \varepsilon G_{nom}(t_i) \rangle$ is the time-averaged omissions and errors in the time-variable signals modeled in the nominal model as in equation (5.3), and $\varepsilon_{other}(T_s)$ are the effects of all the other processing related errors. The signal (and errors) in the nominal models includes variability on a variety of time scales, both short-period and long-period relative to the monthly time-scale of the individual gravity estimates. The time-variable gravity results from GRACE are then defined as the difference between two solutions corresponding to data time span T_A and T_B :

$$\begin{aligned} \delta\hat{G}(T_s) = & \langle G_{hydro}(T_A) \rangle - \langle G_{hydro}(T_B) \rangle + \\ & \langle \varepsilon G_{nom}(T_A) \rangle - \langle \varepsilon G_{nom}(T_B) \rangle + \\ & \varepsilon_{other}(T_A) - \varepsilon_{other}(T_B) \end{aligned} \quad (5.7)$$

For the purposes of this study, only the GRACE gravity solutions and continental hydrology estimates will be discussed (contrasted with the SRL results in chapter 2 that

were attributed to more unmodeled sources of variability). Interpreting GRACE results in terms of continental hydrology will be limited both by the background geopotential used in the nominal models as well as processing related errors. Some aspects of the other terms in equation (5.7) have been discussed in previous chapters (e.g., chapter 3 and 4) and elsewhere in the literature [e.g., *Wahr et al.*, 1998; *Velicogna et al.*, 2001; *Knudsen and Andersen*, 2002; *Kim and Tapley*, 2002]. Updates to the knowledge of the background models for periods on the order of the solution time span or longer (contained in the terms of the second line of equation 5.7) are something that can be corrected for after the gravity estimation process is complete. This requires re-defining of the G_{hydro} contribution as being due to the combined effects of continental hydrology and the correction to new, known source of variability. The effects of short-period temporal variability, data quality, or spacecraft events cannot be corrected for in this manner (contained in the third line of equation 5.7). The impact of unmodeled short-period variability results in a degradation of the gravity products that could not be simply correlated with known geophysical phenomenon (see, e.g., chapter 3). Similarly for spacecraft events that resulted in data gaps, data quality can be improved through editing and more sophisticated processing but data can not be created to account for a time-variable signal that was not sampled.

It is necessary to be clear regarding the definition of “average” as used in this study. While the real variability exhibited in the Earth’s sub-systems is continuous, this is not true for the GRACE observations. Overall data quality is determined on a case-by-case basis for every day. In some cases, small gaps in the data may result without a significant break on continuity. However, entire days are sometimes removed from the processing stream as they result in a serious degradation in gravity estimate. This results in a gravity estimate that can contain an observational gap anywhere during the

“monthly” solution. Therefore, a monthly solution may not necessarily represent the gravity for that entire month, but it represents the variability as sampled on specific days during that time span. It is important to take into account the begin date, end date, and any missing days when comparing the GRACE gravity estimates to any geophysical phenomena. For example, for the sake of consistency a similar type of averaging was applied to the continental hydrology model (discussed below) used in comparisons to the GRACE observations.

5.4 ANNUAL SIGNAL

Using GRACE data collected between April 2002 and December 2003, a sequence of 14 monthly gravity field estimates was computed. The epoch for each monthly solution was taken as the mid-point of the interval contained by each solution. From these monthly estimates, a weighted least-squares solution was derived for the annual cosine (winter-summer) component, the annual sine (spring-fall) component, along with a linear trend for every spherical harmonic coefficient C_{lm} and S_{lm} of the 14 fields:

$$\left\{ \begin{array}{l} C_{lm} \\ \text{or} \\ S_{lm} \end{array} \right\} = A_{lm} \cos(\omega t) + B_{lm} \sin(\omega t) + D_{lm} t + E_{lm} \quad (5.8)$$

where ω is the annual frequency ($1/365.25 \text{ days}^{-1}$), t is time after Jan 1 at 0-hr UTC, A_{lm} and B_{lm} are the cosine and sine amplitude respectively, D_{lm} is the slope, E_{lm} is the mean, and l and m are degree and order respectively. The covariance of each solution was used to allow for a down weighing of the contribution of the error due to the earlier solutions.

While previous determinations of the annual variability from SLR were limited to ~ 5000 -km wavelengths (chapter 2) [e.g., *Cazenave et al.*, 1999; *Nerem et al.*, 2000], the annual cycle was determined by GRACE with a resolution of ~ 400 km to approximately a 2-mm level in geoid anomaly (Figure 5.1) To emphasize the wavelengths of interest in continental and basin scale hydrology applications, the degree two coefficients were omitted and the higher degree coefficients (i.e., short-wavelength spatial scales) were down-weighted using a smoothing function with an effective Gaussian radius of 400 km [*Jekeli*, 1981] before being shown in map form. The rationale for this type of weighting is discussed later.

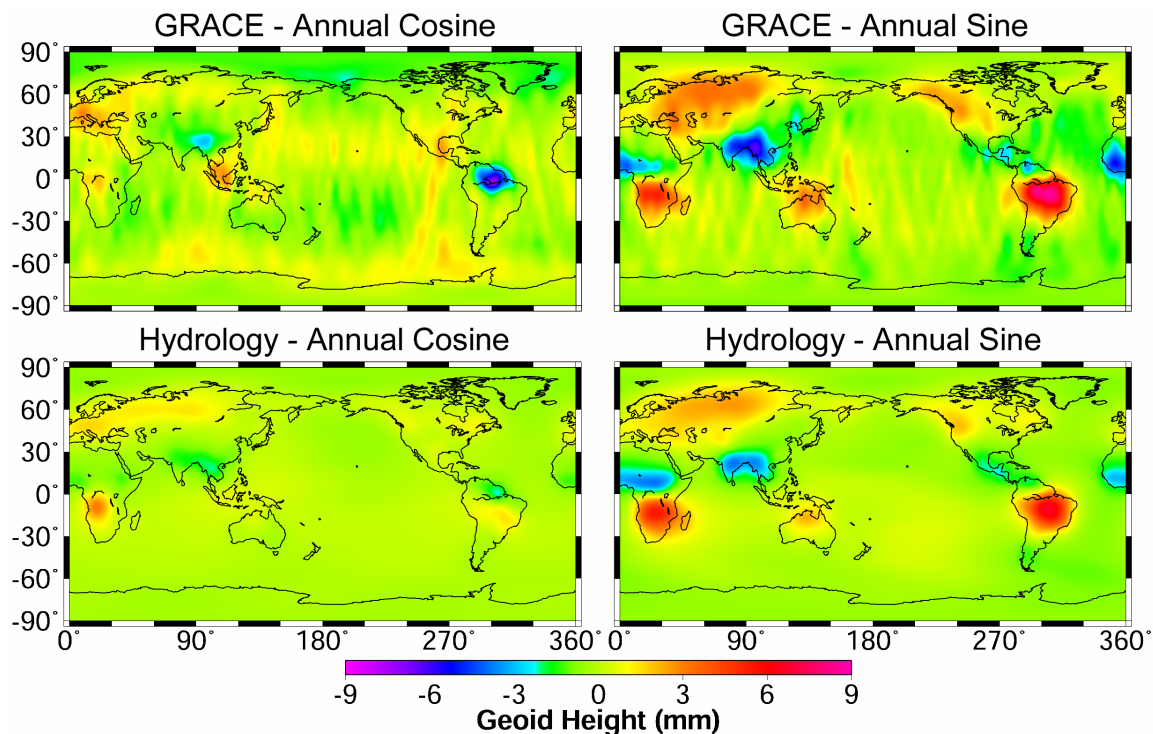


Figure 5.1. Annual variability of the geoid from GRACE and GLDAS hydrology. Geoid height anomaly using a 400-km smoothing radius and with the degree 2 coefficients omitted.

Figure 5.1 also illustrates an estimate for the annual geoid variability due to terrestrial water storage determined from the GLDAS output [Rodell *et al.*, 2004]. The same days and monthly averaging scheme used for the GRACE solutions were used to create the GLDAS results. The magnitude of the annual cosine component from GRACE ranged from -7.2 mm to $+3.0$ mm with a global RMS of 0.9 mm, where a negative value represents a variation that was opposite in phase from the positive values, peaking in summer rather than winter. The annual sine component ranged from -6.4 mm to $+8.9$ mm with a global RMS of 1.3 mm, with a negative value indicating a variation that peaked in fall rather than spring. The cosine component from the GLDAS model ranged from -2.3 mm to $+3.2$ mm with a global RMS of 0.4 mm, while the sine component ranged from -4.0 mm to $+6.7$ mm with a global RMS of 1.0 mm. Overall, the peak annual values across the globe were concentrated in the sine (spring-fall) component.

There is general agreement between the annual features observed by GRACE and the expected hydrologic signal; however, GRACE generally observed larger magnitudes for the variability on a regional basis. Furthermore, while GRACE estimates tend to be dominated by the un-modeled hydrological processes, they also contain a variety of other signals (both real and erroneous) that must be considered when interpreting the results and. As was shown in equation 5.7, perfect agreement with hydrological models is not necessarily expected. Also, as is commonly found with global continental hydrology models, GLDAS does not model deep sub-surface water, snow depth, or variability on the Antarctic continent. This may suggest that the GRACE results can in fact be used as an important additional constraint on the output of such global hydrological models.

5.5 SUB-ANNUAL, BASIN-SCALE VARIABILITY

The Amazon basin is a large watershed in which 20% of the region may be wetlands [Prigent *et al.*, 2001]. The relative importance of this basin for global

hydrology is evidenced by the fact that the water elevation change of a few cm (1-2 mm geoid) in the Amazon flood plain can be greater than the entire annual discharge, on average, of the Mississippi River [*Alsdorf and Lettenmaier, 2003*]. In Figures 5.2-5.12, the regional-scale variability of the geopotential over South America is shown as was observed by GRACE and is contrasted with the GLDAS continental hydrology model. The monthly variations are all taken relative to the 14-solution mean. Also shown are the global degree correlations between GRACE and GLDAS as was defined in equation 2.13; these are global statistics and are not specific to the region shown in the maps. This metric gives a sense of how well specific wavelengths are correlated for the observed geopotential variability (GRACE) and the largest unmodeled geophysical signal (i.e., continental hydrology). The 400-km smoothing radius used in these figures admits more error from the GRACE estimates, but the large signal in this region allowed for this smaller resolution along with a corresponding error of ~4 mm geoid anomaly for some of the months. Smaller regions or smaller amplitudes of variability would not allow for a 400-km smoothing radius to be used, that is, not without a significant reduction in the signal vs. error ratio for the time-variable gravity interpretations.

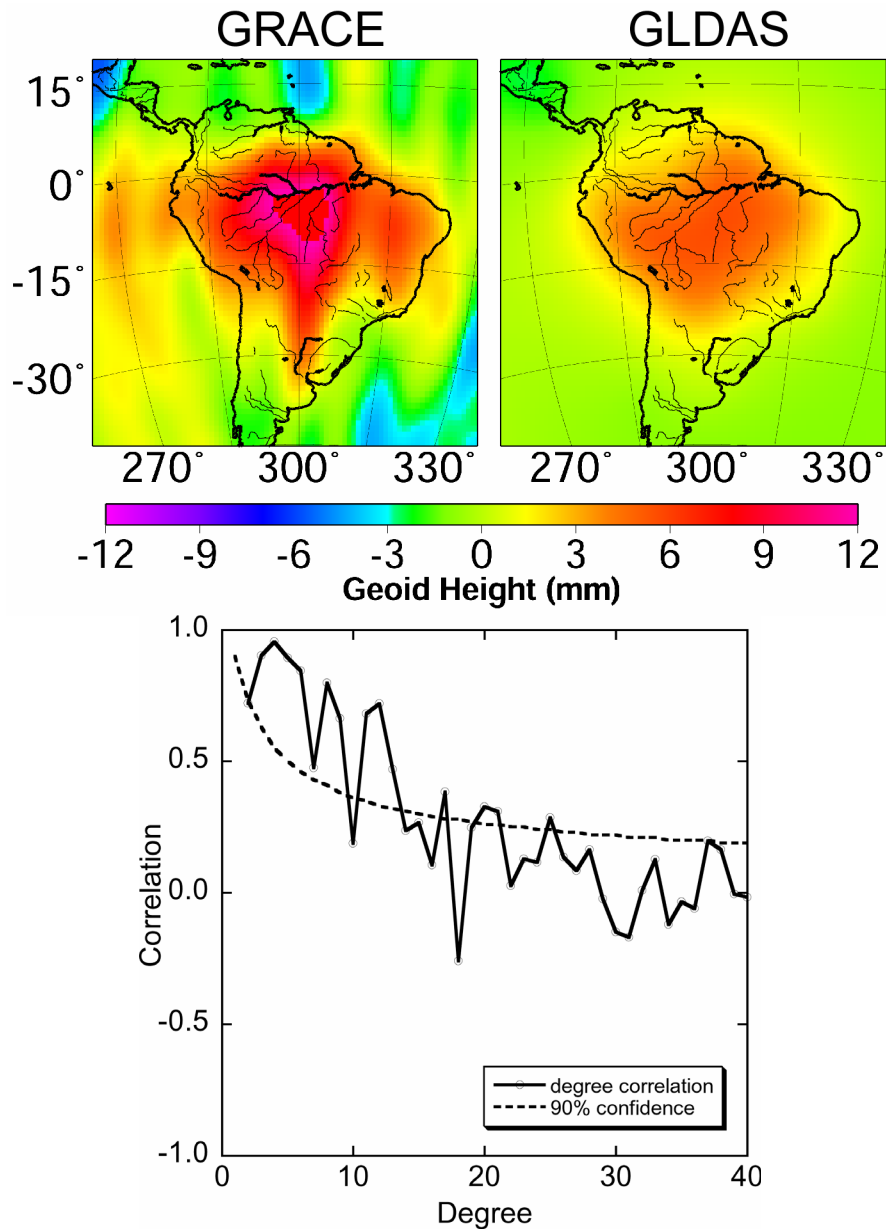


Figure 5.2. Time-variable gravity over South America in April/May 2002 for GRACE (top left) and GLDAS (top right), relative to the average of 14 monthly solutions. The degree 2 coefficients were omitted and a 400-km smoothing radius was used. Degree correlations between GRACE and GLDAS were computed for the global set of geopotential coefficients (bottom).

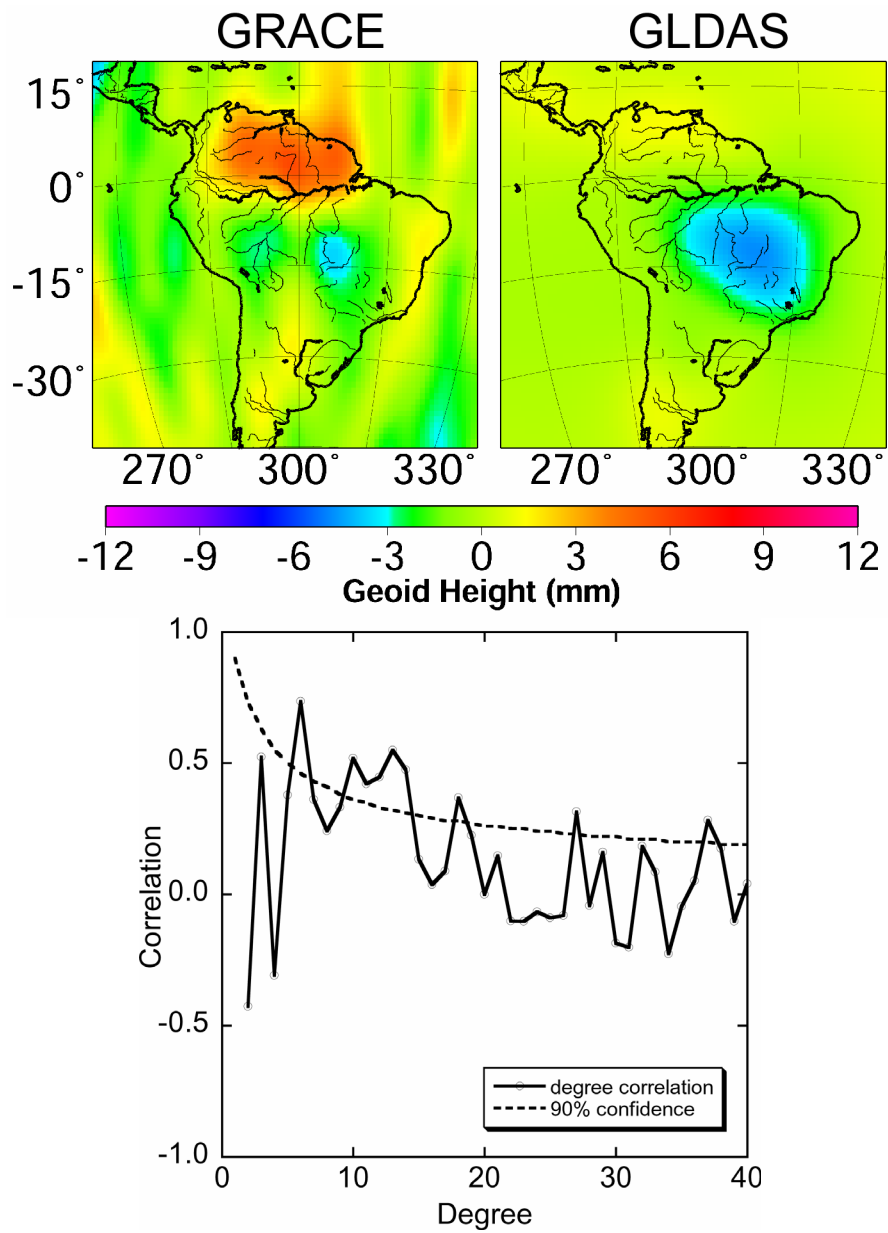


Figure 5.3. Same as Figure 5.2 for August 2002.

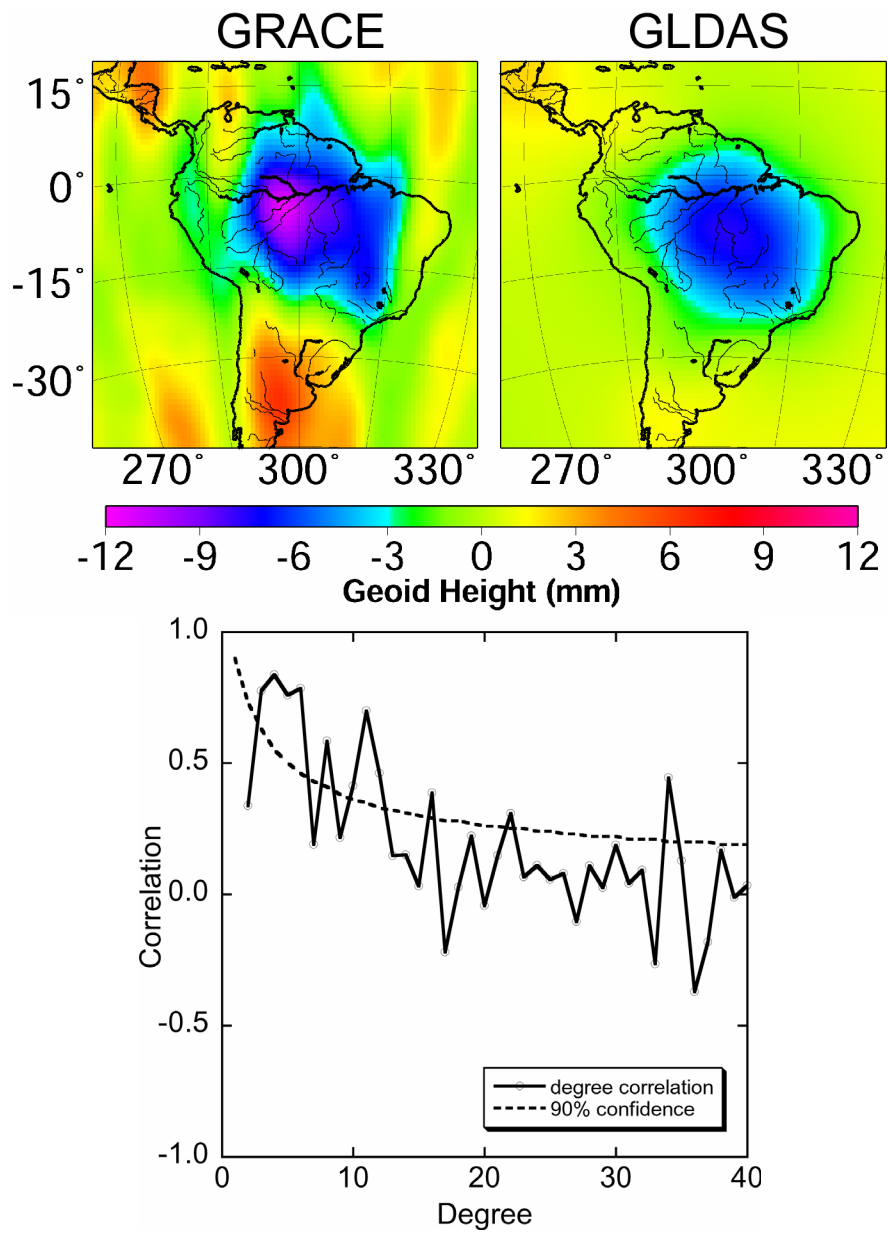


Figure 5.4. Same as Figure 5.2 for October 2002.

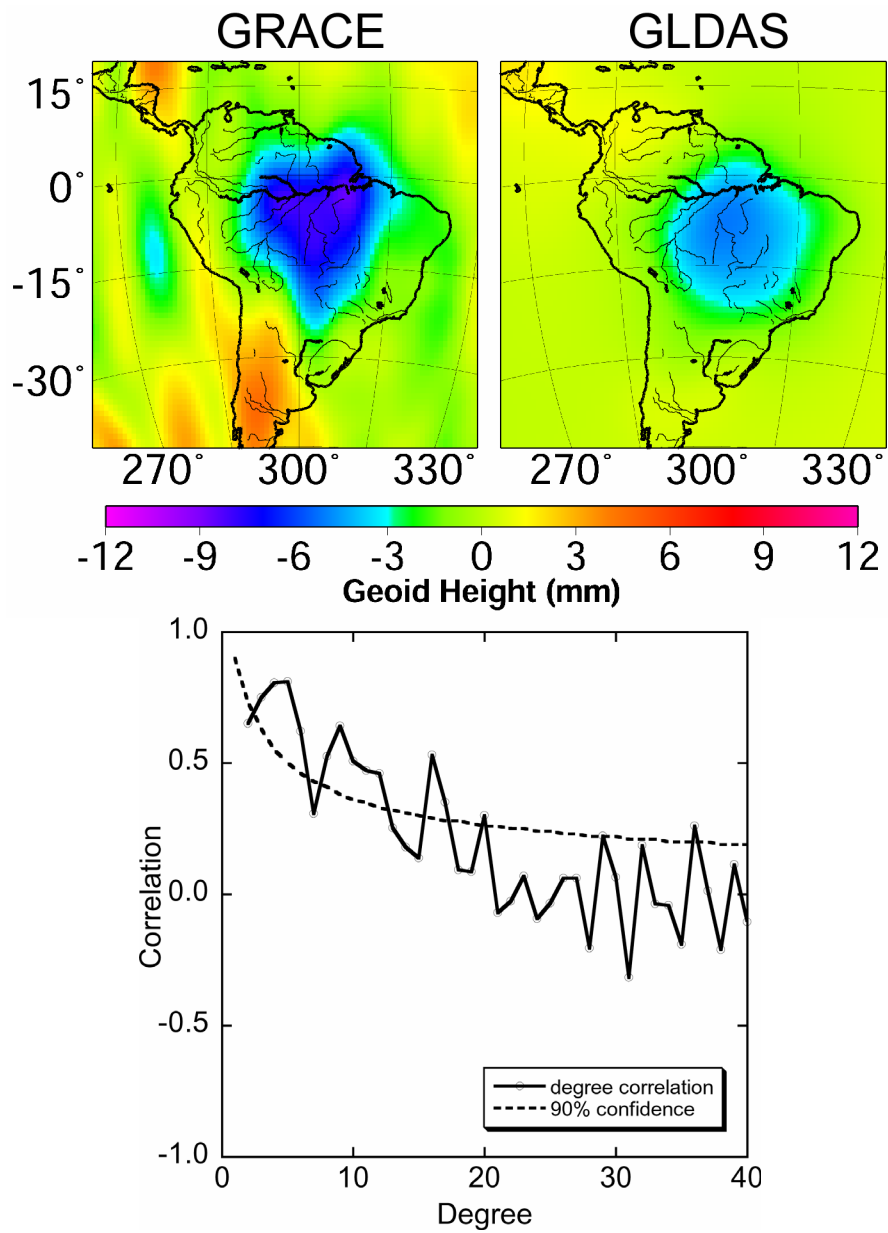


Figure 5.5. Same as Figure 5.2 for November 2002.

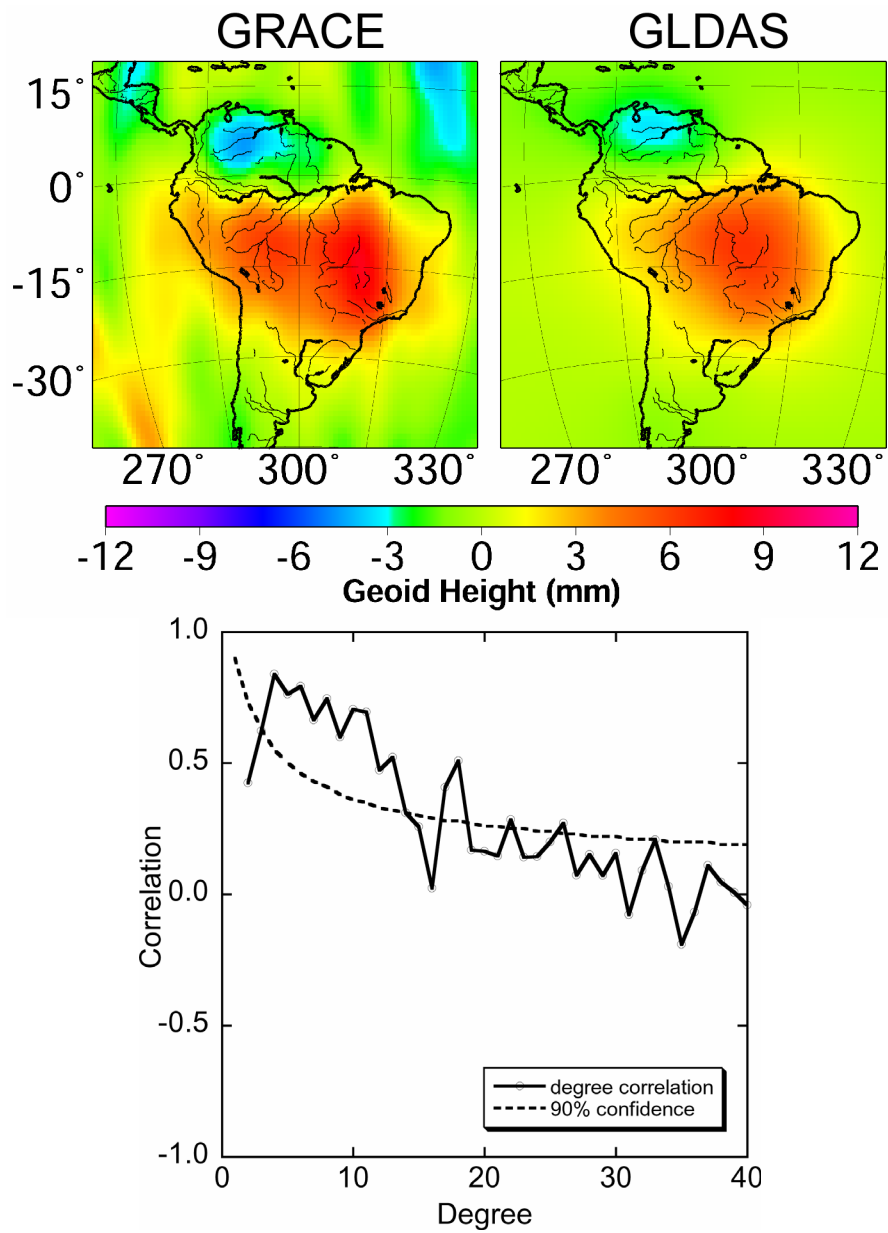


Figure 5.6. Same as Figure 5.2 for February 2003.

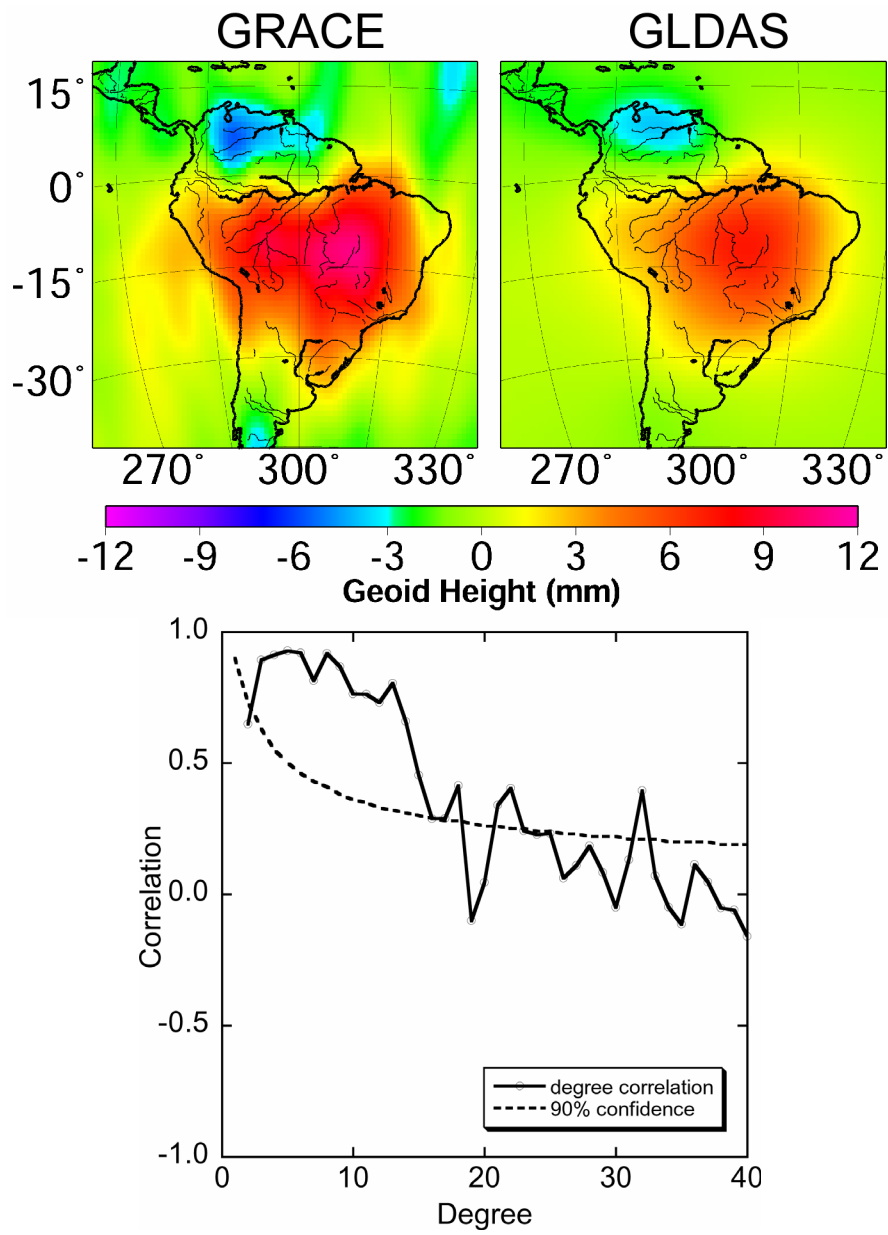


Figure 5.7. Same as Figure 5.2 for March 2003.

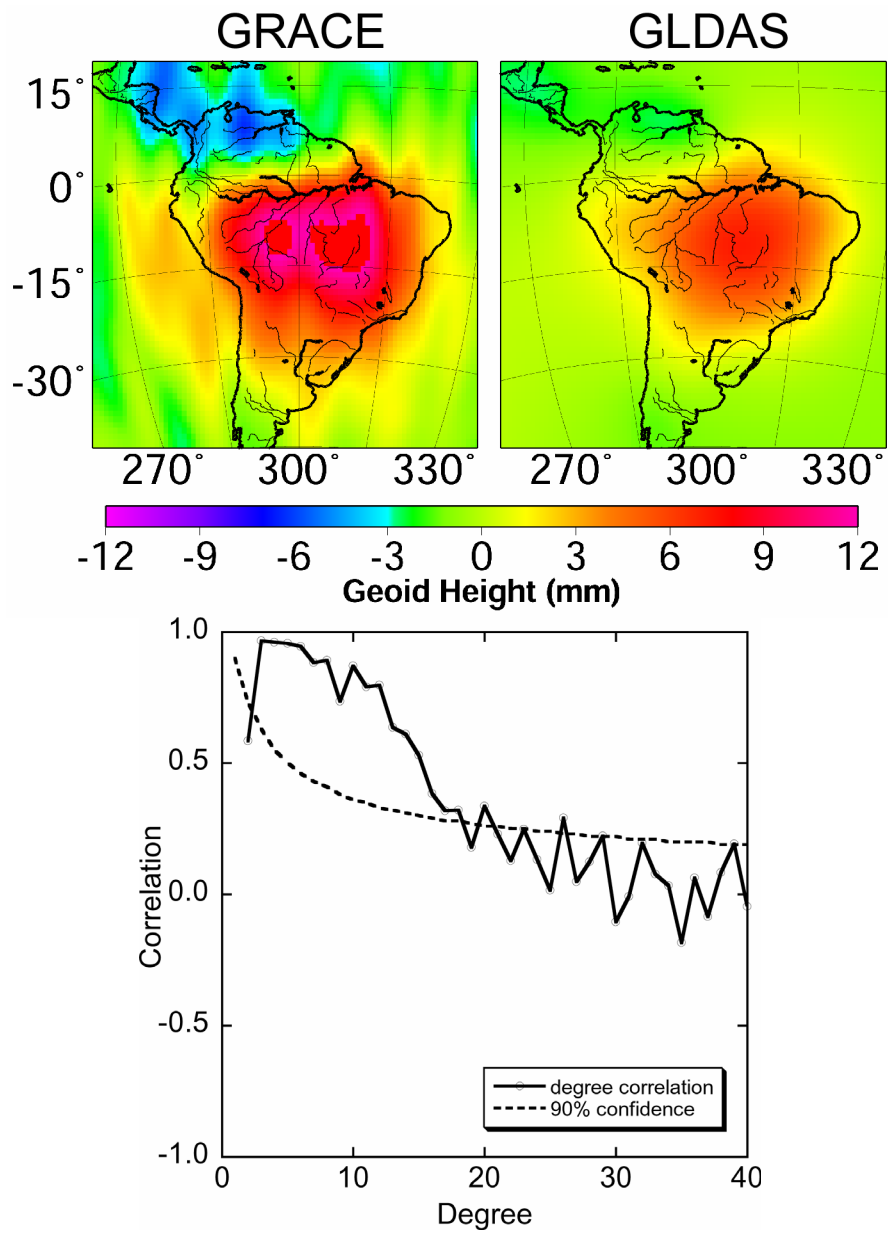


Figure 5.8. Same as Figure 5.2 for April 2003.

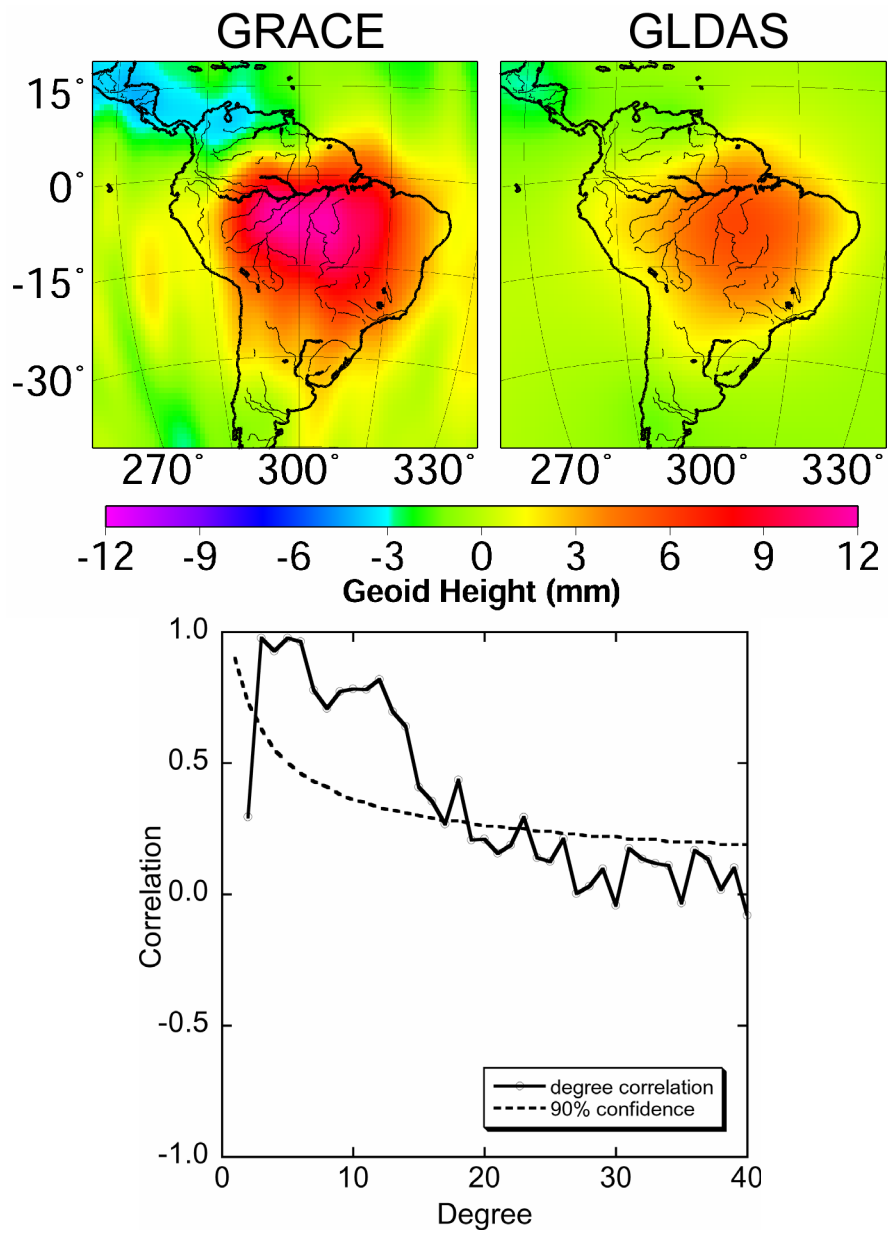


Figure 5.9. Same as Figure 5.2 for May 2003.

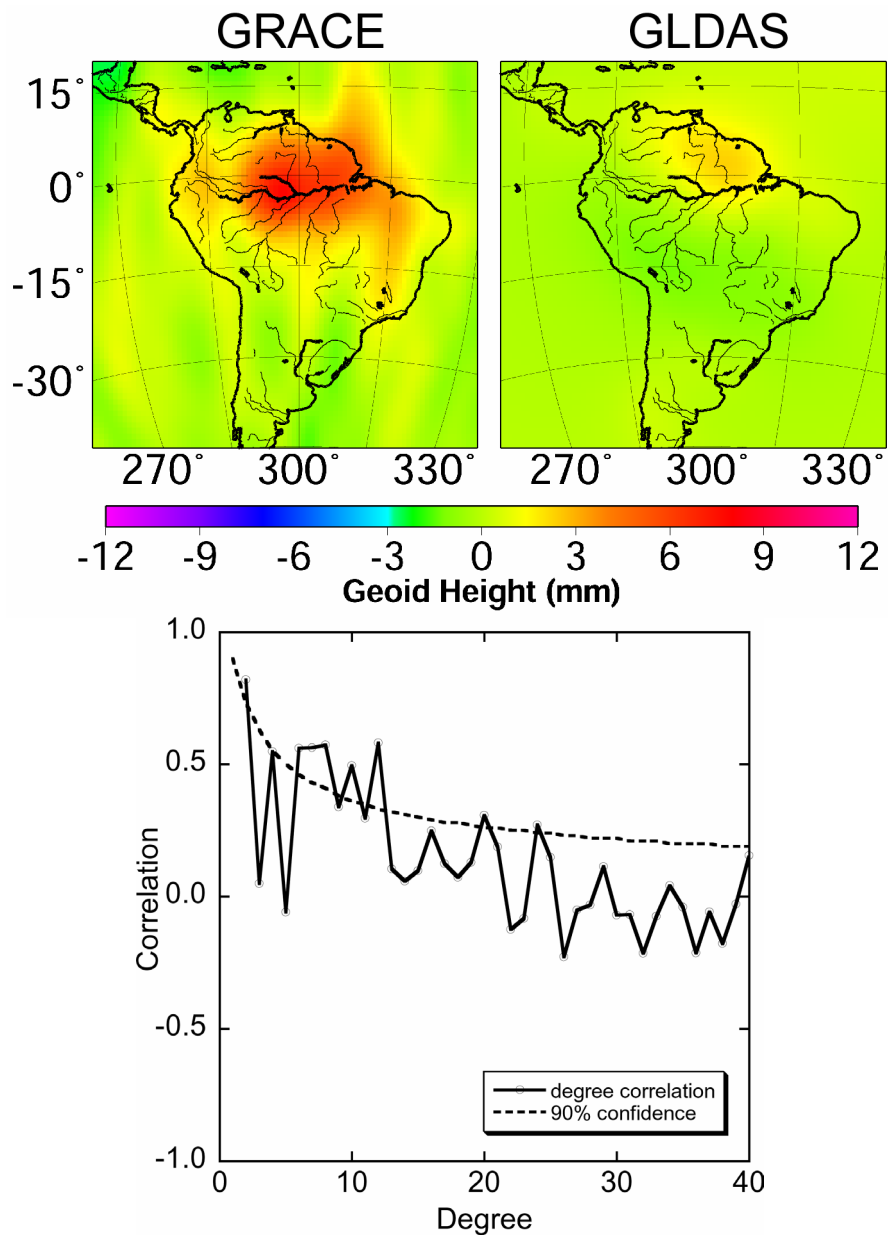


Figure 5.10. Same as Figure 5.2 for July 2003.

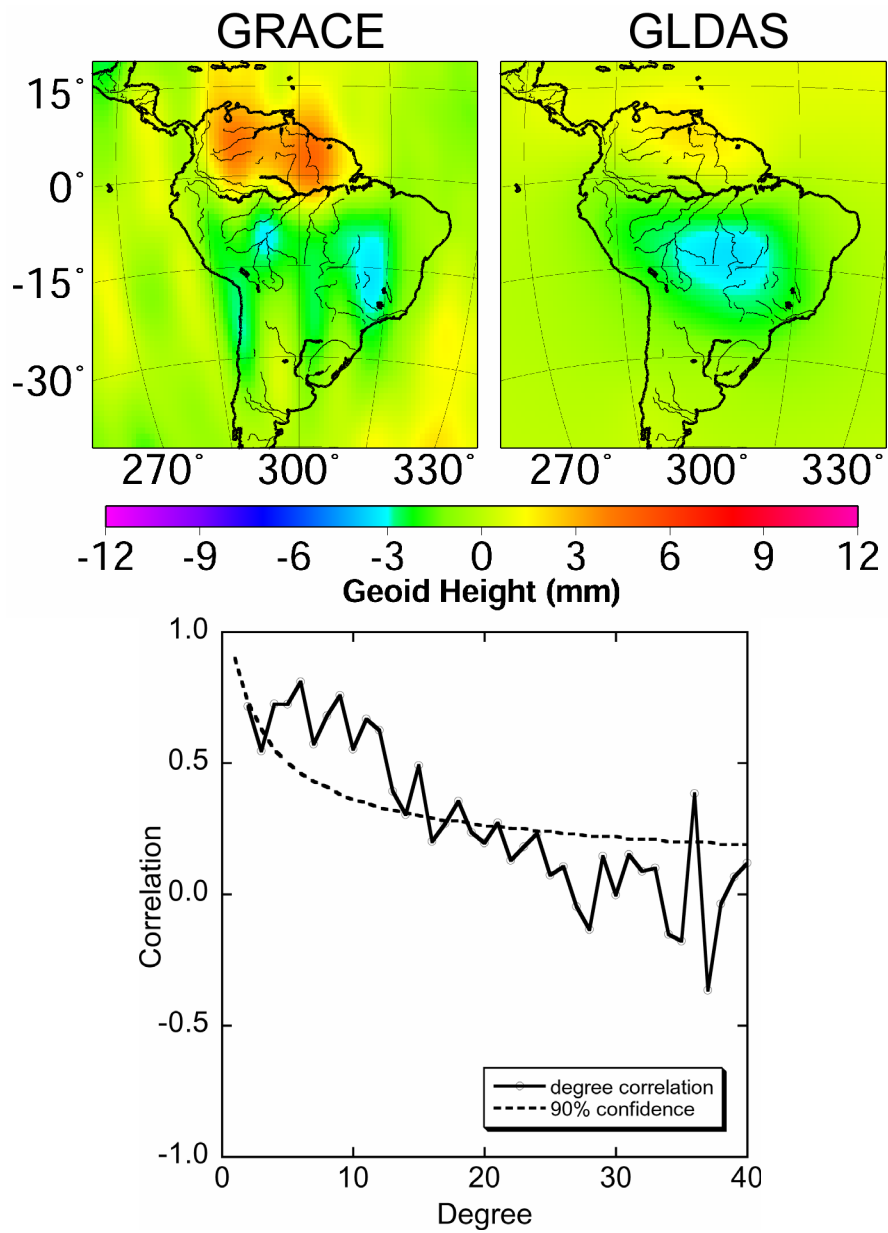


Figure 5.11. Same as Figure 5.2 for August 2003.

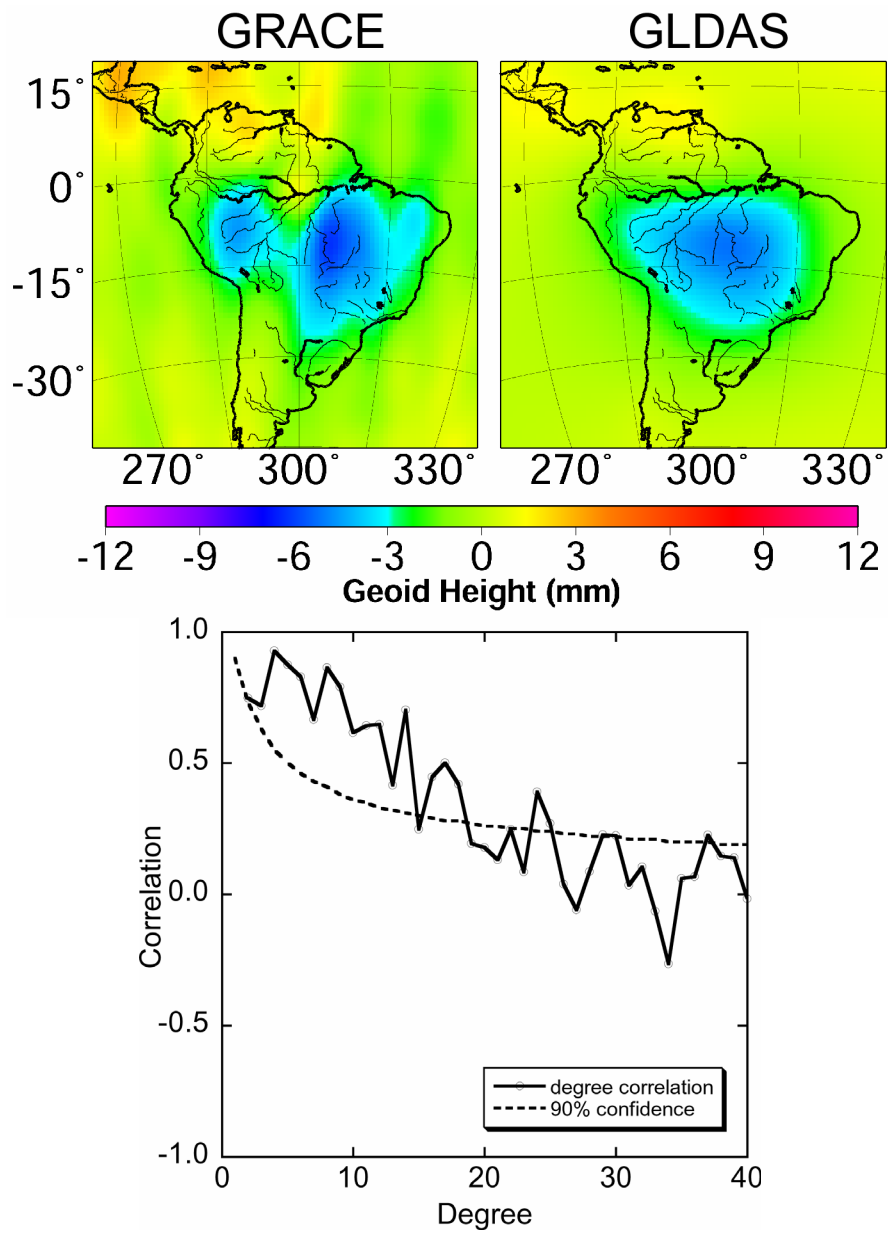


Figure 5.12. Same as Figure 5.2 for September 2003.

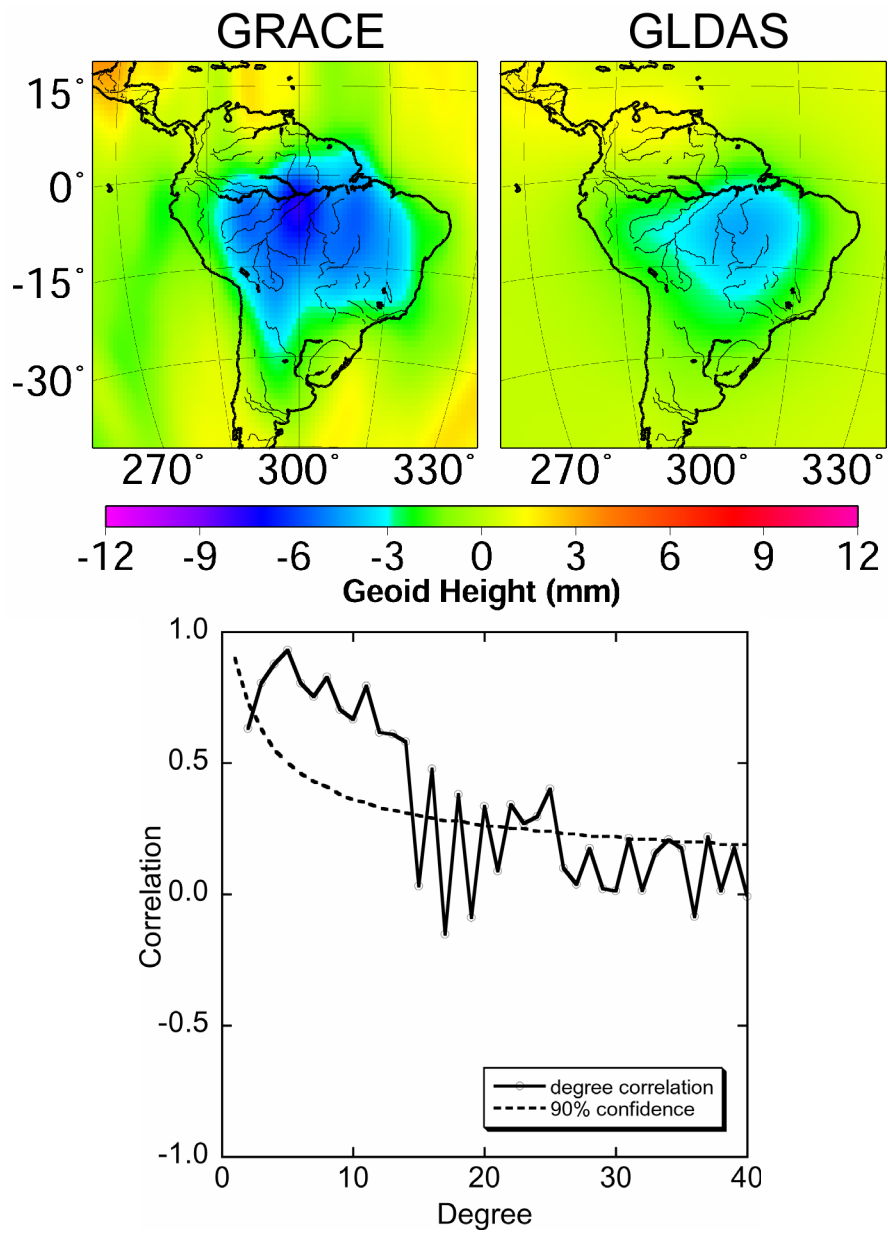


Figure 5.13. Same as Figure 5.2 for October 2003.

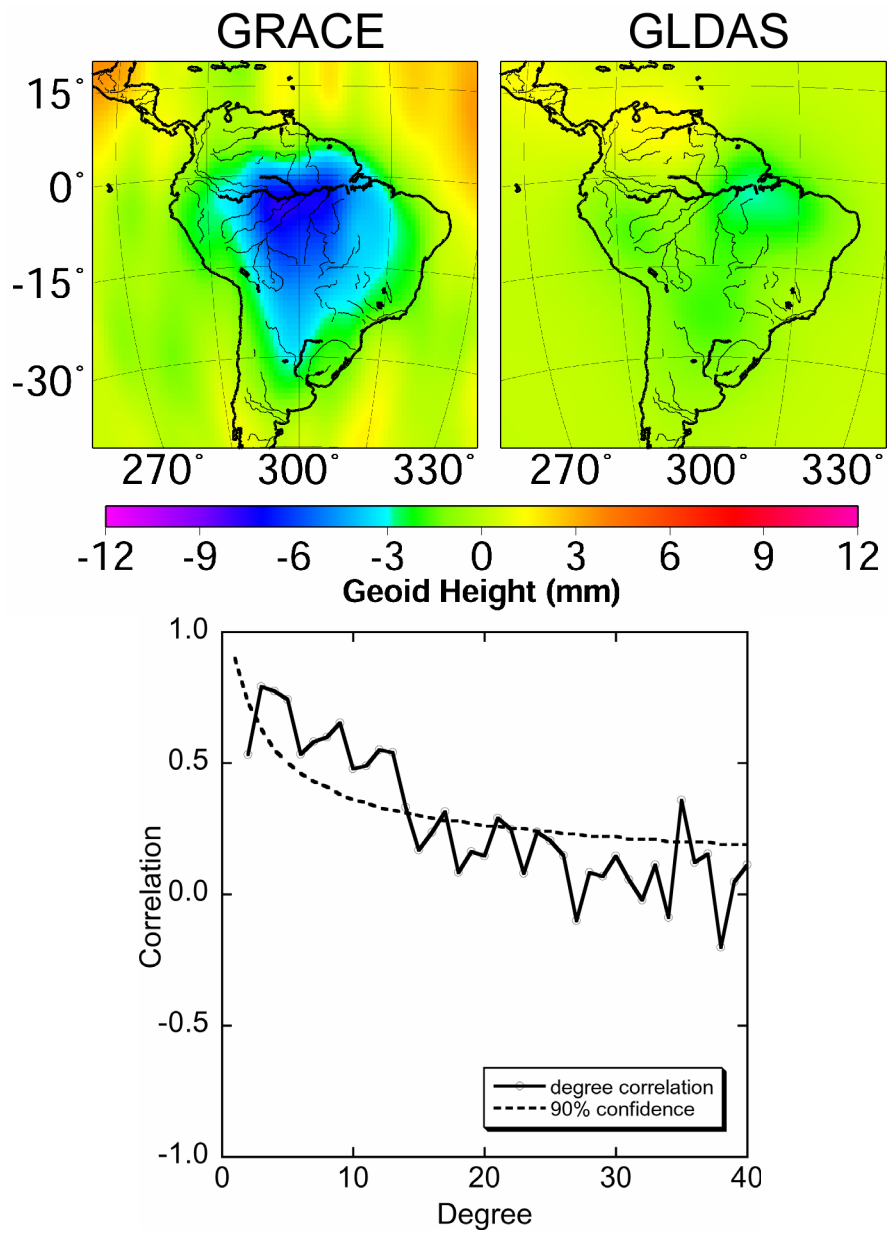


Figure 5.14. Same as Figure 5.2 for November 2003.

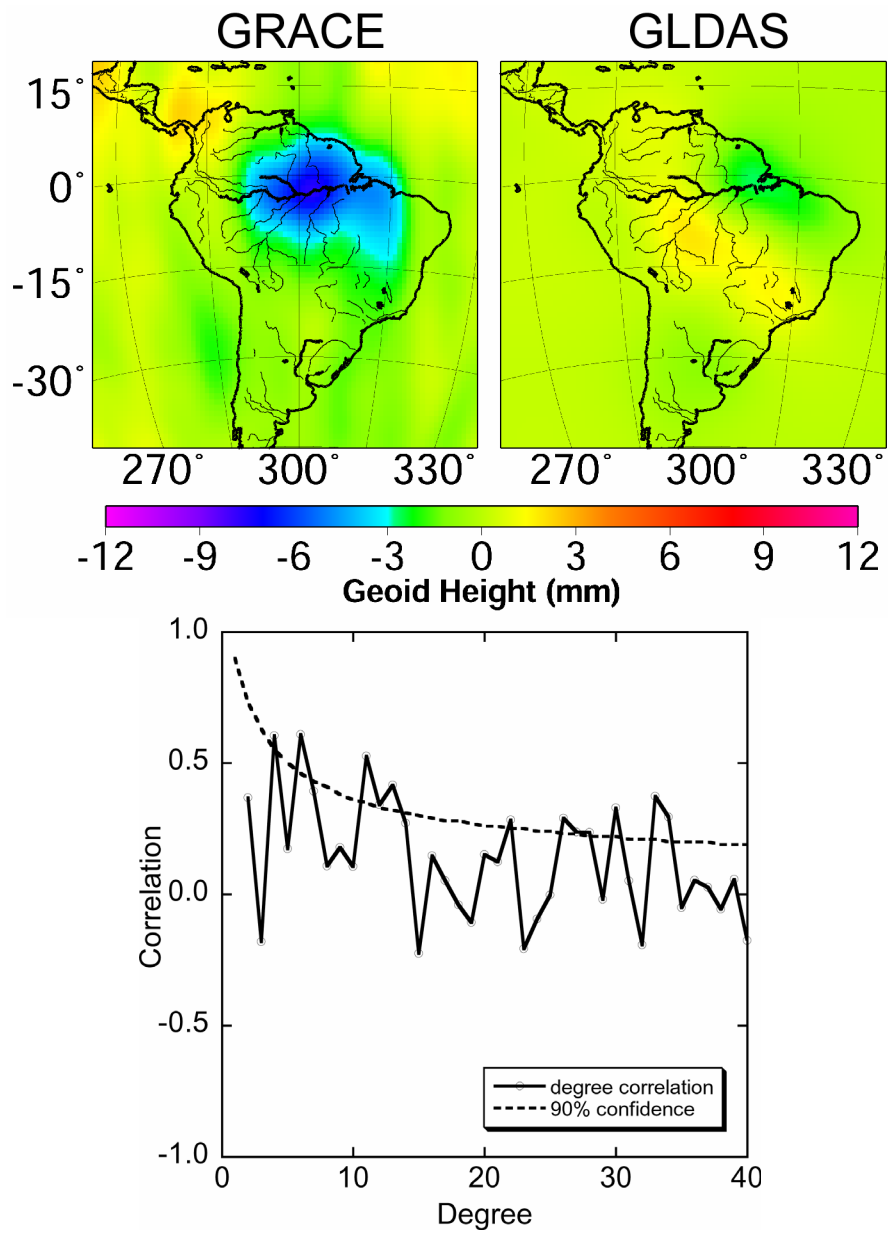


Figure 5.15. Same as Figure 5.2 for December 2003.

Spacecraft events resulted in insufficient date coverage or data quality in order to resolve the gravity field for some of the months during the time span contained by the 14 monthly gravity solutions. For example, January 2003 only had 14 days of usable data, making it difficult to define a “monthly” time span for that particular month. Also, during much of June 2003, data from one of the on-board accelerometers was unavailable, resulting in an incomplete data set for processing those days. As some of these types of issues are resolved, some, but not all, of these omitted months may become available in future data releases by the GRACE project.

For the Amazon basin, a local maximum of 14.0 mm relative to the mean was observed to occur in the month of April 2003 and a local minimum of -7.7 mm was observed to occur in October 2003. A clear separation was observed between the large Amazon watershed and the much smaller watersheds to the north, in particular, the Orinoco watershed. These two watersheds are separated both topographically (due to the Guiana Highlands) and meteorologically (due to the equator).

While GRACE and GLDAS are significantly correlated across a brand range of spatial wavelengths for many of the months considered, perfect agreement should not be expected. GRACE gravity estimates reflect not only the water sources contained within a geophysical model such as GLDAS, but also significant parts of the water cycle missing in most global hydrology models. For example, deep water storage (below about 2 meters) was not modeled, ice and snow flow was not modeled, and the entire Antarctic continent was removed from the GLDAS model.

Two things stood out in regards to the correlation between GRACE and GLDAS: the relatively poorer fit for degree 2 and the gradual reduction in correlation with increasing degree. A clear correlation between existed for most months, frequently showing that GRACE and GLDAS had some level of correlation up to degree 30-35,

corresponding to half-wavelengths on the order of 600 km globally. Beyond degree 35 or so, the GRACE monthly fields were dominated by error in comparison to the expected geophysical signal. These factors suggested that smoothing the GRACE gravity fields with a degree dependent (i.e., spatially wavelength dependent) weighting was an appropriate thing to do.

While the GRACE degree 2 terms were significantly correlated to the expected hydrologic signal, they were more weakly correlated relative to the results for the adjacent degrees ($>$ degree 3). This is not unexpected, and larger relative error was predicted by simulations (chapter 3) [Kim, 2000] and has been observed in the processing of real GRACE data (chapter 4) [Tapley, 2004a]. This is an important issue for time-variable gravity results from GRACE that are compared to geophysical model predictions; the error at these long wavelengths (low degrees) for GRACE will dominate the analysis. There may be a large real signal in the degree 2 coefficients relative to the error in those coefficients. However, in order to focus on the wavelengths that are best resolved by GRACE, the features of the degree 2 coefficients needed to be removed before the comparisons to geophysical models were made.

This is an instance where SLR analysis as conducted in chapter 2 may continue to contribute to the study of time-variable gravity. The degree 2 terms predicted from geophysical models were shown to have a better correlation when compared to SLR observations than when compared to the GRACE observations. Of course, the caveat is that in order to support or constrain GRACE results, SLR data and results will have to be processed in a manner consistent with GRACE data processing. Specifically, the background models of variability used to process the SLR observations in chapter 2 were not the same as the models of variability used to process the GRACE observations. This difference leads to different interpretations for time-variable gravity as observed by

the two methods (SLR vs. GRACE). Care must be taken to ensure that the variability determined from different methods is due to the same processes, for example, continental hydrology. A comparison should not include the effects that have been removed in one instance and not the other, for example, the AOD model that has been removed from the GRACE gravity estimates but not the SLR gravity estimates.

5.6 SPATIAL RESOLUTION

The nature of the errors in different monthly solutions will vary from month to month due to a combination of factors: ground-track coverage, temporal coverage (i.e. missing days), mis-modeled short-period variability, spacecraft events, and data noise. While a 400-km smoothing radius was selected to illustrate annual variability (Figure 5.1) and large amplitude regional signals (Figures 5.2-5.15), this was not necessarily the smoothing that was appropriate for the entire globe for all possible monthly solutions. In order to extract mass variability for specific watersheds, specialized methods of spatial weighting may be more appropriate for taking into account the unique features of a region [Swenson and Wahr, 2002]. The smoothing needed to resolve the signal relative to the errors in the GRACE observations of time-variable gravity depended upon the spatial region of interest as well as the time scale span of interest (monthly versus annual time intervals and global versus regional spatial scales).

There was a clear difference between the monthly GRACE gravity solutions that roughly divided the solutions into two classes: one for the year 2002 and another for the year 2003. The error in the gravity field solutions was slightly reduced soon after changes to the onboard satellite software were implemented in early 2003. A software update for the star camera enabled improved attitude control reconstruction, which resulted in better quality data to be used in the producing the gravity field solutions. Unlike improvements introduced in ground processing, this type of flight software update

can not be retroactively applied. The year 2002 solutions may continue to have a reduced level of accuracy relative to later solutions. This did not make the earlier gravity solutions from 2002 inadequate for analysis, but they did require more smoothing in order to better resolve the time-variability gravity signal relative to the higher degree errors. Such differences in accuracy will continue to make it challenging to compare various monthly solutions that were derived from different data quality and with different levels of error.

The question remains: what level of error is acceptable for a particular application? Using the calibrated error for the monthly solutions, a level of error on the order of 2-3 mm geoid height anomaly for any region on the globe corresponded to signals resolved at spatial scales of ~ 1000 km for the 2002 solutions, while the 2003 solutions were resolved to ~ 400 -600 km. Reducing the amount of smoothing (i.e., smaller smoothing radius) will allow smaller features to become apparent; however, the amount of error in the solution may quickly increase beyond the 2-3 mm level without a significant change in the magnitude of the time-variable signal at the longer spatial wavelengths. More aggressive smoothing (i.e., a larger smoothing radius) may reduce the error even further than illustrated herein, but at the expense of removing more of the interesting time-variable signal. The trade-off will continue to be based on the level of error that the user is willing to accept.

The error structure for two solutions that have different levels of overall error due to data quality is illustrated by a solution for April 2002 and another for April 2003, relative to the average of the 14 monthly solutions (Figure 5.16). These two solutions show that the annual cycle was closely but not exactly repeated. The caveat being that the smoothing radius used was not the same for these two months; there is significantly more smoothing for the April 2002 gravity solutions (1000-km Gaussian radius) relative

to the April 2003 solution (600-km Gaussian radius). This does not allow for a direct quantitative comparison since the magnitude of the signal is dependent upon the level of smoothing; however, a qualitative comparison can be made. Another important difference is that the definition of “monthly” was different between the two solutions. While the April 2003 solution uses days entirely within the calendar month, the 2002 solution required a mix of days in April and May.

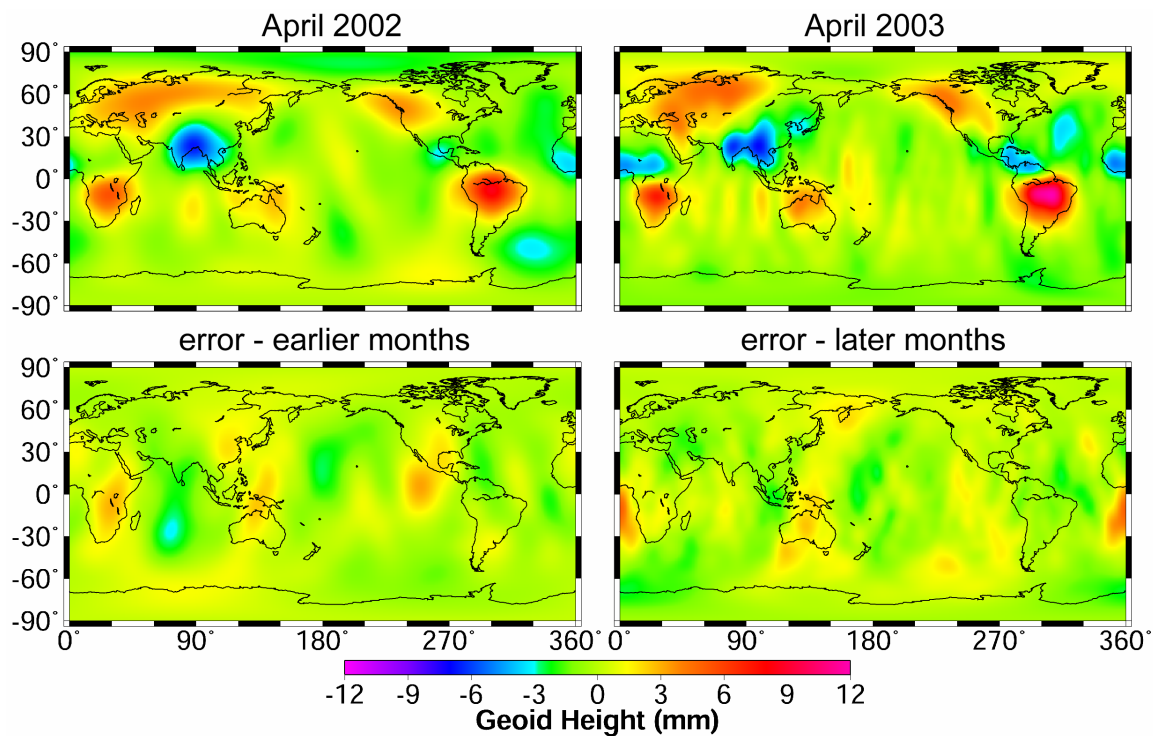


Figure 5.16. Comparisons of signals and errors. Observed geoid height differences relative to a mean geoid (top) and a representation of the expected errors at the same levels of smoothing (bottom) for the April 2002 (left) and April 2003 (right) solutions. A 600-km smoothing radius was used for 2003 and 1000-km for 2002 (degree 2 coefficients not included).

As previously mentioned, the calibrated error differed in the 2002 and 2003 solutions. The error in both cases was based on an approximate calibration of the formal

error covariance taken from a variety of solutions that used the same data or data of similar quality [Tapley *et al.*, 2004a]. This error covariance represents the likely amount of error, but not necessarily the actual errors. The utility of this covariance is that it can be transformed into a randomly generated set of errors that could be applied to the individual coefficients while still being representative of the error that was possible. This is still not the true error, but it can provide a means of calculating how the error might be realized for a particular set of solutions. Two examples of how this error may be realized in terms of a map of geoid height anomaly are also shown in Figure 5.16. What they illustrate is how the error may have spatial features that can appear both in regions where such features are unexpected (e.g., the Pacific Ocean), while also appearing in regions where large signals can mask this level of error (e.g., the Amazon basin). Using the calibrated error to produce realizations of possible error, in order remain at approximately at level of 2-3 mm error in geoid anomaly, the 2002 solutions required a Gaussian smoothing radius of 1000 km while the 2003 solutions permitted a less aggressive level of smoothing using a Gaussian smoothing radius of 600 km.

5.7 DISCUSSION

GRACE was able to resolve variations in the gravity field for a range of spatial scales, down to 400 km for particular time scales and specific regions with large signals. In some cases more aggressive smoothing was required to reduce the high degree (short wavelength) errors. The global monthly solutions required an approximately 600-km smoothing radius for the 2003 solutions, while a 1000-km smoothing radius was more appropriate for the 2002 solutions. In all cases, the degree 2 coefficients were removed before producing maps of the global geoid variability due to the relatively high level of error that masked the real signal at smaller spatial scales (i.e., > degree 2). This suggested that SLR observations still may still contribute to time-variable gravity studies

as SLR observations may produce low-degree geopotential coefficients that correlate more closely with the real geophysical signal.

Basin-scale variability was observed for the particularly active region of South America, resolving differences between neighboring watersheds such as the Amazon and the much smaller Orinoco. Significant correlation was observed globally between GRACE and a representative continental hydrology model (GLDAS), with degree correlations suggesting that sensible signal had been resolved up to approximately degree 30-35, consistent with smoothing radii of several hundred kilometers. While re-processing of the data will improve the accuracy of the GRACE solutions, interpretation requires an understanding of the interaction between the atmosphere, ocean, and land hydrology. Converting GRACE time-variable gravity results into changes in mass within a particular Earth subsystem will require improvement in the sophistication and accuracy of the models of “known” variability as well as recognizing how the acceptable level of error will depend upon the temporal and spatial scales of interest to a particular researcher.

Chapter 6: Conclusions and Recommendations

6.1 CONCLUSIONS

It was possible to show good agreement for the annual cycle in Earth's geopotential as observed from SLR data and one derived from geophysical models, particularly through the inclusion of a continental hydrology model. The agreement was on spatial scales on the order of ~ 5000 km (degree and order 4 gravity field) to about the level of 1 mm geoid anomaly and with degree correlations that generally exceeded the 90% confidence limit. It was clear that in order to explain the geoid variability observed in the Lageos SLR analysis for the annual sine term, a source of mass variability other than atmospheric was required. The NCEP and ECMWF pressure fields compared equally well to the SLR results. For the ocean models, the altimetry-based model (TOPEX/Poseidon) performed slightly, but consistently, better than the numerical model predictions (POP). The most significant difference was observed in the comparison between the continental hydrology models, with the CPC model significantly outperforming the CDAS-1 model. This may be due to the particular nature of the deficiencies of the CDAS-1 model; on a regional basis the maximum and minimum magnitudes of the CDAS-1 model do not occur at the appropriate times (i.e., the phase is wrong), and the frequency of the variations is not consistent with known forcings [*Rodell and Famiglietti, 1999*].

Using orbital simulations of the GRACE spacecraft, I investigated the impact on gravity recovery due to short period, non-tidal temporal mass variability in the atmosphere, oceans, and continental hydrology. Qualitatively, the level of aliasing error was strongly correlated to the high-frequency power present in the models. Degree error

relative to measurement error increased by a factor of ~ 20 due to atmospheric aliasing (corresponding to geoid anomalies of approximately 1 mm at 500-km wavelengths), by a factor of ~ 10 due to the ocean model, and by a factor of ~ 3 due to the continental hydrology model. The benefits of de-aliasing were most evident at the middle to higher degrees while the error at the lowest degrees ($\sim 2-5$) was dominated by other aspects of the GRACE processing methods. For the atmosphere, the residual aliasing error after de-aliasing the ‘true’ mass variability (ECMWF) with an approximate model for the atmosphere (NCEP) was $\sim 1/5$ that of the aliasing error due to a completely unmodeled atmosphere. A barotropic ocean model reduced the aliasing error due to a baroclinic model to nearly the level of measurement noise. Aliasing error predictions based on an NCEP-class continental hydrology were limited by the lack of significant short-period variability. The aliasing error due to a model with such a temporal spectrum was below the level of even an optimistic estimate of the error present after partially de-aliasing the atmospheric effects. In other words, the atmosphere model would have to be improved beyond the current level of accuracy (i.e., approximately the disagreement between ECMWF and NCEP) before a hydrology model similar to the one used in this study would have a significant impact.

The AOD model provided by GFZ and adopted for GRACE processing was shown to result in more accurate gravity solutions. This occurred due to the reduction of the effects of temporal aliasing due to the non-tidal, short period mass variability of the atmosphere and ocean. Aliasing simulation results using NCEP atmospheric pressure data to de-alias the AOD model were consistent with the residual effects of aliasing due to an unmodeled ocean (see appendix A). Using a number of different tests and metrics, accuracy was shown to have consistently improved for solutions that used AOD model during processing. The greatest impact was found to be a reduction of error at the highest

degrees, with the lowest degrees (approximately < 10) being relatively less affected. Highest degrees were better resolved when compared to a surface gravity derived model (TEG4). Ocean circulation statistics comparing velocities derived from the gravity solutions and those based on the Levitus oceanographic atlas showed improvement or no change; significant improvement was shown for the meridional component. Orbit fits with other spacecraft based on these gravity solutions indicated overall improvement for those spacecraft most sensitive to mid-degrees or higher. Time variable gravity interpretations at relatively long wavelengths (> 600 km) were not significantly impacted by the use of the AOD model. Decreased time-variable gravity signal decreased at the higher degrees (approximately > 20) indicated less error overall as the signal at the shorter spatial wavelengths was dominated by error rather than real geophysical signal.

GRACE was able to resolve variations in the gravity field for a range of spatial and temporal scales, in particular, down to 400 km spatial scales for the global annual variability or at monthly time intervals for specific regions with large signals (e.g., the Amazon Basin). In other cases more aggressive smoothing was required to reduce the high degree (long wavelength) errors, thereby reducing the ability to resolve spatial features to the 400-km level. The global monthly solutions required an approximately 600-km smoothing radius for the 2003 solutions while a 1000-km smoothing radius was more appropriate for the 2002 solutions. The annual cycle in the geoid variations observed by GRACE peaked predominately in the spring and fall seasons, with amplitudes up to ~ 10 mm observed in some regions. The South American continent was chosen to highlight regional-scale variability and there was observed a clear separation in signal between the large Amazon watershed and the smaller watersheds to the north. Comparisons of terrestrial water storage estimates from GLDAS to GRACE observations indicated a high degree of correlation up to spatial wavelengths of 600 km or larger,

frequently above the 90% confidence level on a monthly basis. In all the time-variable gravity cases, it was necessary to remove the degree 2 coefficients before producing maps of geoid variability for the purpose of comparing with continental hydrology models. This limitation suggested one way in which SLR observations may still make useful contributions to the longest spatial wavelengths for time-variable gravity. The results of chapter 2 indicated that annual cycle observed by SLR observations agreed well with geophysical model predictions. The challenge will be producing time-variable gravity results from SLR that are consistent with GRACE processing methods, that is, time-variable gravity that can be interpreted as being from the same geophysical phenomenon.

6.2 FUTURE WORK AND RECOMMENDATIONS

It is important that the background time variable models used in GRACE processing contain a reasonably accurate representation of the high-frequency content in the Earth's systems; therefore, accurate estimates of the uncertainty in these models are needed for predicting the level of aliasing error that may be present from using these models. For example, the atmospheric de-aliasing error predictions may be an underestimate and the de-aliasing conclusions optimistic because the errors in the two fields used (ECMWF and NCEP) are partially correlated.

Competitive models sufficiently different from the POP model were not used to assess the inherent accuracy of ocean models in general. The de-aliasing simulations with the ocean models primarily tested the assumption that a barotropic model was sufficient for describing high-frequency ocean behavior. A barotropic model is currently used to model the shorter period variability for the production of GRACE gravity estimates [*Ali and Zlotnicki, 2003*].

An NCEP-class model may even be of limited value in assessing variability at the monthly time scales, requiring models with higher spatial and temporal resolutions in

order to compare with expected GRACE gravity recovery [e.g. *Rodell and Famiglietti, 1999*]. Even if using this type of model in GRACE processing resulted in a more precise gravity estimate, it may introduce significant errors in interpreting monthly gravity solution changes as continental hydrological mass variability. The definition of “time-variable gravity” depends upon what nominal mass variability was assumed during processing. Introducing a model (continental hydrology) that contains more uncertainty than other models already present in the processing stream (e.g., the atmosphere and ocean) may overly complicate the interpreting the time-variable gravity signal.

As accuracy improves, the AOD model may have a more significant impact, but not necessarily the most significant impact. Errors arising from all the different sources of variability may need to be re-considered—modeled sources (e.g., ocean tides) and unmodeled sources (e.g., continental hydrology). Interpretation of the GRACE gravity products (i.e., time-variable gravity) requires an understanding of the interaction between the atmosphere, ocean, and land hydrology as well as understanding the assumptions made during processing to account for some of the “known” geophysical mass variability.

Figure 6.1 summarizes the error assessments in this study based upon both simulated data and real GRACE data processing. The “measurement noise” error curve is based on simulations that contained no other errors sources (e.g., temporal aliasing) and is consistent with previous error assessments [e.g., *Kim, 2000*]. It is an optimistic level of error achievable only with perfect time-variable *a priori* models. A more realistic, though still optimistic, error assessment includes the effects of temporal aliasing as based on the simulated gravity recovery results of chapter 3. The “aliasing error” curve is due to the combined effects of a partially modeled atmosphere, a partially modeled ocean, and completely unmodeled continental hydrology. As the errors in these

geophysical models are better understood or the models are improved, this error assessment should be adjusted.

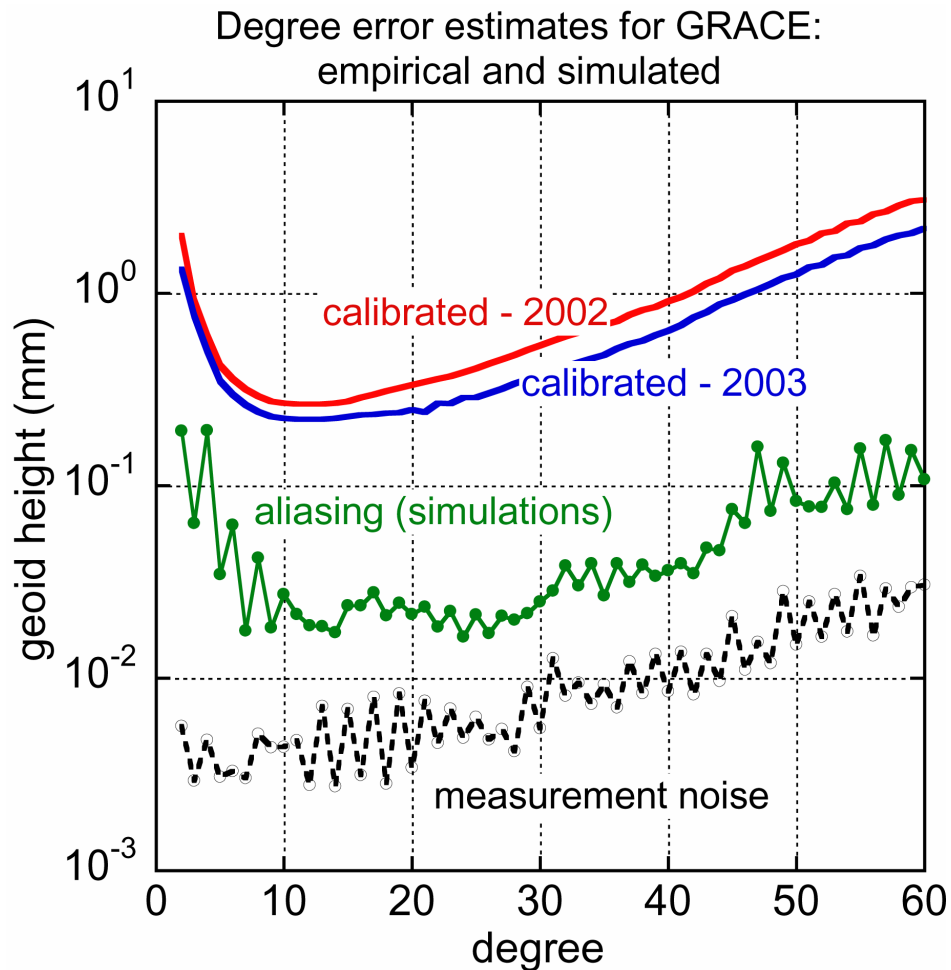


Figure 6.1 Error estimates for GRACE based on simulated and empirical results. Simulation results represent a type of lower bound in the level of error achievable and the empirical results represent an upper bound on the level of error that has been achieved to date. The “measurement noise” and “aliasing” error are based on the aliasing simulations of chapter 3, while the calibrated errors are based on the real-data processing that produced the GRACE solutions used in chapter 5.

Also shown in Figure 6.1 are the calibrated error estimates for both the earlier and later monthly solutions as discussed in chapter 5. The primary difference between these two levels of error arising from onboard software updates implemented in early 2003. These error curves differ from the others as they are based on real data processing experience rather than idealized simulations. Future re-processing of the current data with improved methods is expected to increase both the resolution and the accuracy, reducing the calibrated error. It is reasonable to denote the simulated error results as a lower bound on errors while the calibrated errors represent an upper bound. The true errors level of GRACE errors will continue to be somewhere in-between as the two types of error curves converge.

Appendix A: AOD Model Description and Implementation

The atmosphere-ocean de-aliasing (AOD) model consists of two primary components: ECMWF surface pressure data and a barotropic ocean model driven by ECMWF winds. The details of this combined atmosphere-ocean model as generated by GeoForschungsZentrum (GFZ) Potsdam are contained described by *GRACE Project* [2003]. Discussed herein is a summary of the details relevant to understanding the basic properties of the model, details of the AOD Release 01, a description of how the model was implemented in GRACE processing while the researches in this dissertation was conducted, and how the AOD model affected the usage of GRACE science products (e.g., the gravity field estimates). Furthermore, the orbital simulations of GRACE gravity conducted to test the aliasing impact of the AOD model were found to be comparable with the aliasing results for an unmodeled atmosphere. Simulated de-aliasing of the AOD model using NCEP atmospheric pressure data as an approximate model of the AOD variability gave error results consistent with the residual effects of aliasing due to an unmodeled ocean.

A.1 ATMOSPHERIC DATA

GFZ extracts operational analysis data provided by the ECMWF Integrated Forecast System (IFS). The spatial resolution of the atmospheric data is defined on a Gaussian grid that corresponds roughly to 0.5° . It has a temporal resolution of six hours and is defined at the synoptic times of 0, 6, 12, and 18 hr UTC. To prepare the data for incorporation into the AOD model, the ECMWF data is first transformed to point values of the surface pressure on a regular equiangular grid, representing the pressure for the mean value of the grid cell. Comparisons by GFZ found that the ECMWF operational

data has a slightly larger signal and much higher spatial resolution compared to NCEP atmospheric data. There are also differences between these models at relatively short time scales [e.g., *Velicogna et al.*, 2001] and in regions where there is a sparsity of meteorological data, for example, Antarctica. The differences between ECMWF and NCEP give a measure of error that may be present in any contemporary atmospheric model. This difference implies a level of aliasing that may still be present in a gravity estimate due to short-period variability in the atmosphere.

A.2 OCEAN MODEL

The ocean component of the AOD model is a barotropic model [*Ponte et al.*, 1991; *Ponte*, 1995; *Ponte and Gaspar*, 1999] as modified by *Hirose et al.* [2001]. Some details of the model as used for GRACE processing follow below; further details of the model implementation can be found in *Ali and Zlotnicki* [2003].

The ocean's response can be divided in two classes: barotropic and baroclinic. The barotropic component is a function of pressure alone, while the baroclinic component allows for density variations that are not functions of pressure alone [see, e.g., *Gill*, 1982]. A barotropic numerical ocean model has a single density for the entire water column and is forced only by wind and pressure. In contrast, a baroclinic model allows vertical density changes and their effects, but it requires additional forcings (e.g., evaporation-precipitation, thermal radiation) in order to handle thermodynamic effects. Generally speaking, barotropic motions are fast (sub-daily to a few days), and the baroclinic motions are slow (weeks to centuries). The tides are one example of barotropic motion (though tides are not handled separately from the AOD model), while El Niño is a baroclinic phenomenon. The advantage of using a barotropic model is that it is a simpler analytic model and is less expensive computationally. The differences

between barotropic and baroclinic models are negligible on average globally for periods shorter than 100 days [Tierney *et al.*, 2000]; furthermore, this difference did not result in significant aliasing error (chapter 3).

The ocean component of the AOD model is a barotropic ocean forced by ECMWF winds. The model has coverage for the ocean latitudes from 75° S to 65° N. It also includes the Mediterranean Sea, Hudson Bay, North Sea, and shallow waters, but it is recognized that the model performance in these enclosed or shallow areas is not as good as in the open ocean areas. Spatial resolution is 1.125°x1.125° in latitude and longitude and the integration time step is one minute. Any ocean depths greater than 6000 meters are set to 6000 meters and shallower than 50 meters are treated as land. Wind at various pressure levels is available from the ECMWF operation model and are used to derive a 10-m wind value. It is this 10-m wind that is then converted to wind stress and that forces the ocean surface [Ali and Zlotnicki, 2003]. No assumptions about an IB are made since the output of the model includes the effects of both wind and pressure forcing. It is the sum of the ocean model output plus the atmospheric pressure at each grid point that represents the pressure at the bottom of the ocean.

Fully baroclinic behavior was not be reproduced by this model. Since the model is known to be inaccurate after approximately 120 days, the model output will also vary at these periods relative to the real variability as detected by GRACE. This longer-period variability will be captured in the GRACE gravity estimates along with the other unmodeled time-variable signals (e.g., continental hydrology). In other words, not all of the ocean variability is removed as a consequence of GRACE data processing; there will be long period (~> 120 days) signals present.

A.3 MODEL COMBINATION

Since it is the short-period (i.e., sub-monthly) variability that is of interest, a relatively large bias was removed from the both the atmosphere and ocean models, leaving a residual time series. For the AOD Release 01 data, a year 2001 mean was removed from both the atmospheric and oceanic model components; however, different means may be removed in future AOD releases. For the land grid points, the residual ECWMF atmospheric pressure was calculated for prescribed 6-hr intervals. Over the oceans, the residual ocean model output was converted to pressure on the same 0.5° grid as the atmosphere and at the same 6-hr intervals. Undefined ocean areas outside the 75° S to 65° N latitudes were explicitly set to zero. These residual (i.e., relative to a 2001 mean) oceanic and atmospheric pressure fields were combined into a global time-series of mass variability in units of pressure. This time series was then converted into a spherical harmonics series complete to degree and order 100 at the synoptic times of 0, 6, 12, and 18 hr UTC. It is these geopotential, spherical harmonic coefficients that were and continue to be ingested directly into GRACE data processing.

A.4 IMPLEMENTATION

The inherent time-step currently used in GRACE data processing is five seconds (though the capability exists to change this time-step if necessary). As the AOD model output is provided only at 6-hr intervals, a method must be prescribed to define the AOD model contribution for other times. Nearly all of the spherical harmonic coefficients in the AOD model are sufficiently sampled to allow for linear interpolation between the explicitly defined data point (0, 6, 12, 18 hr UTC). A significant exception to this is the under-sampling of the variability in the atmosphere due to the S2 semi-diurnal tide; it was found that 6-hr sampling of this particular variation introduced measurable error into the

gravity field solution. Since this tidal variation is more precisely determined from other methods, it is better represented by an analytic expression that is defined for any time.

First, an estimate of the change due to this atmospheric tide in the $C_{2,2}$ and $S_{2,2}$ gravity coefficients were derived and removed from the AOD model. This component of the atmospheric tide was combined with the contributions due to the ocean tide model and this combination was thereafter handled by the ocean tide algorithm (with the rest of the ocean tide effects). The residual atmospheric signal left in the AOD model, at the six-hourly sampling, in $C_{2,2}$ and $S_{2,2}$, was treated like the rest of the coefficients in the model, that is, linearly interpolated (Figure A.1).

In order to differentiate this time series from the original, the time series due to any tide-related modifications made to the AOD data was denoted as the AOT model (AOD tide-modified). The modified CSR4.0 tide model and AOD Release 01 as described above was defined time model CSR4.0_MOD and AOT Release 01, respectively. This procedure treated some of the atmospheric variability as a tide and intimately linked the ocean tide model and the AOD model; therefore, any changes to *either* the AOD model *or* the tide model will require a re-generation of the AOT time series with an associated change in the AOT release number.

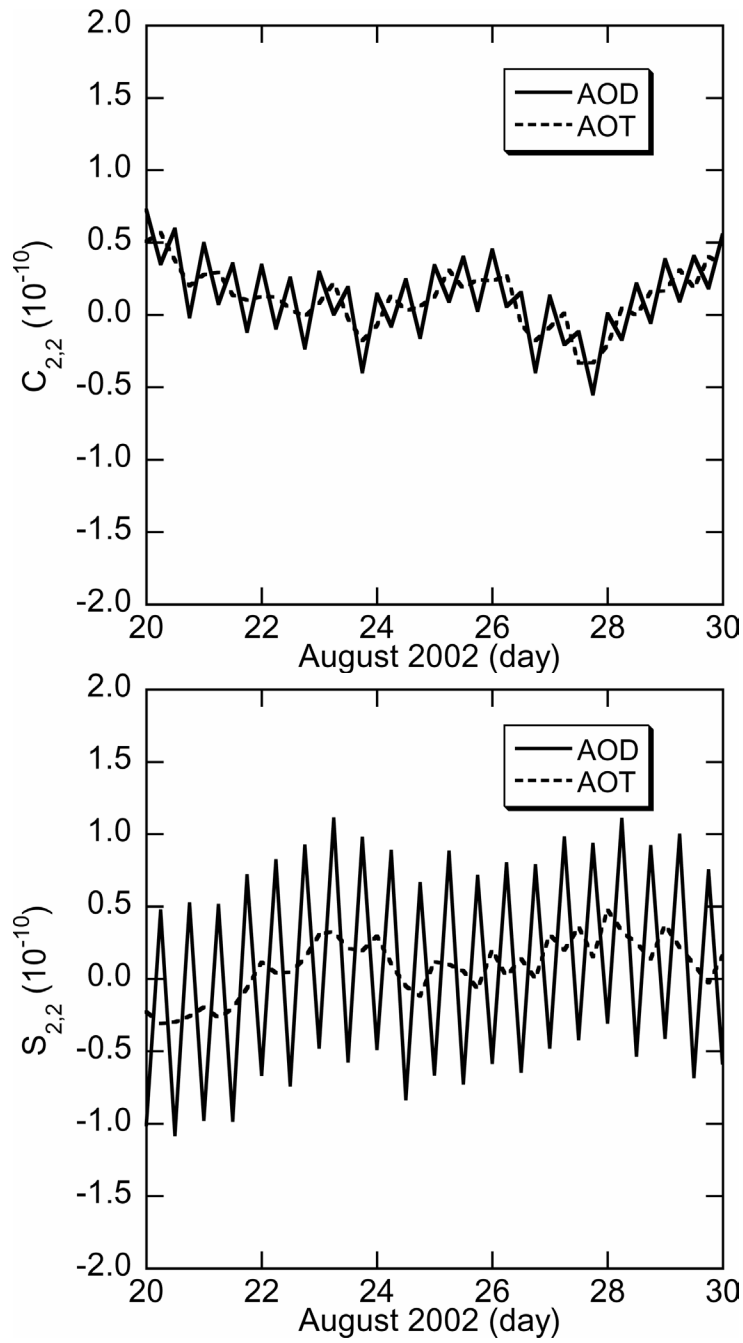


Figure A.1. Representative time series for $C_{2,2}$ (top) and $S_{2,2}$ (bottom) for the original AOD (solid line) and the AOT series created by removing the S2 semi-diurnal tide variability (dashed line).

A.5 BACKGROUND GEOPOTENTIAL MODELS

Along with the non-tidal effects of the atmosphere and ocean (AOD), several other geophysical variations are included in the background gravity model used for GRACE processing. Given a nominal static field, G_{static} , the set of all the spherical harmonic coefficients, C_{lm} and S_{lm} at a specific time, t , can be described by:

$$G(t) = G_{static} + \delta G_{aod}(t) + \delta G_{ot}(t) + \delta G_{st}(t) + \delta G_{pt}(t) + \delta G_{sec}(t) \quad (A.1)$$

where the individual contributions are due to the AOD model, δG_{aod} , ocean tides, δG_{ot} , solid Earth tides, δG_{st} , pole-tide, δG_{pt} , and secular variations, δG_{sec} (Figure A.2). The dominant signals at monthly time-scales are due to solid-body tides, δG_{st} . Diurnal and semi-diurnal periods are dominated by the ocean tides, δG_{ot} . The remaining terms in equation A.1 are small perturbations relative to the tidal variability. For the purposes of this dissertation, the non-AOD contributions to the geopotential were not considered. However, any interpretation of the results will ultimately depend upon and be limited by the accuracy of all of the models used for the purpose of removing the effects of short-period geopotential variability; the AOD model simply being one example of a model used to remove the effects of mass variability on gravity field estimation.

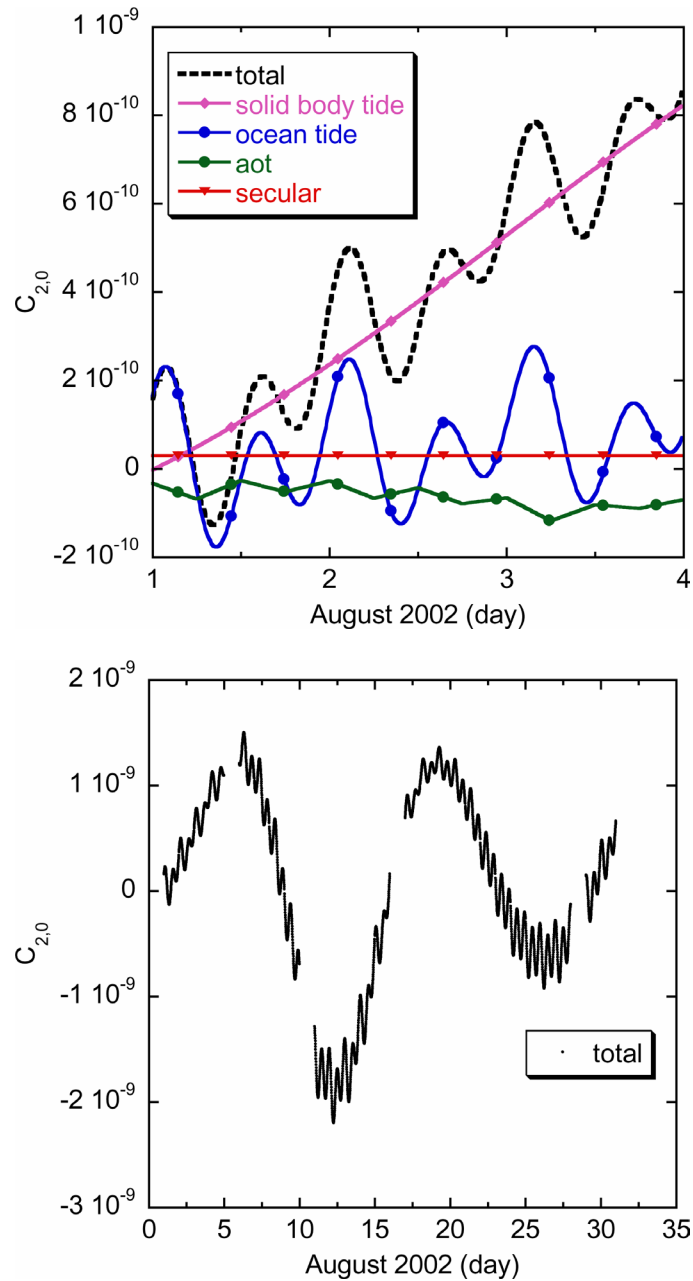


Figure A.2. Time-variable models of $C_{2,0}$ geopotential coefficient as used in GRACE processing for an August 2002 solution. Individual models are shown for a selected 3-day interval (top), while the total is shown for the entire solution time-span (bottom). Gaps in the time series are due to data omitted during processing.

A.6 SIMULATION VALIDATION

Simulations were conducted similar to those done in chapter 3 in order to assess the aliasing impact of completely omitting the AOD model and the residual error left after approximately modeling the effects of the AOD model by using NCEP atmospheric pressure data. August 2002 was selected as the test case, 30 days of data were used, and the simulations were limited to a degree and order 60 geopotential field. The degree difference between these two models was on the order of one-fifth of the signal due to either model (Figure A.3). The difference between ECMWF and NCEP is representative of the error believed to be in both atmospheric models; therefore, the difference between the AOD model and NCEP will be a combination of the error in the atmospheric component (ECWMF-NCEP) along with the full-power due to the unmodeled ocean. As expected, the two models differed most significantly over the ocean (Figure A.4), though the difference on average between the two atmospheric models over the land is comparable to the completely unmodeled signal over the oceans. However, it is important to note that it is not the difference on average that will result in aliasing error, but the mismatch in spectrum of variability between the AOD and NCEP model (Figure A.5) that will corrupt the gravity estimation procedure.

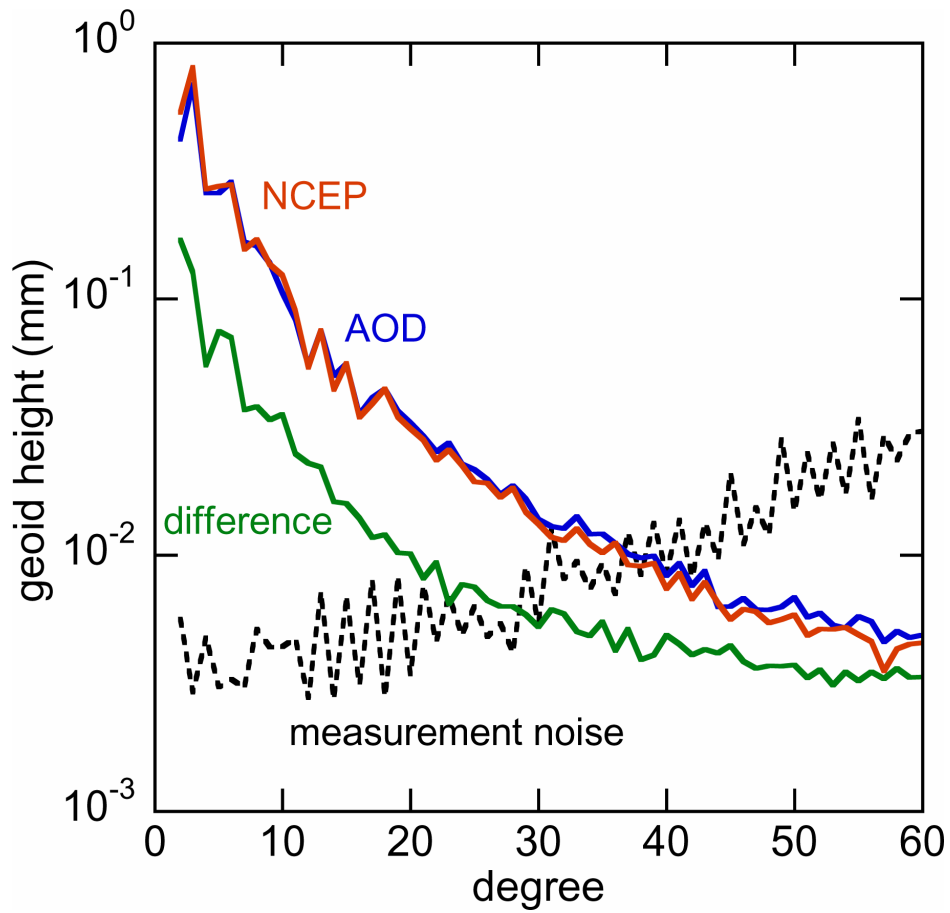


Figure A.3. Comparison of AOD model and NCEP atmospheric pressure in terms of degree amplitude for the month of August 2002. Also shown is representative error due to an optimistic assumption of measurement noise-only (see chapter 3)

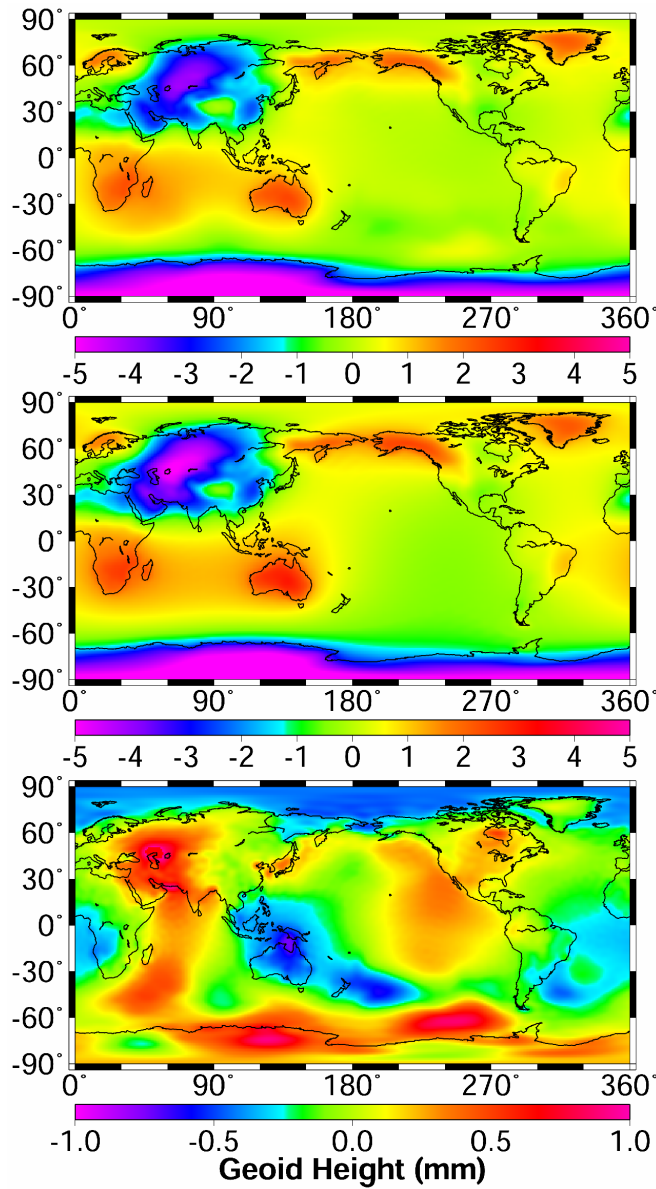


Figure A.4. Average for the month August 2002 relative to the year 2001 mean shown for AOD model (top), NCEP atmosphere (middle), and the difference between the two (bottom). Note that the map scales reflects that the model differences are on the order of one-fifth the model signals.

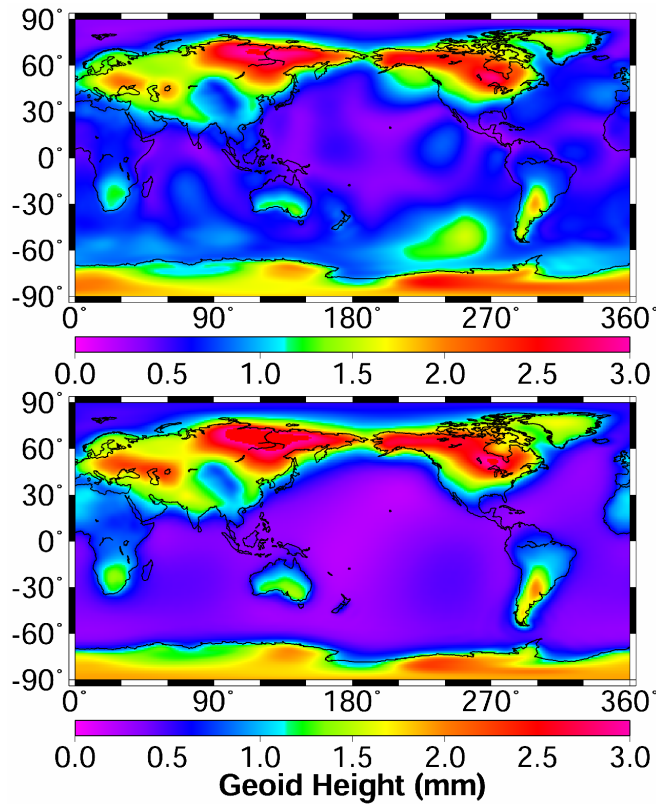


Figure A.5. RMS about the mean for the month August 2002 for AOD model (top) and NCEP atmosphere (bottom).

Due to the nature of orbital dynamics of the GRACE spacecraft, the ground track of GRACE will sample the variability in a manner that will not directly observe the simple mean of that variability. First, assume that the AOD model represented the “true” geopotential variability. If no corruption due to aliasing occurred in the process of estimating the Earth’s gravity field, then the perturbation as sensed by the spacecraft (e.g., Figure A.6) would be approximated by the average of the variation (Figure A.4). Clearly these two representations shown in Figure A.4 and A.6 are not identical, which highlights the effects introduced by sampling of temporal mass variability. In particular,

mass features with a large spatial extent move during the time span corresponding to a gravity solution (~ 30 days) and can be interpreted as short-wavelength spatial features. The GRACE gravity estimation procedure can capture most of the low-degree gravity features, but it is the higher degrees that are predominately corrupted by this unmodeled variability (see, e.g., chapter 3 and 4).

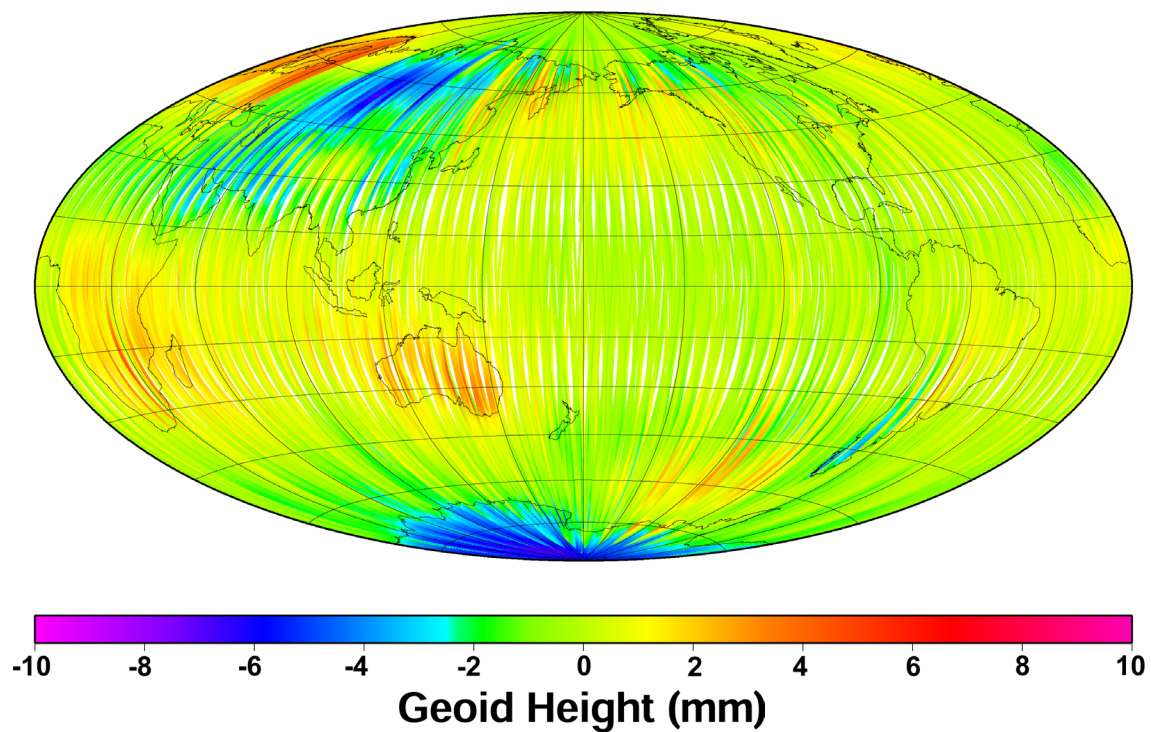


Figure A.6. History of geoid height for AOD taken along the ground track during the August 2002 solution.

Shown in Figure A.7 are the results of the aliasing simulations from using the AOD model as the “true” model. When no “nominal” time-variable mass model was used to attempt to remove the effects of the AOD model, the level of aliasing error was comparable to that predicted for an unmodeled atmosphere (Figure 3.4), i.e., ~ 10 times

the assumed level of measurement noise. Using NCEP as a “nominal” model of this variability had the expected effect of significantly reducing the error at approximately degree 10 and higher, with little to no impact at the lower degrees. The residual error that remains after de-aliasing with NCEP is comparable in magnitude to the level of error found to be possible for a completely unmodeled ocean (Figure 3.6).

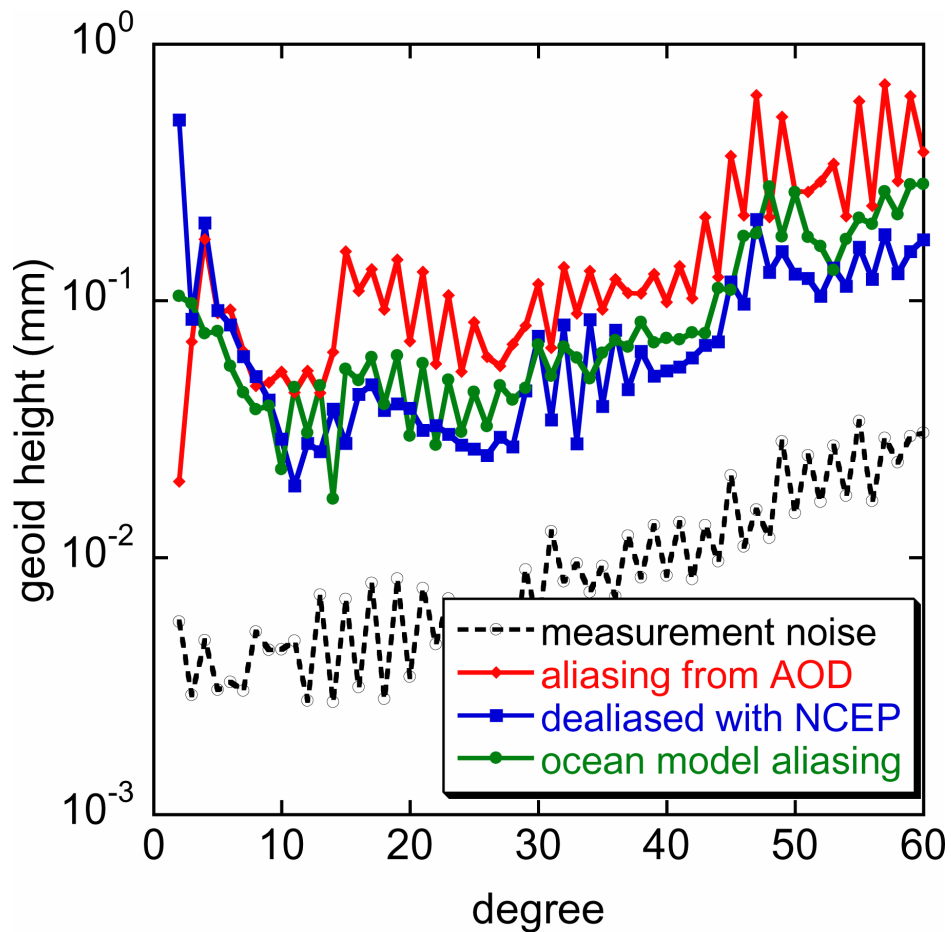


Figure A.7. Degree error using AOD data for August 2002 as the truth model and de-aliasing with NCEP atmosphere as the nominal model. Simulations conducted as in chapter 3. Representative error predicted for an unmodeled ocean and measurement noise-only are also shown.

References

- Ali, A. H., and V. Zlotnicki, Quality of wind stress fields measured by the skill of a barotropic ocean model: Importance of stability of the Marine Atmospheric Boundary Layer, *Geophys. Res. Lett.*, 30(3), 1129, doi:10.1029/2002GL016058, 2003.
- Alsdorf, D. E., and D. P. Lettenmaier, Tracking Fresh Water from Space, *Science*, 301, 1491-1494, doi:10.1126/science.1089802, 2003.
- Blewitt, G., D. Lavallée, P. Clarke, and K. Nurutdinov, A New Global Mode of Earth Deformation: Seasonal Cycle Detected, *Science*, 294, 2342-2345, 10.1126/science.1065328, 2001.
- Bryan, K., A numerical method for the study of the circulation of the world ocean, *J. Comput. Phys.*, 4, 347-376, 1969.
- Cazenave, A., F. Mercier, F. Bouille, and J. M. Lemoine, Global-scale interactions between the solid Earth and its fluid envelopes at the seasonal time scale, *Earth Planet. Sci. Lett.*, 171(4), 549-599, 1999.
- Chambers, D. P., J. Wahr, and R. S. Nerem, Preliminary observations of global ocean mass variations with GRACE, *Geophys. Res. Lett.*, 31, L13310, doi:10.1029/2004GL020461, 2004.
- Chao, B. F., The geoid and Earth rotation, in *Geoid and Its Geophysical Interpretations*, edited by P. Vaníček and N.T. Christou, pp. 285-298, CRC Press, Inc, Boca Raton, Florida, 1994.
- Chao, B. F. and A. Y. Au, Temporal variation of the Earth's low-degree zonal gravitational field caused by atmospheric mass redistribution: 1980-1988, *J. Geophys. Res.*, 96(B4), 6569-6575, 1991.
- Chao, B. F. and R. J. Eanes, Global gravitational changes due to atmospheric mass redistribution as observed by the Lageos nodal residual, *Geophys. J. Int.*, 122, 755-764, 1995.
- Chao, B. F. and W. P. O'Connor, Global surface water-induced seasonal variations in the Earth's rotation and gravitational field, *Geophys. J. Int.*, 94(2), 263-270, 1988.

- Chen, J. L., C. R. Wilson, D. P. Chambers, R. S. Nerem, and B. D. Tapley, Seasonal global water mass budget and mean sea level variations, *Geophys. Res. Lett.*, 25(19), 3555-3558, doi:10.1029/98GL50667, 1998.
- Chen, J. L., C. R. Wilson, R. J. Eanes, and R. S. Nerem, Geophysical interpretation of observed geocenter variations, *J. Geophys. Res.*, 104(B2), 2683-2690, 1999.
- Cheng, M. K. and B.D. Tapley, Seasonal variations in low degree zonal harmonics of the Earth's gravity field from satellite laser ranging observations, *J. Geophys. Res.*, 104(B2), 2667-2681, 1999.
- Degnan, J. J., Millimeter accuracy satellite laser ranging: A review, in *Contributions of Space Geodesy to Geodynamics: Technology, Geodyn. Ser.*, vol. 25, edited by D. E. Smith and D. L. Turcotte, pp. 133-162, AGU, Washington, D.C., 1993.
- Dukowicz, J. K. and R. D. Smith, Implicit free-surface method for the Bryan-Cox-Semtner ocean model, *J. Geophys. Res.*, 99(C4), 7991-8014, 1994.
- Dunn, C., W. Bertiger, Y. Bar-Sever, S. Desai, B. Haines, D. Kuang, G. Franklin, I. Harris, G. Kruizinga, T. Meehan, S. Nandi, D. Nguyen, T. Rogstad, J.B. Thomas, J. Tien, L. Romans, M. Watkins, S.-C. Wu, S. Bettadpur, and J. Kim, Instrument of Grace: GPS augments gravity measurements, *GPS World*, 14(2), 2003.
- Eanes, R. J., A Study of Temporal Variations in Earth's Gravitational Field Using LAGEOS-1 Laser Ranging Observations, Ph.D. dissertation, Department of Aerospace Engineering and Engineering Mechanics, Univ. of Tex. at Austin, Austin, Texas, 1995.
- Eanes, R. J. and S. V. Bettadpur, Temporal variability of Earth's gravitational field from satellite laser ranging, in *Global Gravity Field and Its Temporal Variations, Symposium No. 116*, edited by R. H. Rapp, A. A. Cazenave, and R. S. Nerem, pp. 30-41, Boulder, Colorado, 1995.
- Eckhardt, D. H., Correlations between global features of terrestrial fields, *Mathematical Geology*, 16(2), 155-171, 1984.
- European Centre for Medium-Range Weather Forecasts (ECMWF), The description of the ECMWF/WCRP level IIIA global atmospheric data archive, Data Services publication, Reading, England, 1995.
- Gegout, P. and A. Cazenave, Temporal variations of the Earth's gravity field for 1985-1989 derived from Lageos, *Geophys. J. Int.*, 114(2), 347-359, 1993.
- Gill, A. E., *Atmosphere-Ocean Dynamics*, 662 pp., Academic Press, New York, 1982.

- GRACE (Gravity Recovery and Climate Experiment) Project, AOD1B Product Description Document, GRACE 327-750, Rev. 1.0, 2003.
ftp://podaac.jpl.nasa.gov/pub/grace/doc/AOD1B_20031022.pdf
- Gruber, T. and T. Peters, Time variable gravity field: Using future Earth observation missions for high frequency de-aliasing, in *IERS Technical Note No. 30*, edited by B. Richter, W. Schwegmann, and W. R. Dick, Verlag des Bundesamts für Kartographie und Geodäsie, Frankfurt am Main, 2003.
- Gunter, B., Computational methods and processing strategies for estimating Earth's gravity field, Ph.D. thesis, Department of Aerospace Engineering and Engineering Mechanics, Univ. of Tex. at Austin, Austin, Texas, 2004.
- Hirose, N., I. Fukumori, V. Zlotnicki, and R.M Ponte, Modeling the high-frequency barotropic response of the ocean to atmospheric disturbances: Sensitivity to forcing, topography, and friction, *J. Geophys. Res.*, *106*(C12), 30987-30996, 2001.
- Huang, J., H. M. van den Dool, and K. P. Georgakakos, Analysis of model-calculated soil moisture over the United States (1931-1993) and applications to long-range temperature forecasts, *J. Climate*, *9*(6), 1350-1362, 1996.
- James, T. S. and E. R. Ivins, Global geodetic signatures of the Antarctic ice sheet, *J. Geophys. Res.*, *102*(B1), 605-633, 1997.
- Jayne, S. R., J. M. Wahr, and F. O. Bryan, Observing ocean heat content using satellite gravity and altimetry, *J. Geophys. Res.*, *108*(C2), 3031, doi:10.1029/2002JC001619, 2003.
- Jekeli, C., Alternative methods to smooth the Earth's gravity field, Rep. 327, Dep. Of Geod. Sci. and Surv., Ohio State Univ., Columbus, Ohio, 1981.
- Kalnay, E., M. Kanamitsu, R. Kistler, W. Collins, D. Deaven, L. Gandin, M. Iredell, S. Saha, G. White, J. Woollen, Y. Zhu, M. Chelliah, W. Ebisuzaki, W. Higgins, J. Janowiak, K. C. Mo, C. Ropelewski, J. Wang, A. Leetmaa, R. Reynolds, R. Jeanne, and D. Joseph, The NCEP/NCAR 40-year reanalysis project, *Bull. Amer. Meteor. Soc.*, *77*(3), 437-471, 1996.
- Kaula, W. M., *Theory of Satellite Geodesy*, 124 pp., Blaisdell Publishing Co., Waltham, Massachusetts, 1966.
- Kim, J., Simulation study of a low-low satellite-to-satellite tracking mission, Ph.D. dissertation, Department of Aerospace Engineering and Engineering Mechanics, Univ. of Tex. at Austin, Austin, Texas, 2000.

- Kim, J. and B.D. Tapley, Error analysis of a low-low satellite-to-satellite tracking mission, *J. Guid. Control. Dynam.*, 25 (6), 1100-1106, 2002.
- Knudsen, P. and O. Andersen, Correcting GRACE gravity fields for ocean tide effects, *Geophys. Res. Lett.*, 29(8), 1178, doi:10.1029/2001GL014005, 2002.
- McCarthy, D. D. (Ed.), IERS Conventions (1996), *IERS Technical Note 21*, Observatoire de Paris, France, 1996.
- Métris, G., D. Vokrouhlický, J. Ries, and R. Eanes, Nongravitational effects and the LAGEOS eccentricity excitations, *J. Geophys. Res.*, 102(B2), 2711–2730, 1997.
- Muller, P. A., and W. L. Sjogren, Mascons: Lunar mass concentrations, *Science*, 161, 680-694, 1968.
- National Research Council (U.S.). Committee on Earth Gravity from Space, *Satellite Gravity and the Geosphere: Contributions to the Study of the Solid Earth and Its Fluid Envelope*, 112 pp., National Academies Press, Washington, D.C., 1997.
- Nerem, R. S., B. F. Chao, A. Y. Au, J. C. Chan, S. M. Klosko, N. K. Pavlis, and R. G. Williamson, Temporal variations of the Earth's gravitational field from satellite laser ranging to LAGEOS, *Geophys. Res. Lett.*, 20(7), 595-598, 1993.
- Nerem, R. S., C. Jekeli, and W. M. Kaula, Gravity field determination and characteristics: Retrospective and prospective, *J. Geophys. Res.*, 100(B8), 15053-15074, 1995.
- Nerem, R. S., R. J. Eanes, P. F. Thompson, and J. L. Chen, Observations of annual variations of the Earth's gravitational field using satellite laser ranging and geophysical models, *Geophys. Res. Lett.*, 27(12), 1783-1786, 2000.
- Nerem, R. S., J. M. Wahr, and E. W. Leuliette, Measuring the distribution of ocean mass using GRACE, *Space Sci. Rev.*, 108, 331-344, doi:10.1023/A:1026275310832, 2003.
- Ponte, R. M., Nonequilibrium response of the global ocean to the 5-day Rossby-Haurwitz wave in atmospheric surface pressure, *J. Phys. Oceanogr.*, 27, 2158-2168, 1997.
- Ponte, R. M. and P. Gaspar, Regional analysis of the inverted barometer effect over the global ocean using TOPEX/POSEIDON data and model results, *J. Geophys. Res.*, 104(C7), 15587-15601, 1999.
- Ponte, R. M., D. Salstein, and R. Rosen, Sea level response to pressure forcing in a barotropic numerical model, *J. Phys. Oceanogr.*, 21(7), 1043-1057, 1991.

- Prigent, C., E. Matthews, F. Aires, and W. B. Rossow, Remote sensing of global wetland dynamics with multiple satellite data sets, *Geophys. Res. Lett.*, 28(24), 4631-4634, 2001.
- Rim, H. J., TOPEX orbit determination using GPS tracking system, Ph.D. dissertation, Department of Aerospace Engineering and Engineering Mechanics, Univ. of Tex. at Austin, Austin, Texas, 1992.
- Rodell, M. and J. S. Famiglietti, Detectability of variations in continental water storage from satellite observations of the time-variable gravity field, *Water Resour. Res.*, 35(9), 2705-2723, 1999.
- Rodell, M., P. R. Houser, U. Jambor, J. Gottschalck, K. Mitchell, C.-J. Meng, K. Arsenault, B. Cosgrove, J. Radakovich, M. Bosilovich, J. K. Entin, J. P. Walker, D. Lohmann, and D. Toll, The Global Land Data Assimilation System, *Bull. Am. Meteorol. Soc.*, 85(3), 2004.
- Roesset, P. J., A simulation study of the use of accelerometer data in the GRACE mission, Ph.D. dissertation, Department of Aerospace Engineering and Engineering Mechanics, Univ. of Tex. at Austin, Austin, Texas, 2003.
- Schutz, B. E., B. D. Tapley, P. A. M. Abusali, and H. J. Rim, Dynamic orbit determination using GPS measurements from TOPEX/POSEIDON, *Geophys. Res. Lett.*, 21(19), 2179-2182, 1994.
- Semtner, A. J., Jr., Finite-difference formulation of a world ocean model, in *Advanced Physical Oceanographic Numerical Modelling*, edited by J. J. O'Brien, pp. 187-202, D. Reidel, Norwell, Massachusetts, 1986.
- Swenson, S. and J. Wahr, Methods for inferring regional surface-mass anomalies from Gravity Recovery and Climate Experiment (GRACE) measurements of time-variable gravity, *J. Geophys. Res.*, 107(B9), 2193, doi:10.1029/2001JB000576, 2002.
- Tapley, B. D. and C. Reigber, The GRACE Mission: Status and future plans, *Eos Trans. AGU*, 82(47), Fall Meet. Suppl., Abstract G41C-02, 2001.
- Tapley, B. D., J. C. Ries, G. W. Davis, R. J. Eanes, B. E. Schutz, C. K. Shum, M. M. Watkins, J. A. Marshall, R. S. Nerem, B. H. Putney, S. M. Klosko, S. B. Luthcke, D. Pavlis, R. G. Williamson, and N. P. Zelensky, Precision orbit determination for TOPEX/POSEIDON, *J. Geophys. Res.*, 99(C12), 24383-24404, 1994.
- Tapley, B. D., M. M. Watkins, J. C. Ries, G. W. Davis, R. J. Eanes, S. R. Poole, H. J. Rim, B. E. Schutz, C. K. Shum, R. S. Nerem, F. J. Lerch, J. A. Marshall, S. M.

- Klosko, N. K. Pavlis, and R. G. Williamson, The Joint Gravity Model 3, *J. Geophys. Res.* 101(B12), 28029-28050, 1996.
- Tapley, B., D. Chambers, M. Cheng, M. Kim, S. Poole, and J. Ries, The TEG-4 Earth Gravity Field Model, paper presented at 25th General Assembly, EGS, Nice, France, April, 2000.
- Tapley, B. D., D. P. Chambers, S. Bettadpur, and J. C. Ries, Large scale ocean circulation from the GRACE GGM01 Geoid, *Geophys. Res. Lett.*, 30(22), 2163, doi:10.1029/2003GL018622, 2003.
- Tapley, B. D., S. Bettadpur, M. Watkins, and C. Reigber, The gravity recovery and climate experiment: Mission overview and early results, *Geophys. Res. Lett.*, 31(9), L09607, doi:10.1029/2004GL019920, 2004a.
- Tapley, B. D., S. Bettadpur, J. C. Ries, P. F. Thompson, and M. M. Watkins, GRACE measurements of mass variability in the Earth system, *Science*, 305(5683), 503-505, doi:10.1126/science.1099192, 2004b.
- Tapley, B. D., B. E. Schutz, and G. H. Born, *Statistical Orbit Determination*, 546 pp., Academic Press, Boston, Massachusetts, 2004c.
- Thompson, P. F., S. V. Bettadpur, J. Kim, and M. M. Watkins, Short period time variations in the gravity field and their impact on GRACE science, *Eos Trans. AGU*, 81(48), Fall Meet. Suppl., Abstract G61A-08, 2000.
- Tierney, C., J. Wahr, F. Bryan, and V. Zlotnicki, Short-period oceanic circulation: Implications for satellite altimetry, *Geophys. Res. Lett.*, 27(9), 1255–1258, 2000.
- Velicogna, I. and J. Wahr, Postglacial rebound and Earth's viscosity structure from GRACE, *J. Geophys. Res.*, 107(B12), 2376, doi:10.1029/2001JB001735, 2002.
- Velicogna, I., J. Wahr, and H. Van den Dool, Can surface pressure be used to remove atmospheric contributions from GRACE data with sufficient accuracy to recover hydrological signals?, *J. Geophys. Res.*, 106(B8), 16415-16434, 2001.
- Vonbun, F. O., W. D. Kahn, W. T. Wells, and T. D. Conrad, Determination of 5 x 5 degree gravity anomalies using satellite-to-satellite tracking between ATS6 and Apollo, *Geophys. J. R. Astron. Soc.*, 61, 645-658, 1980.
- Wahr, J., M. Molenaar, and F. Bryan, Time variability of the Earth's gravity field: hydrological and oceanic effects and their possible detection using GRACE, *J. Geophys. Res.*, 103(B12), 30205-30229, 1998.

- Wahr, J. M., S. R. Jayne, and F. O. Bryan, A method of inferring changes in deep ocean currents from satellite measurements of time-variable gravity, *J. Geophys. Res.*, *107*(C12), 3218, doi:10.1029/2001JC001274, 2002.
- Wahr, J., S. Swenson, V. Zlotnicki, and I. Velicogna, Time-variable gravity from GRACE: First results, *Geophys. Res. Lett.*, *31*, L11501, doi:10.1029/2004GL019779, 2004.
- Watkins, M. M. and R. J. Eanes, Long term changes in the Earth's shape, rotation, and geocenter, *Adv. Space Res.*, *13*, 11251-11255, 1993.
- Wolff, M., Direct measurements of the Earth's gravitational potential using a satellite pair, *J. Geophys. Res.*, *74*(22), 5295-5300, 1969.
- Wunsch, C. and V. Zlotnicki, Measuring Ocean Bottom Pressure Changes from Space: Report of a Meeting, *JPL Tech. Report D-19027*, Jet Propul. Lab., Pasadena, Calif., 1999.
- Wu, X., M. M. Watkins, E. R. Ivins, R. Kwok, P. Wang, and J. M. Wahr, Toward global inverse solutions for current and past ice mass variations: Contribution of secular satellite gravity and topography change measurements, *J. Geophys. Res.*, *107*(B11), 2291, doi:10.1029/2001JB000543, 2002.
- Yoder, C. F., J. G. Williams, J. O. Dickey, B. E. Schutz, R. J. Eanes, and B. D. Tapley, Secular variation of Earth's gravitational harmonic J_2 coefficient from Lageos and nontidal acceleration of Earth rotation, *Nature*, *303*, 757-762, 1983.
- Yunck, T. P., W. I. Bertiger, S. C. Wu, Y. E. Bar-Sever, E. J. Christensen, B. J. Haines, S. M. Lichten, R. J. Muellerschoen, Y. Vigue, and P. Willis, First assessment of GPS-based reduced dynamic orbit determination on TOPEX/Poseidon, *Geophys. Res. Lett.*, *21*(7), 541-544, 1994.

Vita

Paul Frank Thompson, Jr. was born in Long Beach, California on 11 January 1969, the son of Paul Frank Thompson, Sr. and Esther Ann Thompson. After obtaining his diploma at Eureka High School, Eureka, California in 1987, he attended college at the University of California, Los Angeles (UCLA). He received the degree of Bachelor of Science in Physics from the University of California in March 1991 and received the degree of Masters of Science in Geophysics and Space Physics from the University of California in August 1997. During the period of November 1995 to August 1997 he also worked at the Jet Propulsion Laboratory in Pasadena, California as a Sequence Integration Engineer for the Galileo Project Mission to Jupiter. In September 1997 he entered the Graduate School of The University of Texas at Austin.

Permanent address: 3235 G Street, Eureka, California 95503

This dissertation was typed by the author.